Finite volume approximations for some equations arising in mathematical physics

by

Aderogba Adebayo Abiodun

Submitted in partial fulfillment of the requirements for the degree

Philosophiae Doctor

In the Faculty of Natural and Agricultural Sciences

University of Pretoria
Pretoria

May, 2014

Declaration

I, Adebayo Abiodun, Aderogba declare that the thesis, which I hereby submit for the degree Philosophiae Doctor at the University of Pretoria, is my own work and has not previously been submitted by me for a degree at this or any other tertiary institution.

SIGNATURE:

DATE:

To

τ & Ω

Acknowledgement

You know how it feels when you pick up a book, flip to the acknowledgement page, and discover, once again, the author missed out your name. This time it is different, therefore, I appreciate everybody who contributed in one way or the other to the success of this work. I will not forget to mention the following:

The Almighty God for life and all provisions.
Drs. Chapwanya M and Djoko JK for guidance.
University of Pretoria for financial support and conducive research environment.
The Dean, Faculty of Natural and Agricultural Science.
Department of Mathematics and Applied Mathematics, University of Pretoria staff, friends and colleagues.
Obafemi Awolowo University for support and grant of my study leave.
Department of Mathematics, Obafemi Awolowo University, staff, friends and colleagues.
All my colleagues for advise and counsels.
DCLM, Pretoria.
CGMC, Ibadan, Nigeria.
My Parents and the entire Aderogba's and Adebayo's family.
Praise, Goodness, Halleluyah, for understanding.
My sweetheart for the love.

Contents

List of Tables

List of Figures

Title	Finite volume approximations for some equations arising in mathematical physics
Name	Aderogba Adebayo Abiodun
Supervisor	Dr. Jules Djoko Kamdem
Co-Supervisor	Dr. Chapwanya Michael
Department	Mathematics & Applied Mathematics
Degree	Philosophiae Doctor

Abstract

In this thesis we design and implement finite volume schemes to approximate the solution of 1-dimensional (partial) differential equations. Most of these partial differential equations (PDEs) are made up of not only mathematically interesting but also physically relevant terms such as the hyperbolic convective and parabolic diffusive operators. The coupling of higher order, linear and nonlinear operators and the presence of a small parameter multiplying the highest derivative imposes some stiffness into the equations thereby making both their numerical and mathematical analysis interesting but very challenging. For example, singularly perturbed second order ordinary differential equations (ODEs) possess boundary layers and/or oscillatory solutions which make their numerical approximation by difference-type schemes expensive.

We design two uniformly convergent finite volume schemes for a singularly perturbed ODE: the Schrödinger equation. The first scheme is based on the nonstandard finite difference (NSFD) method which is known to preserve the qualitative properties of the physical model and the second is based on boundary layer analysis.

We employ fractional splitting method for the analysis of higher order equations in order to isolate the linear and nonlinear terms thereby resolving the stiffness in the equation. The nonlinear hyperbolic term is solved by shock capturing schemes while the fourth order linear parabolic term is handled by A-stable schemes. We also utilize the idea of the NSFD method to design a scheme for the hyperbolic, nonlinear parabolic and the linear fourth order PDEs. Each of the terms is solved sequentially within every time step and their solutions are pieced together in such a way as to preserve the properties of the original equations.

We observe uniform convergence with better approximation at relatively low computation cost when the Schrödinger equation was solved by the proposed schemes. We also examined the computational strength of our schemes on two fourth order equations: the Kuramoto-Sivashinsky equation and Cahn-Hilliard equation. We studied the effect of combining different schemes for each of the split sub-problems on the convergence of the fractional splitting scheme. We are able to reproduce all the expected properties of the selected equations. We observed a better convergence when the nonstandard finite volume method was applied to these PDEs. Throughout this work, numerical simulations are provided to validate the computational power of the proposed schemes.

Chapter 1

Introduction

In this thesis, numerical investigations of 1-dimensional singularly perturbed (partial) differential equations are presented. The finite volume method is employed throughout. Each chapter represents scientific contribution in form of published, accepted, submitted or work in progress.

The real world is filled with different challenges ranging from social, physical and engineering sciences. Reliable mathematical models offer the cheapest way of investigating these challenges. These mathematical models range from algebraic, differential, integral, algebraic-differential, algebraic-integral or differential-integro equations. Designing well-possed mathematical models is essential so as to provide realistic solutions under reasonable and dynamically consistent assumptions. Surprisingly, most of these equations, because of their complexity, as we will see later, are not amenable to analytical solutions. For this reason, there is need to develop approximate numerical solutions for these models. The size of system of equations, the number of unknowns, the nonlinearity in the equations and some other complexities in such equations coupled with limited space, time and human capacity constrained individuals to make assumptions which at the end of the day reduces the strength and quality of the results, and consequently their applicability to real life models. Thanks to the advent of computer system, now we only need to develop numerical algorithms which are able to handle such equations with more realistic assumptions.

Computational/numerical mathematics has gained much ground over a century now. It is a strong tool for scientific computing and very useful in solving problems from physical, economical, engineering and biological models. There are many different numerical methods for solving mathematical models. We have among many, the finite element method, finite difference method and finite volume method. Some of the common features of these methods are as follows.

- *Grid generation*: This is the process by which the continuous space is represented by discrete points/grids in a numerical domain.

- *Time discretization*: The whole time interval is sub-divided into finite intervals called time steps.
- Lastly, the continuous equation is transformed into algebraic system of equations.

In the present work, we will employ the finite volume method to approximate the solutions of three important models

1. The Kuramoto-Sivashinsky equation,
2. The Cahn Hilliard equation,
3. The Schrödinger equation.

This will help us to treat each of the differential equation models in their integral forms. The process of discretization will be discussed in the next sections. Appeal is made to the fractional splitting method for its stability and the nonstandard finite difference method for their qualitative stability, monotonicity and positivity preserving properties.

1.1 Higher order equations

Pattern formation resulting from phase transition has been observed in alloys, glasses, polymer solutions, binary liquid mixtures, ecological contexts among many. The fourth order Cahn-Hilliard equation,

$$u_t + \gamma u_{xxxx} = \phi(u)_{xx} + \delta u u_x \ \ (a < x < L, 0 < t), \tag{1.1}$$

where

$$\phi(u) = \alpha u^3 + \beta u^2 + \kappa u, \tag{1.2}$$

has been a successful model for such transitions (see for example [18, 19, 62] and the references therein). The research into the Cahn-Hilliard equation (1.1) has been documented in the literature. The authors in [19] established the global existence or blow up in a finite time of problem (1.1)-(1.2) when $\delta = 0$ under some certain conditions. They observed that if $\alpha > 0$, there exists a unique solution for any initial data $u_0 \in H^2$ and satisfying $u_x(0,t) = 0 = u_x(L,t)$, but the solution must blow up in finite time for large initial data if $\alpha < 0$. Along side this, they noted that if $\gamma > L^2/\pi^2$ and the initial data is small, there will be a unique global solution which decays to the constant M as $t \to \infty$ no matter the sign of α. This was later verified in [18] via the Galerkin finite element method provided that

$$\int_I (\mathcal{F}(u_0) - \mathcal{F}_m)dx + \frac{\gamma}{2}|u_0|_1^2,$$

is sufficiently small, $\mathcal{F}(u_0) > \mathcal{F}_m \ \forall x$, where $\mathcal{F}_m$ is of the local minimal of $\mathcal{F}(s)$ on $\mathbb{R}$, M is sufficiently close to u_m, where $\mathcal{F}_m = \mathcal{F}(u_m)$ and the seminorm $\|D^s v\|$ is denoted by $|v|_s$. Next,

a semi-discrete finite element scheme for the solution of the Cahn-Hilliard equation (1.1) - (1.2) was derived in [20]. They also derived optimal order error bounds in various norms. The Cahn-Hilliard equation (1.1) with boundary conditions $u(0,t) = u(1,t) = u_{xx}(0,t) = u_{xx}(1,t) = 0$ was considered in [16]. They showed the existence and uniqueness of solution based Faedo-Galerkin semi-discrete scheme and also presented a new finite element based fully discrete scheme which has a Lyapunov functional. The Lyapunov functional helped them to obtain point-wise estimate of the solution.

These theoretical results were verified numerically by several authors (see [12, 13, 14, 22, 48] among others). Eyre [22] studied the solution of the Cahn-Hilliard equation (1.1) employing a splitting method in which the contractive and expansive terms of the equation are separated across the time step. They noted that the flops reported in their work do not directly apply to solving the Cahn-Hilliard equation in more than one spatial dimension. Later, their type of splitting was employed in [13] to solve the Cahn-Hilliard equation subject to free boundary condition and showed that unconditionally gradient stability is achieved in one, two and three dimensions with large time steps. Recently, Cueto-Felgueroso and Peraire [12] studied numerically the two dimensional phase separation problem governed by the Cahn-Hilliard equation using a time adaptive procedure. They were able to provide a quantitative characterization of the different time scales present in phase separation processes. The work in [85] on the Cahn-Hilliard equation with degenerate mobility enjoyed the use of tanh, homotopy perturbation and Adomian decomposition methods. The tanh method was used to find the traveling wave solution while the main equation was solved by the homotopy perturbation and the Adomian decomposition separately. The work of Dehghan and Mirzaei [14] reproduce most of the properties of the Cahn-Hilliard equation. The authors employed a numerical method based on the boundary integral equation and dual reciprocity methods. Most recently, Lee et al. [48] introduced a gradient stable scheme to solve the N-component Cahn-Hilliard system. The method helped them to reduce the N-component system to a system of $N-1$ binary Cahn-Hilliard equations which they solved with the aid of a nonlinear multi grid method.

If $\delta > -\sqrt{2}$, $\gamma = 1$, $\beta = 0$, the asymptotic solution of equation (1.1) takes the form of a valley and is called a kink while it takes the form of a hill (anti-kink) if $\delta < \sqrt{2}$ [26]. The occurrence of a kink and anti-kink together is referred to as kink-anti-kink pair. In 1996, Emmott and Bray [21] studied the Cahn-Hilliard equation (1.1) in the presence of a driving force (i.e. $\delta \neq 0$). They examined the effects of the driving force on the solution of the equation. They observed that it has an asymmetric effect on the solution for a kink and the direction of the field determines whether the analytic solutions derived earlier by Leung [49] are unique. They also studied the dynamics of a kink-anti-kink pair. Later, this problem was investigated by Golovin et al. [26] where they observed that the kink-anti-kink pair actually comes as the final result of coarsening on a periodic domain. They noted that such a solution does not exist for $\delta > \sqrt{2}$ and that the far field solution becomes unstable when $\delta > 0.94$. This was also confirmed by the work of Watson [86] and

Watson et al. [87]. Watson [86] derived the convective Cahn-Hilliard equation (1.1) when examining the coarsening dynamics of crystal growth. He performed the direct simulation of the equation with $\delta = 0.1$ while Watson et al. [87] performed a matched asymptotic analysis on the equation (1.1) ($\delta = 1$, $\gamma = 0.01$) on a periodic domain. Both teams, Watson [86] and Watson et al. [87], agree on the impossibility of binary coalescence of phase boundary and the occurrence of ternary coalescence only through the kink-ternary interaction (i.e., two kinks meet an anti-kink resulting in a kink). They also concluded that when $\delta \gg 1$ the solution of the convective Cahn-Hilliard equation behaves like that of the Kuramoto-Sivashinsky equation. This was shown for a two dimensional case in [26]. Recently, the dynamics of domain walls (kinks) governed by the equation (1.1) with special interest in the dynamics of kink pairs and triplets that play crucial role in the coarsening process was investigated by Podolny et al. [69]. They were able to derive an analytical formula that describes the motion of the kink pairs and the triplets.

Scaling the equation (1.1) by δ and letting $\bar{u} = \frac{u}{\delta}$ gives rise to another interesting fourth order unsteady equation [26], the *Kuramoto-Sivashinsky* equation,

$$\begin{cases} u_t + uu_x + \alpha u_{xx} + \gamma u_{xxxx} = 0, \quad \forall\ (x,t) \in \mathbb{R} \times (0,\infty), \\ u(x,0) = \psi(x), \end{cases} \tag{1.3}$$

as $\delta \to \infty$ after dropping the bar. Here, $\alpha, \gamma > 0$ are constant coefficients accounting for the long wave instability (gain) and short wave dissipation, respectively. Equation (1.3) is a well known model of one dimensional turbulence which was derived in various physical contexts including chemical-reaction waves, propagation of combustion fronts in gas, surface waves in a film of a viscous liquid flowing along an inclined plane, patterns in thermal convection, rapid solidification, and many others (see for example [41, 44, 80, 74, 75, 76]).

Various approaches have been presented in the literature to find the properties of the solutions of the Kuramoto-Sivashinsky (K-S) equation, with special attention on the energy bound derived theoretically in the form

$$\limsup_{t\to\infty} \|u(x,t)\|_2 = \limsup_{t\to\infty} (L\mathcal{E}(t))^{1/2} \leq CL^p, \tag{1.4}$$

where

$$\mathcal{E}(t) = \frac{1}{L}\int_0^L u^2 dx. \tag{1.5}$$

For example, Nicolaenko *et al.* [61] determined $p = 5/2$ with the assumption that initial data is L-periodic, antisymmetric about the origin and of zero mean. In Collet et al. [10] removed the antisymmetry requirement and observed that $p = 8/5$. A 1-dimension version of the equation was considered by Goodman [27] where they removed the requirement of odd solutions and arrived at the same value of p following a generalization of the Nicolaenko *et al.* 's Lyapunov function argument. Giacomelli and Otto [24] obtained two integral identities in $L^4 - norm$ of u and employed these to determine a bound for equation (1.4). Through

their analysis, they arrived at $p = 3/2$. A weaker bound which was proved to be necessary in the presence of a linear destabilizing term was later introduced in [9]. Recently, a Lyapunov argument was followed in [63] to obtain bounds that are independent of the system size.

The numerical solutions of the K-S equation have been widely investigated in the literature. In particular, we highlight the Galerkin method [89], the Chebyshev spectral methods [43], the B-splines [46], the meshless method of lines [28], etc. The aim of these investigations have been on the accuracy [89], and/or how these solutions compare with the well documented benchmark solutions [64]. In [89], an explicit Runge Kutta method was used to avoid the restrictive stability limit of the fourth order derivative. Further advantage of the method is that the approach can easily be tweaked to obtain any required order of accuracy. Other approaches are based on simplifying the partial differential equation in order to reduce difficulties in its numerical approximation. For example, the B-spline approach by Lakestani and Dehghan [46] reduced the problem to a set of algebraic equations, while in [43] the equation was reduced to a system of ODEs that were solved by implicit-explicit BDF method.

In this theses, we employ the fractional splitting method to simplify the analysis of equations (1.1) and (1.3).

1.2 Singularly perturbed equation

The steady state of the Cahn-Hilliard equation (1.1) shows that it is probably a singularly perturbed equation [70]. Equations of such type are known to be either strongly oscillatory or possess boundary, interior or inversion layers. As $\gamma \to 0$ (see equation (1.1)) they become very stiff and computationally expensive to be handled by classical methods. Here, we motivate the numerical study of the steady state CH equation via a well known second order differential equation. A general expression of a second order singularly perturbed boundary value problem is

$$\begin{aligned} &-\epsilon^2 u''(x) + a(x)u'(x) + b(x)u(x) = f(x),\ x \in (a,b), \\ &u(a) = \alpha,\ u(b) = \beta, \end{aligned} \tag{1.6}$$

where $0 < \epsilon \ll 1$. Analytical approximation of equation (1.6) has been the subject of many research activities (see for example [71, 88] and the references therein). Wollkind [88] compared the effectiveness of the method of matched asymptotic expansion and the multiple scale method in solving equation of type (1.6) when the coefficient of the diffusion term is positive and $a(x)$ is either only increasing or decreasing in the entire interval. They observed that the two methods yield valid asymptotic approximation. Many algebraic calculations are involved in the multiple scale method while the method of matched asymptotic expansion needs more terms for greater accuracy. He also observed that the method of matched asymptotic expansion is very useful when studying flows past a body at high Reynold's number

than the method of multiple scales. In fact, later, an asymptotic estimate was derived in [71] for the Reynold's equation. They also established existence and a uniformly valid asymptotic expansion following the matched asymptotic expansion method.

Here, our focus will be on the *Schrödinger* equation

$$\begin{cases} \epsilon^2 u''(x) + q(x)u(x) &= 0, \\ \epsilon u'(a) + \imath p u(a) &= 2\imath p, \quad \imath = \sqrt{-1}, \ p > 0, \\ \epsilon u'(b) &= \imath p u(b), \end{cases} \tag{1.7}$$

where $q(x) > 0$, $\epsilon \ll 1$. It has its relevance ranging from industrial purposes to domestic usage such as design of semiconductor appliances, resonant tunneling diodes, microwaves, in quantum and plasma physics, etc. Therefore, a lot of numerical analysis and simulations have been done on the system (1.7) based on finite difference (both classical and adaptive mesh), finite volume, finite element and Wentzel-Kramers-Brillouin (WKB) methods (see [8] and references therein). Two different iteration techniques for the numerical solution of the self-consistent Poisson-Schrödinger equation subject to Dirichlet boundary condition (with zero values at both ends) was suggested in [79]: the extrapolated-convergence-factor and the perturbation-iteration method. The advantage of the perturbation-iteration method over the extrapolated-convergence-factor method is its fast convergence even though it takes longer computing time per round. This model was employed by Inoue et al. [35] to determine the electronic states in a selectively doped double-heterojunction system. The system of equation was solved by the finite element method. Their observed electron concentration variation with gate voltage agreed with experiment. Later, a two-dimensional Schrödinger-Poisson equation was solved by Laux and Stern [47] by the finite difference method on a non uniform mesh using a conjugate gradient method. They employed a Lanczos iteration in order to tridiagonalize the Schrödinger equation and self-consistency is obtained by a damped Newton iteration using an approximate Jacobian matrix. Their aim was to determine the electron states under narrow gate in metal-oxide-silicon. They observed that the states for motion parallel to the silicon-oxide-silicon interface are more closely spaced than the state for motion perpendicular to the interface. The same equation was solved by the finite difference method on a uniform grid in [77] where Snider et al. determined the conduction band, electron states and electron concentration in quantum well wires. Their simulation agreed well with experiment for shallow mesa but not for deep mesa. Next, a finite difference scheme on a non-uniform grid was proposed for the one dimensional Schrödinger-Poisson equation in [83]. Their matrix transformation preserves symmetry, hence reduces computation time. They validated their result by comparing it with exactly calculated eigen-states of GaAs/AlGaAs rectangular wells. Another application of the Schrödinger equation is found in the resonant tunneling diodes. Equation (1.7) was solved subject to open boundary condition coupled with the Poisson equation (subject to Dirichlet boundary condition) in [68]. The authors achieved self-consistence and fast convergence by a Gumel approach. Later, Abdallah and Pinaud [1] improved on this result and were able to approximate the solution

of the Schrödinger-Poisson equation on a coarser grid. They accomplished this by discretizing the equation on a finite element space with WKB oscillating interpolation basis. This scheme was later analyzed in [59] for consistency and stability. Recently, another numerical scheme for the Schrödinger equation (1.7) subject to the open boundary condition was proposed and analysed in [8]. Their scheme based on a WKB-type transformation was able to filter out the dominant oscillations, and the reduced equation was then solved on a coarser grid with less computational cost.

Here, we will employ nonclassical finite volume schemes to approximate the Schrödinger equation.

1.3 Numerical approach

This section introduces the several numerical methods used in this work. Here we highlight the fractional split method, finite volume method and the NSFD method. All the schemes in this thesis were implemented via the MATLAB programming language.

1.3.1 Fractional Splitting

The fractional splitting method originates from Alternating Direction Implicit method (ADI) and the Local One Dimensional (LOD) method used by Peaceman and Rachford [66] and Douglas and Rachford [15]. Yanenko [90] later built on these methods and designed the fractional step method to solve problems in mathematical physics. This method was analyzed by Crandall and Majda [11] when applied to conservation laws in 2-D. Since then, it has been a very effective tool in solving incompressible Navier-Stokes equation [23, 67], nonlinear convection diffusion equations [31, 39, 40], the Kortewg de Vries (KdV) equation [30, 32], the thin film equation [91] and the Fisher equation [45]. The method simplifies the numerical analysis and computation of complicated differential equations. The complicated unsteady partial differential equation is split into simpler equations which may either be steady or unsteady partial or ordinary differential equations. These are solved sequentially within every time step until the final time of integration is reached. The method is always exact when dealing with linear equations while the order of accuracy may be reduced when employed to solve non linear equation. It is essential to note that the stability of each of the solver of the sub problems guarantees the stability of the entire scheme. The idea of the method is best illustrated using examples.

Example 1.1 *We want to show the accuracy of the fractional splitting method for the solution of the equation*

$$u_t + u_x - 2u_{xxxx} = 0,\ u(0,x) = g(x),\ x \in \mathbb{R}R,\ t > 0. \tag{1.8}$$

An exact solution of (1.8) is $g(x-t)\exp(2t)$. In order to apply the method of fractional splitting to this equation, we first split it into two subproblems that can be solved independently:

$$u_t + u_x = 0,\ u(0,x) = g(x), \tag{1.9}$$

$$w_t - 2w_{xxxx} = 0,\ w(0,x) = w_0(x). \tag{1.10}$$

The solution of (1.9) is $g(x-t)$, while that of the equation (1.10) is $w_0\exp(2t)$. Note that the fractional step method requires the initial data of the second subproblem to be the final solution of the first subproblem within that same time step. Hence, $w_0 = g(x-t)$ and therefore, the solution of the entire equation gives $g(x-t)\exp(2t)$ which just reproduces the exact solution of the equation (1.8).

We are interested in illustrating the general approach of fractional splitting method to linear equations. We pick linear equation just for the simplicity of presentation. We will consider the general equation

$$u_t = (\mathbf{A}+\mathbf{B})u, \tag{1.11}$$

where $\mathbf{A}$ and $\mathbf{B}$ are differential operators, for example $-\frac{\partial}{\partial x}$ and $\frac{\partial^4}{\partial x^4}$ as in (1.8). Given that $\mathbf{A}$ and $\mathbf{B}$ are time independent then

$$u_{tt} = (\mathbf{A}+\mathbf{B})u_t = (\mathbf{A}+\mathbf{B})^2 u.$$

For this case it is generally acceptable that [51]

$$u_t^j = (\mathbf{A}+\mathbf{B})^j u.$$

If the operators are time dependent then

$$u_{tt} = (\mathbf{A}_t+\mathbf{B}_t)u + (\mathbf{A}+\mathbf{B})u_t,$$

which leads to some other complications. If they are nonlinear operators, we can still appeal to Taylor's expansion to handle the higher derivatives as long as the solution is smooth. For equation (1.11)

$$\begin{aligned} u(x,\Delta t) &= u(x,0) + \Delta t u_t(x,0) + \frac{1}{2}\Delta t^2 u_{tt}(x,0) + \cdots \\ &= u(x,0) + \Delta t(\mathbf{A}+\mathbf{B})u(x,0) + \frac{1}{2}\Delta t^2(\mathbf{A}+\mathbf{B})^2 u(x,0) + \cdots \\ &= \left(I + \Delta t(\mathbf{A}+\mathbf{B})(I + \frac{1}{2}\Delta t(\mathbf{A}+\mathbf{B})) + \cdots\right) u(x,0) \\ &= \sum_{j=0}^{\infty} \frac{\Delta t^j}{j!}(\mathbf{A}+\mathbf{B})^j u(x,0). \end{aligned} \tag{1.12}$$

By the aid of Taylor's series this can be written as

$$u(x,\Delta t) = e^{\Delta t(\mathbf{A}+\mathbf{B})}u(x,0).$$

The operator $e^{\Delta t(\mathbf{A}+\mathbf{B})}$ is called the solution operator for the unsplit equation. For the fractional split method, following the same procedure we compute

$$u^*(x,\Delta t) = e^{\Delta t\mathbf{A}}u(x,0),$$

for problem (1.9) and

$$u^{**}(x,\Delta t) = e^{\Delta t\mathbf{B}}u^*(x,\Delta t),$$

for (1.10). This means that the solution through the fractional split method will be

$$u^{**}(x,\Delta t) = e^{\Delta t\mathbf{B}}e^{\Delta t\mathbf{A}}u(x,0).$$

Therefore, the splitting error is given by

$$u(x,\Delta t) - u^{**}(x,\Delta t) = (e^{\Delta t((\mathbf{A}+\mathbf{B}))} - e^{\Delta t\mathbf{B}}e^{\Delta t\mathbf{A}})u(x,0). \tag{1.13}$$

The second term in (1.13) is

$$\begin{aligned} e^{\Delta t\mathbf{B}}e^{\Delta t\mathbf{A}}u(x,0) &= (I+\Delta t\mathbf{B}+\frac{1}{2}\Delta t^2\mathbf{B}^2+\cdots)(I+\Delta t\mathbf{A}+\frac{1}{2}\Delta t^2\mathbf{A}^2+\cdots)u(x,0) \\ &= (I+\Delta t(\mathbf{A}+\mathbf{B})+\frac{\Delta t^2}{2}(\mathbf{A}^2+\mathbf{B}^2+2\mathbf{B}\mathbf{A})\cdots)u(x,0). \end{aligned} \tag{1.14}$$

We can easily see that the term $I+\Delta t(\mathbf{A}+\mathbf{B})$ agrees with the expansion in (1.12) while the term

$$\frac{1}{2}(\mathbf{A}^2+\mathbf{B}^2+2\mathbf{B}\mathbf{A}),$$

will only be the same as in (1.12) only if the operators $\mathbf{A}$ and $\mathbf{B}$ commute. When dealing with nonlinear operators or whenever the operators do not commute, the above scheme tends to reduce the order of accuracy in time by $O(\Delta T)$. We will quickly talk about some of the types of splitting we have. The two major types of splitting are

1. Godunov Splitting: This was introduced in the previous section and we have already ascertain that it is first order accurate unless the operators commute. We will discuss another type which is an improvement on this.

2. Strang Splitting: Instead of taking the solution operator of problem (1.9) over the entire time step, it is taken over half a time step and used as initial data for problem (1.10) which will be integrated over the entire time step and finally use as initial to solve the problem (1.9) again to be integrated over half a time step. We have the Taylor's expansion of the solution operator as

$$\begin{aligned} e^{\Delta t\frac{\mathbf{A}}{2}}e^{\Delta t\mathbf{B}}e^{\Delta t\frac{\mathbf{A}}{2}} &= (I+\frac{\Delta t}{2}\mathbf{A}+\frac{\Delta t^2}{8}\mathbf{A}^2+\cdots)(I+\Delta t\mathbf{B}+\frac{\Delta t^2}{2}\mathbf{B}^2+\cdots) \\ &\quad (I+\frac{\Delta t}{2}\mathbf{A}+\frac{\Delta t^2}{8}\mathbf{A}^2+\cdots) \\ &= I+\Delta t(\mathbf{A}+\mathbf{B})+\frac{\Delta t^2}{2}(\mathbf{A}^2+\mathbf{B}^2+\mathbf{A}\mathbf{B}+\mathbf{B}\mathbf{A})+O(\Delta t^3). \end{aligned} \tag{1.15}$$

From equation (1.15), one can see that the $O(\Delta t^2)$ is captured correctly as in (1.12). Hence, the Strang splitting scheme is second order accurate.

Remark 1.1 *When dealing with much complicated equations, it has been advised that the Godunov splitting is often sufficient [51]. Also, in the presence of rough solutions it was argued in [11] that the order of accuracy is always reduced to one no matter the type of splitting employed. This may be due to the fact that at the region of discontinuity, the order of accuracy always reduces to one [51].*

1.3.2 Finite volume method

The finite volume method, like the finite difference and the finite element methods, is a discretization method for differential equations. Unlike the finite difference method in which the equation is approximated at the grid points and the finite element method in which it is approximated element-wise, the finite volume approximation is evaluated at the intercell. The domain of integration is first subdivided into cells (finite volumes), then the approximation are evaluated at the intercell average. Therefore, the approximation is kept away from shock regions, since discontinuities that leads to shock occurs at grid points. Also, the flux entering each cell (finite volume) is identical to the flux leaving, then the flux in each cell is conserved. Hence, its application to conservation equations. Here, we will introduce this by applying it to hyperbolic conservation laws.

Example 1.2 *Consider the finite volume discretization of the hyperbolic equation*

$$u_t + f(u)_x = 0, \tag{1.16}$$

by the finite volume method.

The idea of finite volume follows the weak formulation. The domain of integration is subdivided into grid cells called finite volumes, say,

$$\mathcal{I}_j = [x_{j-\frac{1}{2}},\ x_{j+\frac{1}{2}}],\ \ j = 1, 2, 3, ..., m, \tag{1.17}$$

with interfaces $x_{j-\frac{1}{2}} = x_j - \frac{\Delta x}{2}$ and $x_{j+\frac{1}{2}} = x_j + \frac{\Delta x}{2}$, see Figure 1.1. m is the number of volumes and $\Delta x = x_{j+1} - x_j = x_{j+\frac{1}{2}} - x_{j-\frac{1}{2}}$ is the cell size on uniform grids. Here, $x_{\frac{1}{2}}$ and $x_{m+\frac{1}{2}}$ are the boundaries. We will always employ boundary conditions to handle ghost points where applicable. The integral formulation is approximated in each of the cells at the cell interfaces for one dimensional problems.

We will integrate the equation (1.16) over $\mathcal{I}_j$ with respect to x.

$$\frac{\partial}{\partial t}\int_{\mathcal{C}_j} u(x,t)dx + f(u(x_{j+\frac{1}{2}}),t) - f(u(x_{j-\frac{1}{2}}),t) = 0,$$

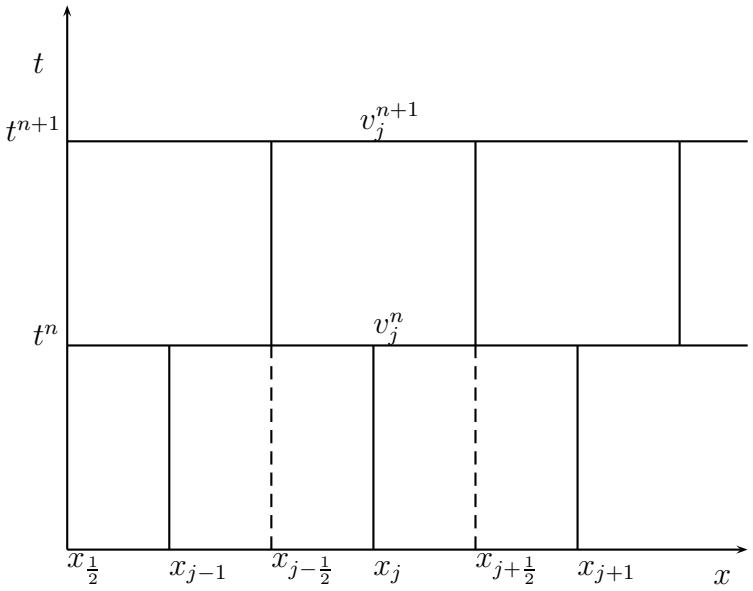

Figure 1.1: Finite volume domain discretization

integrating the above equation over time from t^n to t^{n+1} yields

$$\int_{\mathcal{C}_j} u(x,t^{n+1})dx - \int_{\mathcal{C}_j} u(x,t^n)dx = \int_{t^n}^{t^{n+1}} f(u(x_{j-\frac{1}{2}}),t) - \int_{t^n}^{t^{n+1}} f(u(x_{j+\frac{1}{2}}),t).$$

Dividing the above equation by Δx and letting the average

$$v_j^n = \frac{1}{\Delta x}\int_{\mathcal{C}_j} u(x,t^n)dx,$$

we have

$$v_j^{n+1} = v_j^n - \frac{1}{\Delta x}\left(\int_{t^n}^{t^{n+1}} f(u(x_{j+\frac{1}{2}}),t) - \int_{t^n}^{t^{n+1}} f(u(x_{j-\frac{1}{2}}),t)\right). \tag{1.18}$$

However, we can write this as

$$v_j^{n+1} = v_j^n - \frac{\Delta t}{\Delta x}\left(F_{j+\frac{1}{2}}^n - F_{j-\frac{1}{2}}^n\right), \tag{1.19}$$

where

$$F_{j+\frac{1}{2}} = \frac{1}{\Delta t}\int_{t^n}^{t^{n+1}} f(u(x_{j+\frac{1}{2}}),t),$$

is the numerical flux. The definition of this flux gives rise to many finite volume methods for approximating the solution of (1.16). We will discuss more on this in later chapters.

1.3.3 Nonstandard finite difference method

NSFD originates from the work of Mickens [57]. It has been employed to solve several differential models including singularly perturbed equations [53, 54]. We will adapt the NSFD procedure to design nonstandard finite volume schemes when solving some of the equations in order to preserve some physical and dynamical properties of the equation. To the best of our knowledge, this has not been employed to equations with complex solutions like the Schrödinger equation and higher order equations.

Example 1.3 *We will design a nonstandard finite difference scheme for the harmonic oscillator equation [57]*

$$\frac{d^2y}{dt^2} = -\lambda^2 y, \ \lambda \in \mathbb{R}. \tag{1.20}$$

The derivation is based on the two linearly independent solutions to (1.20), namely $y_1 = \exp(\imath\lambda t)$, $y_2 = \exp(-\imath\lambda t)$. The linear independence of y_1 and y_2 implies

$$\begin{vmatrix} y_j & e^{\imath\lambda\Delta tj} & e^{-\imath\lambda\Delta tj} \\ y_{j+1} & e^{\imath\lambda\Delta t(j+1)} & e^{-\imath\lambda\Delta t(j+1)} \\ y_{j+2} & e^{\imath\lambda\Delta t(j+2)} & e^{-\imath\lambda\Delta t(j+2)} \end{vmatrix} = 0. \tag{1.21}$$

The determinant in equation (1.21) leads to the difference equation

$$y_{j+2} - 2y_{j+1}\cos(\lambda\Delta t) + y_j = 0. \tag{1.22}$$

Employing the trigonometric identity $\cos(\theta) = 1 - 2\sin^2(\frac{\theta}{2})$ and shifting the index j simplifies (1.22) to

$$y_{j+1} - 2y_j + 4y_j \sin^2\left(\frac{\lambda\Delta t}{2}\right) + y_{j-1} = 0.$$

Finally, we have the exact finite difference scheme

$$\frac{y_{j+1} - 2y_j + y_{j-1}}{\frac{4}{\lambda^2}\sin^2\left(\frac{\lambda\Delta t}{2}\right)} + \lambda^2 y_j = 0. \tag{1.23}$$

Equation (1.23) is an exact nonstandard finite difference scheme for the harmonic oscillator equation (1.20). This method shall be adapted to the finite volume space in this thesis.

1.4 Thesis outline

This thesis is divided into self-contained papers that represent specific scientific contributions.

- In Chapter 2, we design finite volume schemes for fourth order equations: the Kuramoto-Sivashinsky and the (convective) Cahn-Hilliard equations. The fractional splitting

method is employed to split the linear higher order terms from the nonlinear lower order terms. We employ shock capturing schemes for the nonlinear hyperbolic sub-equations; design A-stable schemes for the fourth order equation and a $\theta-$ scheme for the nonlinear diffusion equation. This way, we are able to resolve the restrictive stability condition, $\Delta t \sim O(\Delta x^4)$, common to most explicit schemes and the stiffness imposed by the coupling of the linear and the nonlinear terms. The physical behaviour of these models are all verified numerically.

This is the first time these two equations will be investigated by the fractional splitting method. The results in this chapter are the subject of the papers [2, 3]. The presence of the small parameter in the Cahn-Hilliard equation led us to the study of singularly perturbed equations. This is the subject of the succeeding chapters.

- Chapter 3 is devoted to the study of singularly perturbed differential equations with a special interest on the Schrödinger equation. The presence of the reduced Planck's constant, the oscillatory behaviour of its solution and the complex boundary conditions makes its simulation challenging. Here, two different uniformly convergent finite volume schemes were designed for this equation. These schemes, semi-analytical scheme based on perturbation analysis and the nonstandard finite volume scheme proved efficient in resolving the challenges stated earlier. Their efficiency were shown through a series of computation.

  This is the first time nonclassical schemes of this type are being applied to the Schrödinger equation and we are able to design exact schemes for the complex dependent boundary conditions. Some of our observations are subject of [4] while our major results are being prepared for submission.

- In Chapter 4, we design finite volume scheme for the Kuramoto-Sivashinsky equation and the Cahn-Hilliard equation. The schemes enjoy several properties which include preserving the properties of the original equation. Each of the sub-equations is approximated by nonstandard finite volume schemes. The significance of this work includes the reliability of the scheme in handling the small parameter. We also verified all the properties tested for in Chapter 2.

  The importance of this includes the construction of a nonstandard finite volume scheme for the fourth order partial differential equation. Our observations are being prepared for submission.

- The last chapter is dedicated to discussion, conclusions on and possible further research work.

Chapter 2

Fractional splitting method for higher order differential equations

In this chapter, we implement finite volume schemes to solve the 1-dimensional Kuramoto-Sivashinsky equation and the Cahn-Hilliard equation. We design operator splitting algorithm to resolve the restrictive stability condition ($\Delta t \sim O(\Delta x^4)$) imposed by the coupling of the linear and the nonlinear terms. Our results on the K-S equation have been published in Aderogba et al. [2] while our results on the CH equation [3] will soon appear in Engineering Computations.

2.1 Introduction

We design operator splitting based finite volume schemes to solve some fourth order unsteady partial differential equations. The operator splitting method is used in order to simplify the computation of the solution of these nonlinear equations. We apply the schemes to approximate the Kuramoto-Sivashinsky (K-S) equation and the Cahn-Hilliard (CH) equation.

The first equation under investigation in this chapter is the K-S equation (2.1),

$$\begin{cases} u_t + uu_x + \alpha u_{xx} + \gamma u_{xxxx} = 0, \quad \forall\ (x,t) \in \mathbb{R} \times (0,\infty), \\ u(x,0) = u_0(x). \end{cases} \tag{2.1}$$

Unless otherwise stated, the initial condition $u_0(x)$ is considered to be a L-periodic function with zero average, that is

$$u_0(x+L) = u_0(x) \quad \text{and} \quad \int_0^L u_0(x)dx = 0. \tag{2.2}$$

Our focus is to implement finite volume scheme to solve equation (2.1). This is the object of discussion in Section 2.3.4. This method allows us to treat the nonlinear hyperbolic term

with optimal shock capturing schemes explicitly while the linear terms are approximated by the backward differentiation formula. Consequently, our results validate all the physical properties of this model: the existence of regular and oscillatory shock achieved through the traveling wave solution, the chaotic behaviour of the solution and the bound on the energy.

We also examined the convective Cahn-Hilliard equation (cCH)

$$u_t + \gamma^2 u_{xxxx} = \phi(u)_{xx} + \delta u u_x, \quad x \in \Omega,\ 0 < t, \tag{2.3}$$

where $\Omega \in (a, L)$ and

$$\phi(u) = \alpha u^3 - u, \ \ \alpha > 0,$$

which has been a successful model of phase transition observed in alloys, glasses, polymer solution and binary liquid mixtures (see for example [18, 19, 62], and the references therein).

Our numerical approach for these equations through the fractional time splitting method is discussed in Section 2.2 where we introduce the shock preserving schemes for the nonlinear hyperbolic term, the θ-method for the nonlinear diffusion term and the schemes for the linear fourth order term. Section 2.3.4 is dedicated to the analysis of the K-S equation while we study the CH equation in Section 2.3.5 and 2.3.6 and discuss our observations in Section 2.4.

2.2 Numerical approach

We will employ the fractional time-splitting method to solve our desired equations. From an abstract point of view, suppose we are dealing with a differential equation

$$u_t + \mathcal{A}(u) = 0,$$

and the operator $\mathcal{A}(u)$ is decomposable to either $\mathcal{H}(u) + \mathcal{N}(u) + \mathcal{L}(u)$ or $\mathcal{H}(u) + \mathcal{L}(u)$, the space discretized problem can be written as:

$$\begin{cases} u_t + \mathcal{H}(u) + \mathcal{N}(u) + \mathcal{L}(u) = 0, \\ u(0) = u_0, \end{cases} \tag{2.4}$$

or

$$\begin{cases} u_t + \mathcal{H}(u) + \mathcal{L}(u) = 0, \\ u(0) = u_0, \end{cases} \tag{2.5}$$

where $\mathcal{H}$ is the discretization of the nonlinear (convection) operator, $\mathcal{N}$ is the discretization of the nonlinear diffusion operator and $\mathcal{L}$ is the discretization of the linear operator. Apart from the fact that the fractional step method substantially reduces computational time, it has the advantage of simplifying a complex process efficiently. This method permits the treatment of each segment of the original equation separately, thus

$$\begin{cases} u_t + \mathcal{H}(u) = 0, \\ u(0) = u_0, \end{cases} \tag{2.6}$$

$$\begin{cases} w_t + \mathcal{N}(w) = 0, \\ w(0) = w_0, \end{cases} \tag{2.7}$$

and

$$\begin{cases} y_t + \mathcal{L}(y) = 0, \\ y(0) = y_0. \end{cases} \tag{2.8}$$

Let $H_t u_0$, $N_t u_0$ and $L_t u_0$ describe the approximate numerical solution operators for each of the split models (2.6), (2.7) and (2.8) respectively. We will use the first order scheme based on Marchuk splitting which can be written as $v^0 = u_0$ for $n = 0$; and for $n > 0$, we obtain v^{n+1} from v^n via the solution of

$$v_k(x, nk) = [L_k \circ N_k \circ H_k]^n v_0(x), \tag{2.9}$$

or

$$v_k(x, nk) = [L_k \circ H_k]^n v_0(x), \tag{2.10}$$

for some time step $\Delta t = k$, where the notation $\circ$ denotes the composition of two operators [30] and n denotes the time discretization step. Our splitting scheme will follow this algorithm throughout this work. This algorithm can be explained as below

1. We initialise the solution via $v^0 = u_0(x_j)$ for $j = 0, 1, 2, 3, \cdots, m$ i.e., $m+1$ grid points.
2. For $n > 0$, we compute the intermediate solution H_k, from the advection equation.
3. Within the same time step, we use the solution from Step 2 to compute the solution of the nonlinear equation to obtain N_k.
4. Within the same time step, we use the solution from Step 3 to compute the solution of the linear equation to obtain L_k.
5. We use the solution from Step 4 in Step 1 to initialise the next time step.
6. We repeat until the final computational time.

Remark 2.1 *The boundary conditions of each of the subproblems were corrected to first order accuracy in time following a similar procedure in [42], and the references therein.*

Remark 2.2 *In the case where the original equation has only two discretized operator, there will only be two split equations and hence only two solution operators. Consequently, one of the steps 3 and 4 will not be essential in the described algorithm above.*

In the succeeding sections, we will describe the numerical solution operators that will be employed in our numerical experiments.

2.2.1 Schemes for the hyperbolic equations (2.6)

The design of finite volume numerical schemes for equations of type

$$u_t + f(u)_x = 0, \tag{2.11}$$

has been introduced earlier on. It is noteworthy that the robustness of existing schemes on equations of this type is embedded in the way the numerical fluxes are handled and the temporal order of convergence. In this work, we employed

1. Godunov scheme
2. The non-staggered scheme (NSTG), [5, 81]
3. Semi-discrete scheme (SemiD)
4. Fully discrete (FD), [82]
5. Weighted essentially non-oscillatory scheme (WENO), [72, 73]
6. Implicit schemes

It is worth mentioning here that apart from the implicit schemes, all the schemes listed above are total variation diminishing (TVD), monotonicity preserving and conservative.

Remark 2.3 *A TVD scheme is one in which* $TV(v^{n+1}) \leq TV(v^n)$ *where TV(u) is the total variation of the function, u. This type of scheme preserves monotonicity and guarantees the absence of spurious oscillation in our numerical simulations.*

We will briefly outline these schemes.

2.2.1.1 Godunov scheme

Godunov methods, founded by Godunov (1959), rely on the solution of the Riemann problem. The basic version of the scheme is only first order accurate but by updating the reconstruction process with the introduction of slope limiters, there is a possibility of extending this to higher order. Since the flux is convex, the application is direct. The intercell average at the interface $x_{j+1/2}$ is given as

$$v_j^n = \frac{1}{\Delta x} \int_{x_{j-\frac{1}{2}}}^{x_{j+\frac{1}{2}}} u(x, t^n) dx, \tag{2.12}$$

and the numerical flux is

$$f(u_{j+1/2}^n) \simeq f(v_j^n) + \frac{h}{2} f'(v_j^n) \left(1 - f'(v_j^n) \frac{\Delta t}{h}\right) \sigma_j^n,$$

where σ_j^n is a slope limiter and $h = \Delta x = x_{j+\frac{1}{2}} - x_{j-\frac{1}{2}}$ is the space width. Several limiters are documented in the literature, but throughout this thesis we will employ the monotonized centered (MC) limiter, which is given as

$$\sigma(j) = \text{minmod}\left(2\frac{v_{j+1} - v_j}{h}, \frac{v_{j+1} - v_{j-1}}{2h}, 2\frac{v_j - v_{j-1}}{h}\right).$$

The minmod function compares the absolute value of the arguments and returns the one with minimum absolute value as the slope. If $\sigma_j^n = 0$, the scheme will switch to the basic first order Godunov scheme. For more information on limiters and the Godunov scheme, the reader can consult [51, 84, 91] among others.

2.2.1.2 Non staggered central difference scheme

The non staggered central difference scheme (NSTG) is a second order extension of the non staggered version of the central difference scheme by Lax-Friedrich (see for example [81, 82]). It follows a process of reconstruction, evolution and projection step and takes an easily implemented predictor-corrector form,

$$v_j^{n+1/2} = v_j^n - \frac{\lambda f_j'}{2}, \tag{2.13}$$

$$v_j^{n+1} = \frac{1}{2}\left(v_{j+1}^n + v_{j-1}^n\right) + \frac{1}{4}\left(v_{j-1}'^n - v_{j+1}'^n\right) - \frac{\lambda}{2}\left(f(v_{j+1}^{n+1/2}) - f(v_{j-1}^{n+1/2})\right), \tag{2.14}$$

where $\lambda = \frac{k}{h}$ is the CFL number. Furthermore, the non oscillatory behavior of this second order scheme is guaranteed by the choice

$$v_j' = \text{minmod}\left(\Delta v_{j+1/2}, \Delta v_{j-1/2}\right),$$

and

$$f_j' = a(v_j)v_j',$$

where $a(v_j)$ is the derivative of the flux function with respect to the argument v_j which should be interpreted as the Jacobian when dealing with systems of conservation laws.

2.2.1.3 Semi discrete central-upwind scheme

The second order semi-discrete central (SemiD) difference scheme (see [5, 6, 82]) in the conservative form is given by

$$[v_j]_t = -\frac{F_{j+1/2} - F_{j-1/2}}{h}, \tag{2.15}$$

with the numerical flux

$$F_{j+1/2} = \frac{f(v_{j+1/2}^+) + f(v_{j+1/2}^-)}{2} - \frac{a_{j+1/2}}{2}(v_{j+1/2}^+ - v_{j+1/2}^-), \tag{2.16}$$

where the intermediate values $v^{\pm}_{j+1/2}$ are given by

$$v^{+}_{j+1/2} = v_{j+1} - \frac{h}{2}(u_x)_{j+1},$$
$$v^{-}_{j+1/2} = v_{j} + \frac{h}{2}(u_x)_{j},$$

and the $a_{j+1/2}$ term is the maximal local speed given in the generic case as

$$a_{j+1/2} = \max\left[\rho\left(\frac{\partial f}{\partial u}(v^{+}_{j+1/2})\right), \rho\left(\frac{\partial f}{\partial u}(v^{-}_{j+1/2})\right)\right].$$

In the scalar case with convex flux the maximal local speed simplifies to

$$a_{j+1/2} = \max(|f'(v^{-}_{j+1/2})|, |f'(v^{+}_{j+1/2})|).$$

Also, the slope $(u_x)_j$ is given by the minmod function

$$(u_x)_j = \text{minmod}\left(\frac{v_{j+1} - v_j}{h}, \frac{v_j - v_{j-1}}{h}\right),$$

and the time derivative in (2.15) is evaluated by the Euler's scheme.

2.2.1.4 Weighted Essentially Non-Oscillatory Scheme

The scheme presented here follows the work of [72]. The hyperbolic conservation law (2.11) can be cast into the semi-discrete form as

$$\frac{dv_j}{dt} = \mathcal{A}(v_j), \tag{2.17}$$

where

$$\mathcal{A}(v_j) = -\frac{f_{j+1/2} - f_{j-1/2}}{h}. \tag{2.18}$$

The left hand side of the equation (2.17) will be handled by the third order Total Variation Diminishing Runge-Kutta scheme as developed in [73]:

$$\begin{aligned} u^1 &= v^n + \Delta t\mathcal{A}(v^n), \\ u^2 &= \frac{3}{4}v^n + \frac{1}{4}u^1 + \frac{1}{4}\Delta t\mathcal{A}(u^1), \\ v^{n+1} &= \frac{1}{3}v^n + \frac{2}{3}u^2 + \frac{2}{3}\Delta t\mathcal{A}(u^2). \end{aligned} \tag{2.19}$$

The discretized flux terms $f_{j\pm1/2}$ are given as

$$f_{j\pm1/2} = g(v^{-}_{j\pm1/2}, v^{+}_{j\pm1/2}),$$

where

$$g(a,b) = \frac{1}{2}\left(f(a) + f(b) - \alpha(b-a)\right), \tag{2.20}$$

is the Lax-Friedrich monotone flux and $\alpha = \max_u |f'(u)|$ is a constant. The maximum is taken over the relevant range of u. The values of $v^-_{j+1/2}$ and $v^+_{j-1/2}$ are computed through the intercell average of the conserved variable u given in equation (2.12).

$$v^-_{j+1/2} = \sum_{r=0}^{l-1} \omega_r v^r_{j+1/2}, \;\; v^r_{j+1/2} = \sum_{i=0}^{l-1} c_{ri} v_{j-r+i},$$

and

$$v^+_{j-1/2} = \sum_{r=0}^{l-1} \tilde{\omega}_r v^r_{j-1/2}, \;\; v^r_{j-1/2} = \sum_{i=0}^{l-1} \tilde{c}_{ri} v_{j-r+i},$$

where $r = 0, ..., l-1$. The linear weights

$$\omega_r = \frac{\alpha_r}{\sum_{s=0}^{l-1} \alpha_s}, \;\; \alpha_r = \frac{d_r}{(\epsilon + \beta_r)^2},$$

and

$$\tilde{\omega}_r = \frac{\tilde{\alpha}_r}{\sum_{s=0}^{l-1} \tilde{\alpha}_s}, \;\; \tilde{\alpha}_r = \frac{\tilde{d}_r}{(\epsilon + \beta_r)^2},$$

where $\epsilon = 10^{-6}$, β_r are smooth indicators and $\tilde{d}_r = d_{l-1-r}$ are constants. The order of accuracy is $2l-1$. We use $l = 2$ in our computations, consequently, we only need $d_0 = 2/3$ and $d_1 = 1/3$. The values of constants $\tilde{c}_{ri} = c_{r-1,i}$ are given in Table 2.1 as extracted from [72]. Also, the smooth indicators are given as

$$\beta_0 = (v_{j+1} - v_j)^2, \;\; \beta_1 = (v_j - v_{j-1})^2.$$

Table 2.1: The values of c_{ri}

r	$i = 0$	$i = 1$
-1	1.5	-0.5
0	0.5	0.5
1	-0.5	1.5

2.2.1.5 Fully discrete scheme

The fully discrete scheme for the convective equation (2.11) is given by [5]

$$(u)^{n+1}_j = \frac{1}{h} \int_{x_{j-1/2}}^{x_{j+1/2}} \tilde{w}(\xi, t^{n+1}) d\xi = \lambda a^n_{j-1/2} w^{n+1}_{j-1/2} + \left(1 - \lambda(a^n_{j-1/2} + a^n_{j+1/2})\right) w^{n+1}_j$$

$$+ \lambda a^n_{j+1/2} w^{n+1}_{j+1/2} + \frac{h}{2} \left((\lambda a^n_{j-1/2})^2 (u_x)^{n+1}_{j-1/2} - (\lambda a^n_{j+1/2})^2 (u_x)^{n+1}_{j+1/2} \right), \qquad (2.21)$$

and

$$(u_x)^{n+1}_{j+1/2} = \frac{2}{h}\text{minmod}\left(\frac{w^{n+1}_{j+1} - w^{n+1}_{j+1/2}}{1+\lambda(a^n_{j+1/2} - a^n_{j+3/2})}, \frac{w^{n+1}_{j+1/2} - w^{n+1}_{j}}{1+\lambda(a^n_{j+1/2} - a^n_{j-1/2})}\right),$$

$$w^{n+1}_{j+1/2} = \frac{u^n_j + u^n_{j+1}}{2} + \frac{h - a^n_{j+1/2}\Delta t}{4}((u_x)^n_j - (u_x)^n_{j+1}) - \frac{1}{2a^n_{j+1/2}}\left(f(u^{n+1/2}_{j+1/2,r}) - f(u^{n+1/2}_{j+1/2,l})\right),$$

$$w^{n+1}_j = u^n_j + \frac{\Delta t}{2}(a^n_{j-1/2} - a^n_{j+1/2})(u_x)^n_j - \frac{\lambda}{1-\lambda(a^n_{j-1/2} + a^n_{j+1/2})}\left(f(u^{n+1/2}_{j+1/2,l}) - f(u^{n+1/2}_{j-1/2,r})\right),$$

with

$$u^{n+1/2}_{j+1/2,l} = u^n_{j+1/2,l} - \frac{\Delta t}{2}f(u^n_{j+1/2,l})_x, \quad u^n_{j+1/2,l} = u^n_j + h(u_x)^n_j\left(\frac{1}{2} - \lambda a^n_{j+1/2}\right),$$

$$u^{n+1/2}_{j+1/2,r} = u^n_{j+1/2,r} - \frac{\Delta t}{2}f(u^n_{j+1/2,r})_x, \quad u^n_{j+1/2,r} = u^n_{j+1} - h(u_x)^n_{j+1}\left(\frac{1}{2} - \lambda a^n_{j+1/2}\right).$$

The local speed of propagation is

$$a^n_{j+1/2} = \max\left[\rho\left(\frac{\partial f}{\partial u}(u^-_{j+1/2})\right), \rho\left(\frac{\partial f}{\partial u}(u^+_{j+1/2})\right)\right],$$

where ρ is the spectral radius,

$$u^+_{j+1/2} = u^n_{j+1} - \frac{h}{2}(u_x)^n_{j+1}, \quad u^-_{j+1/2} = u^n_j + \frac{h}{2}(u_x)^n_j,$$

and

$$(u_x)^n_j = \text{minmod}(\frac{u^n_j - u^n_{j-1}}{h}, \frac{u^n_{j+1} - u^n_j}{h}),$$

with

$$\text{minmod}(a,b) = \frac{\text{sgn}(a) + \text{sgn}(b)}{2}\min(|a|,|b|).$$

Remark 2.4 *It is worth mentioning at this point that the convergence of the above schemes for the convection equation has been documented in the literature as quadratic (see [5, 6, 51, 81, 91] for example). Throughout, we choose the CFL number to be less than* 1*, which is within the stability requirement of all the schemes considered.*

2.2.1.6 Implicit schemes

When the intercell time average is

$$f(u^n_{j+1/2}) \simeq \frac{1}{2}((1-\theta)(f(v^n_j) + f(v^n_{j+1})) + \theta(f(v^{n+1}_j) + f(v^{n+1}_{j+1}))),$$

then the corresponding numerical scheme

$$v^{n+1}_j = v^n_j - \frac{\Delta t}{2h}((1-\theta)(f(v^n_{j+1}) - f(v^n_{j-1})) + \theta(f(v^{n+1}_{j+1}) - f(v^{n+1}_{j-1})), \tag{2.22}$$

is either fully implicit ($\theta = 1$) or Crank-Nicolson ($\theta = 0.5$).

2.2.2 Schemes for the nonlinear diffusion equation

In this section, we implement finite volume schemes for a nonlinear diffusion equation. We solve the nonlinear diffusion equation explicitly and implicitly by considering a conservative scheme in which case the equation is written as

$$u_t = \alpha(u^3)_{xx}. \tag{2.23}$$

We discretized (2.23) using the θ-method to give

$$v_j^{n+1} = v_j^n + r\left(\theta[\phi_{j+1}^{n+1} - 2\phi_j^{n+1} + \phi_{j-1}^{n+1}] + (1-\theta)[\phi_{j+1}^n - 2\phi_j^n + \phi_{j-1}^n]\right), \tag{2.24}$$

where $\phi_j^n = (v_j^n)^3$, $r = \frac{k}{h^2}$ and v_j^n is the intercell averages. For the purpose of comparison, we also solve (2.23) with second order non conservative schemes, in which case the equation is re-written as

$$u_t = \alpha(\varphi u_x)_x, \tag{2.25}$$

where $\varphi = 3u^2$. Similarly, this is discretized using the θ method to give

$$\begin{aligned} v_j^{n+1} = v_j^n + r\theta\left(\varphi_{j+1/2}^{n+1}[v_{j+1}^{n+1} - v_j^{n+1}] - \varphi_{j-1/2}^{n+1}[v_j^{n+1} - v_{j-1}^{n+1}]\right) + \\ r(1-\theta)\left(\varphi_{j+1/2}^{n}[v_{j+1}^{n} - v_j^{n}] - \varphi_{j-1/2}^{n}[v_j^{n} - v_{j-1}^{n}]\right), \end{aligned} \tag{2.26}$$

where

$$\varphi_{j\pm1/2} = \frac{\varphi_{j\pm1} + \varphi_j}{2},$$

and θ is a weighting factor. The schemes (2.24) and (2.26) will be fully implicit if $\theta = 1$, Crank-Nicolson if $\theta = 0.5$ and fully explicit when $\theta = 0$. The explicit schemes result in a system of linear equations while the implicit schemes give a system of nonlinear equations. While the linear equations can be solved directly, the nonlinear equations are solved by the iterative Newton-Raphson method. Coupled with the corresponding second order boundary conditions, the expected rate of convergence is 2 for all these schemes.

2.2.3 Schemes for the linear (diffusion) equation

In this section, we consider three different schemes for the numerical solution of the linear subproblem

$$u_t + u_{xx} + \gamma^2 u_{xxxx} = 0. \tag{2.27}$$

Via the θ-scheme, we consider the implicit schemes in the following form

$$v_j^{n+1} + \theta F_j^{n+1} = v_j^n - (1-\theta)F_j^n, \;\; j = 1, 2, \cdots, m-1, \tag{2.28}$$

where

$$F_j^n = r(v_{j-1}^n - 2v_j^n + v_{j+1}^n) + \mu(v_{j-2}^n - 4v_{j-1}^n + 6v_j^n - 4v_{j+1}^n + v_{j+2}^n),$$

$\mu = \gamma^2 \frac{k}{h^4}$ and $r = \frac{k}{h^2}$. The scheme is fully implicit if $\theta = 1$ and Crank-Nicolson (C-N) if $\theta = 0.5$. We have chosen not to include the explicit scheme ($\theta = 0$) in the analysis because of its restrictive stability condition which requires a time step of $\mathcal{O}(h^4)$. Scheme (2.28) obviously include ghost nodes which are eliminated via the boundary conditions. This will be explained later in this chapter.

We will also consider the backward differentiation formula (BDF2) in the form

$$3v_j^n + 2F_j^n = 4v_j^{n-1} - v_j^{n-2}, \quad n = 2, 3, 4, 5, \cdots, \tag{2.29}$$

where the backward Euler scheme

$$v_j^n = v_j^{n-1} + F_j^n,$$

is used for the $n = 1$ time step and F_j^n is as given above.

Lastly, we employ the Diagonally Implicit Runge-Kutta (DIRK) scheme which is given as

$$v_j^* = v_j^{n-1} - \frac{1}{2}F_j^*,$$
$$v_j^n = v_j^{n-1} - F_j^*.$$

For periodic boundary conditons, we will also solve the linear equation using the `Matlab` built-in `fft-solver` to serve as a benchmark for the other schemes.

2.3 Numerical experiments

In this section we apply each of the numerical schemes discussed in Section 2.2 to specific examples in order to validate their effectiveness.

2.3.1 Hyperbolic equation

In this Section, we apply and compare the performance of the schemes listed in Section 2.2.1 in approximating the inviscid Burgers equations.

Example 2.1 *Here we solve the following convection problem,*

$$\begin{cases} u_t + uu_x = 0, \quad \forall\ (x,t) \in (0,L) \times (0,T], \\ u(0,x) = 0.5 + \sin(x)\,, \end{cases} \tag{2.30}$$

with periodic initial and boundary conditions.

Solution to the convection term preserves the average energy density until the formation of the shock [24]. The profiles of $\mathcal{E}(t)$ in Figure 2.1 show the conservation of $\mathcal{E}(t)$ before the development of shock. This is a generic behaviour of the solution of hyperbolic equations.

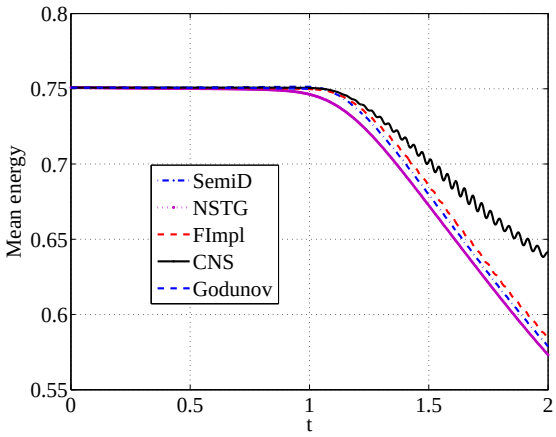

Figure 2.1: Mean energy density profiles for problem (2.30).

Giacomelli and Otto [24] also claimed that the convection term preserves the mean energy density before the onset of shock. This is confirmed by all the schemes through Figure 2.1. These profiles also show that the shock develops at about time $T = 1$ except for the Godunov scheme. The semi-discrete central and the implicit schemes agreed with the approximation of time of shock development while the non-staggered central scheme depict shock as setting in a little earlier before $T = 1$. These all agree with the assertion in [5]. The down-hill sawtooth behavior of the mean energy after the shock in the implicit schemes (which is more pronounced in the Crank-Nicolson scheme) may be due to oscillation about the shock region as observed in the earlier work of Yong-Jung et al. [91]. Moreover, it is note worthy that out of all the schemes, the mean energy climbs uphill after the shock only in the Godunov scheme. Thus from here forthwith, we will drop the simulations based on the Godunov scheme because of its poor performance.

2.3.2 Nonlinear diffusion equation

Here we consider the following example.

Example 2.2 *Solve*

$$\begin{cases} u_t - (u^3)_{xx} = f(x), \ x \in [0, \pi], \\ u(0,t) = u(\pi,t) = 0, \\ u(x,0) = \sin(x), \end{cases} \tag{2.31}$$

where $f(x) = -\frac{3}{4}[3\sin 3x - \sin x]$, to test the effectiveness of schemes (2.24) and (2.26). We compare our results with the exact steady state solution $u(x,t) = \sin(x)$ at time $T = 0.5$. The $\infty - norm$ error, $e(m_j)$, for different number of grid points, m_j, were computed and the convergent rates, p, were calculated based on the relation

$$p = \frac{\log(e(m_2)/e(m_1))}{\log(m_2/m_1)}. \tag{2.32}$$

The errors and the convergent rates due to each of the scheme are given in Table 2.2 for different grid points. It is obvious that all the schemes are equally good.

Table 2.2: Convergence rate of the schemes for the nonlinear equation (2.48)

Grid points	L^∞ error$\times 10^{-3}$ (p) at T = 0.5			
	Conservative		Non Conservative Schemes	
	CN	Explicit	CN	Explicit
20	18.1	18.2	23.0	20.0
40	6.34 (1.46)	6.39 (1.46)	7.86 (1.49)	7.30 (1.50)
80	2.03 (1.62)	2.02 (1.63)	2.50 (1.63)	2.39 (1.64)
160	0.58 (1.78)	0.58 (1.78)	0.72 (1.78)	0.70 (1.78)

Remark 2.1 *We highlight here that it is not necessary to determine the convergence through other norms. This guaranteed by the equivalence of all norms in* $\mathbb{R}^d$ *[52].*

2.3.3 Linear diffusion equation

For finite domains, the boundary conditions are either periodic or non periodic. For the non-periodic case we have nonhomogeneous Dirichlet and Neumann boundary conditions as follows

$$u(0,t) = g(0,t), \quad u_x(0,t) = g_x(0,t), \quad u(L,t) = g(L,t), \quad u_x(L,t) = g_x(L,t),$$

where $g(x,t)$ is a known function related to the exact solution. In particular, we introduce ghost nodes, v_{-1}^n and v_{m+1}^n, which are eliminated using the following discretization,

$$v_0^n = g_0^n, \quad \frac{-3v_{-1}^n + 4v_0^n - v_1^n}{2h} + O(h^2) = g_x(0,t), \tag{2.33}$$

and

$$v_m^n = g_m^n, \quad \frac{v_{m-1}^n - 4v_m^n + 3v_{m+1}^n}{2h} + O(h^2) = g_x(L,t), \tag{2.34}$$

respectively.

Example 2.3 *We solve*

$$\begin{cases} u_t + u_{xx} + \gamma^2 u_{xxxx} = 0, & \forall\ t \in (0,T], \\ u(x,0) = \Phi(x), \end{cases} \tag{2.35}$$

subject to periodic boundary condition.

Grid points	L^∞ error$\times 10^4$ at T = 1			
	CNS	Spectral	BDF2	DIRK
20	74.4087	1516.61	74.4253	81.1000
40	19.1106	773.780	19.1108	19.4500
80	5.02760	390.024	5.02761	4.8850
160	1.28539	195.709	1.28539	1.6900

Table 2.3: Error due to each scheme for the numerical approximation of the linear equation.

We compare the numerical approximations by each of the scheme discussed in Section 2.2.3 to the exact solution $u(x,t) = \sin\left(\frac{x}{\gamma}\right)$ and compute the $\|\cdot\|_\infty$ error. These are shown in Table 2.3. This computation is done with $\Phi(x) = \sin\left(\frac{x}{\gamma}\right)$.

It is claimed, see for example [24], that the energy density for this diffusion equation grows exponentially. We validate this claim by considering Example 2.3 with different initial conditions.

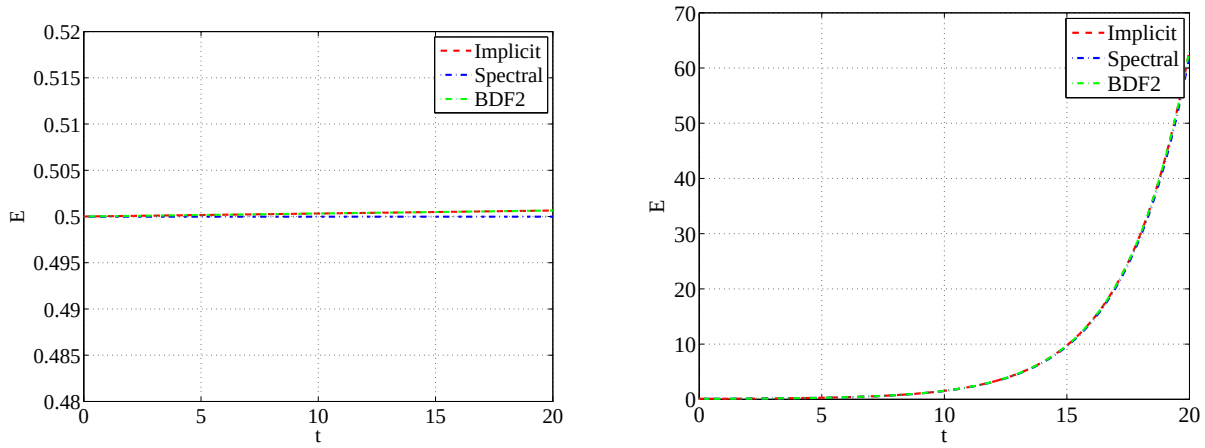

(a) $\Phi(x) = \sin(x)$ (b) $\Phi(x) = e^{-x^2}$

Figure 2.2: Mean energy density profile for the diffusion term for $T = 20$, $\gamma = 1$ and (a) $x \in [0, 2\pi]$ and (b) $x \in [-2\pi, 2\pi]$.

The growth of the mean energy of the diffusion equation as shown in Figure 2.2(b) agrees with the earlier observations (see [24] and the references therein). No growth is expected when the initial condition is a periodic exact steady state solution of the problem as was shown in Figure 2.2(a).

From here forthwith, the convection term is solved by any of the above mentioned schemes while the diffusion term is solved by the BDF2 scheme (for K-S equation) or DIRK scheme (for CH equation). The C-N scheme was dropped basically because of the stiffness of the problem under consideration. Hence, we will refer to the method of solution of the K-S equation by the scheme used to handle the convection term. In all the schemes we will

choose 320 grid points.

2.3.4 Kuramoto-Sivashinsky equation

In this Section, we will consider equation (2.1). The split scheme used here is motivated by observing that the K-S equation consists of two different spatial operators: the linear and the nonlinear operators. Interestingly, the nonlinear operator is hyperbolic, i.e., it is known to introduce discontinuity in finite time while the linear fourth order term has a stabilizing effect. Therefore, it is advantageous to split the equation into the nonlinear and the linear equations for easy treatment. Hence, we split equation (2.1) into the following two partial differential models

$$u_t + uu_x = 0, \tag{2.36}$$

and

$$u_t + \alpha\ u_{xx} + \gamma^2\ u_{xxxx} = 0. \tag{2.37}$$

It is noteworthy at this point that while (2.37) accounts for the long wave instability (gain) the equation (2.36) accounts for short wave dissipation. Consequently, the equation is split into two physical processes evident in the equation: the convection (inviscid Burgers) equation and the linear fourth order equation. Each of the equations is solved numerically using finite volume method [50] in such a way as to preserve some qualitative properties of the solutions related to each continuous problem.

Our aim in this work is to present reliable and efficient solution approach and, in the process, numerically validate some of the theoretical results of the K-S equation documented in the literature. We verify the results stated above on the bound of the solution, preservation of the periodicity and zero average as observed in [24].

The schemes that we will employ to treat the convective equation have been discussed in the preceding section. We will only test the efficiency of four of these when combined with the solver that will be used for the linear term. The four schemes are the Implicit, Godunov, NSTG and SemiD schemes as outlined in Section 2.2.1 while we will make use of the BDF2 scheme outlined in Section 2.2.3 for the linear equation (2.37).

Example 2.4 *We consider the computational domain to be* $[-L, L]$ *with a focus on computing the solution of the entire K-S equation using the fractional time step method described in Section 2.2. We test the convergence of the following problem as given by [89], solving*

$$\begin{cases} u_t + uu_x + u_{xx} + u_{xxxx} = 0, \quad \forall\ (x,t) \in (-L, L) \times (0, T], \\ u(x, 0) = \Phi(x). \end{cases} \tag{2.38}$$

First, we solve equation (2.38) with $\Phi(x) = g(x, 0)$ and subject to boundary conditions

$$u(-L,t) = g(-L,t), \quad u(L,t) = g(L,t), \quad u_x(-L,t) = g_x(-L,t), \quad u_x(L,t) = g_x(L,t), \tag{2.39}$$

where $g(x,t)$ is the exact solution given by

$$g(x,t) = c + \frac{15}{19}\sqrt{\frac{11}{19}}(-9\tanh[l(x-ct-x_0)] + 11\tanh^3[l(x-ct-x_0)]). \tag{2.40}$$

The ghost points are removed via equations (2.33) and (2.34). Here, c, l and x_0 are constants and in the computations we take $L = 30$, $x_0 = -12$, $c = 5$ and $l = \sqrt{11/19}/2$ as documented in [7, 89].

For comparison we also solve equation (2.38) for $\Phi(x) = \exp(-x^2)$ subject to periodic boundary conditions. We will follow the fractional step algorithm as given in Section 2.2. The convergence results due to different numerical schemes for the convection equation are all presented in Tables 2.4 and 2.5. The numbers inside the brackets are the convergent rates, q. These are computed from the errors e_m and e_{2m} corresponding to number of grid points m and $2m$ respectively, that is

$$q = \frac{\log(e_{2m}/e_m)}{\log 2}.$$

From Table, 2.5 the Godunov scheme admits the largest error followed by the non-staggered central scheme and then by the implicit schemes, while the semi-discrete central scheme appears to produce the best result. Interestingly, from Table 2.4, when the initial data that corresponds to the exact solution of the K-S equation was employed, the explicit schemes behave far better than the implicit ones. The semi-discrete is consistent in producing the least possible error out of the explicit schemes. It is also evident that the convergent rate non-staggered central scheme is better than any of the other schemes.

Table 2.4: Convergence rate of the fractional step for the K-S equation with initial data that corresponds to the exact solution.

Grid points	L^∞ error (convergence rate, p) at T = 1				
	Godunov	SemiD	NSTG	CNS	FUIM
40	1.040	1.373	1.883	1.588	1.608
80	1.512 (-0.54)	0.535 (1.36)	1.258 (0.58)	0.709 (1.16)	0.688 (1.22)
160	0.950 (0.67)	0.137 (1.97)	0.6011 (1.07)	0.206 (1.78)	0.222 (1.63)
320	0.268 (1.82)	0.178 (2.94)	0.2197 (1.45)	0.056 (1.88)	0.068 (1.71)
640	0.099 (1.43)	0.007 (1.41)	0.0698 (1.65)	0.021 (1.45)	0.028 (1.26)

The profiles of the solution generated by the different schemes in comparison with the exact solution including the 'close-up near the peaks' are shown in Figure 2.3. The deviation of all the numerical schemes from the exact solution is shown in Figure 2.3(a) while Figure 2.3(b) reveals the deviation of each of the schemes at the highest peak. Of particular interest, the NSTG scheme gives the largest deviation from the exact solution at the peak.

Table 2.5: Convergence rate of the fractional step scheme for the K-S equation with Gaussian initial data. The exact solution is taken as the solution of the most refined grid ($m = 640$)

Grid points	L^∞ error $\times 10^3$ (convergence rate, p) at T = 1				
	Godunov	SemiD	NSTG	CNS	FUIM
40	281	241	391	263	263
80	268 (0.07)	107 (1.18)	178 (1.14)	113 (1.22)	113 (1.22)
160	83.6 (1.68)	46.6 (1.20)	60.4 (1.56)	48.1 (1.24)	47.9 (1.23)
320	34.8 (1.26)	15.6 (1.58)	17.8 (1.76)	15.9 (1.59)	15.9 (1.59)

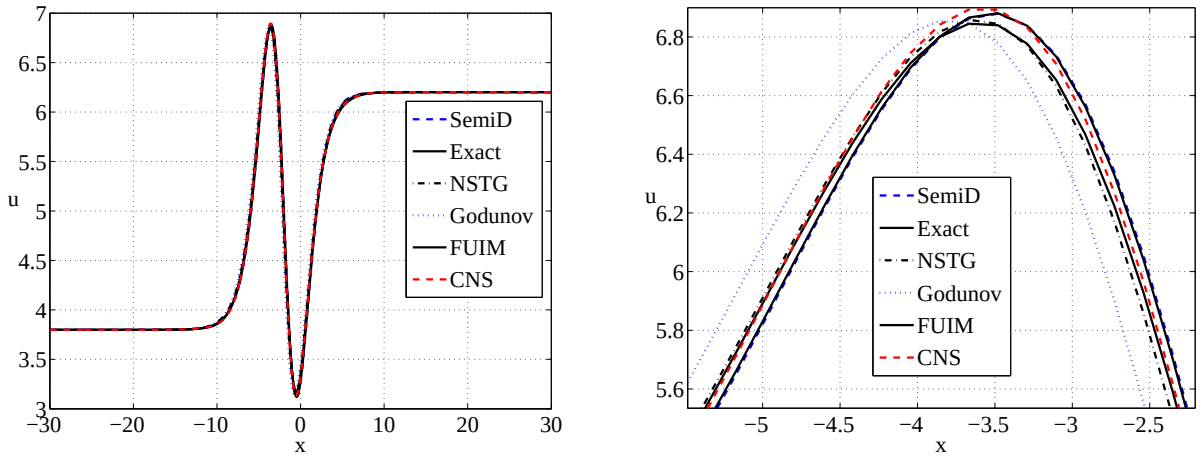

(a) All schemes with the exact solution. (b) Close peaks.

Figure 2.3: Comparison of the exact solution with the numerical solutions.

2.3.4.1 Comparison with the traveling wave solution

The traveling wave solution of every time-dependent partial differential equation gives the solution at all times. Therefore to test the accuracy of the numerical schemes, it makes sense to initialize the solution with the traveling wave solution and check the deviation of the schemes from the traveling wave solution as time advances, [91]. This section is dedicated to traveling wave solution of the K-S equation. This is advantageous over any other solution since the chaotic behavior of (2.38) is restricted to it being integrated over a finite $x-$domain with periodic boundary conditions. Therefore, following the work of Hooper and Grimshaw [34] and Yong-Jung et al. [91] (and references therein) we use the transformation $u(x,t) = u(z)$ where $z = x - st$, s is the wave speed, so that the traveling wave solution is defined over the entire $z-$domain, $-\infty < z < +\infty$. The boundary conditions are such that $u \to u_l$ as $z \to -\infty$ and $u \to u_r$ as $z \to +\infty$. The substitution above reduces equation (2.38) to an ordinary differential equation which can be integrated once to give

$$u''' = c + su - \frac{1}{2}u^2 - u', \tag{2.41}$$

where the prime denotes the derivative with respect to z. The wave speed s and the constant of integration c are determined by the far field solutions as

$$s = \frac{u_l + u_r}{2}, \quad c = -\frac{u_l u_r}{2}.$$

The wave speed is found via the Rankine-Hugoniot condition to be

$$s = \frac{f(u_r) - f(u_l)}{u_r - u_l}.$$

The spatiotemporal behavior of the solution of (2.42) had been recorded by many authors (see [24, 34, 55, 60] among many). Michelson [55] gave the steady solution of (2.38) and studied the solution as a function of the square of a parameter c. With this, he classified the behavior of the solution as conical (for large value of c^2), periodic or quasi-periodic (for small values of c^2). Later, Hooper and Grimshaw [34] classified the solution based on the shock development as either regular shocks, solitary waves or oscillatory shocks. This they did by observing the far field behavior of the solution. They also noted that experiments may show chaotic behavior with respect to traveling waves. Recently, Nickel [60] employed the conditions for solitary and periodic waves to derive an exact solution to the traveling wave. Here we implement the oscillatory shock behavior as given in [34]. Thus, we solve the non homogeneous ordinary differential equation

$$\begin{cases} u''' + u' - (s - 0.5u)u = c, \\ u(-\infty) = u_l, \\ u(+\infty) = u_r. \end{cases} \tag{2.42}$$

The nonlinear boundary value problem (2.42) was discretized and the system of equations derived were solved by the Newton's method. In the numerical computations, we choose a sufficiently large domain such that u' vanishes at the truncated boundaries. We highlight here that our numerical approach was able to reproduce most of the different families of solutions predicted in [34]. For the oscillatory shock considered here, we impose the far field boundary values, $u_l = 1 = -u_r$, consistent with the work of Hooper and Grimshaw [34].

The results in Figure 2.4 were all generated as outlined in Section 2.2. We highlight that all the schemes produced the same quantitative behavior. Nevertheless, NSTG and the fully implicit scheme solution are the closest to the traveling wave solution with the NSTG giving the least deviation from the traveling wave solution. The Godunov and the semi-discrete scheme solution gave the largest deviation of all the schemes.

2.3.4.2 Chaotic property of the Kuramoto-Sivashinsky equation

In this section we verify the chaotic nature of the solution of the K-S equation by solving (using the time-splitting scheme) equation (2.38) subject to periodic boundary conditions. We can see that the numerical simulations in Figure 2.5 are consistent with the work of [89]. We highlight the convergence of the presented scheme in Figure 2.5(a) and Figure 2.5(c).

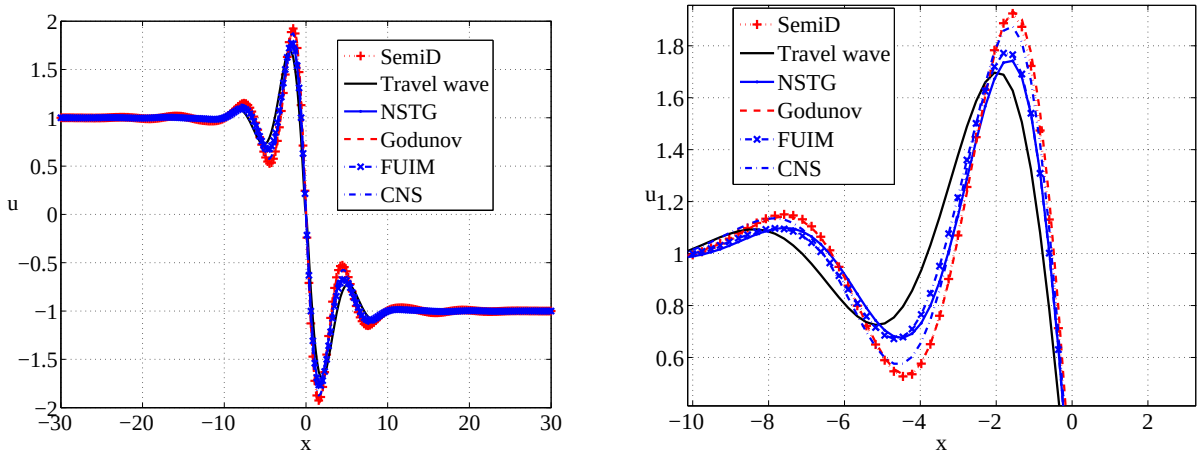

(a) All schemes with the traveling wave. (b) Close peaks of all the schemes.

Figure 2.4: Traveling wave solution as standard compared to other schemes at $T = 10$.

2.3.4.3 Solution properties of the Kuramoto-Sivashinsky equation

We begin this section by validating the bound for the mean energy density of the full K-S equation. In particular, Giacomelli and Otto [24] claimed that the effect of (2.30) will balance the exponential growth of (2.35) resulting in a bound for the mean energy of the entire K-S equation. We consider equation (2.38) with $\Phi(x) = \sin(x)$ subject to periodic boundary conditions. The validation is given in Figure 2.6. We note that all the schemes determine approximately the same bound. However the NSTG scheme gives a largest deviation from the other schemes.

In addition to the boundedness of the mean energy density of the full equation, we also performed numerical experiments to validate the periodicity preserving property. In Figure 2.7(a), we show the conservation of the conserved variable. It is shown here by the zero mean in Figure 2.7(b).

Next, in order to show the effectiveness of our proposed scheme, we validate the bound as proved in earlier literature. We write the inequality (1.4) as

$$\limsup_{t\to\infty} \|u\|_2 = \left(\int_0^L u^2 dx\right)^{\frac{1}{2}} = \mathcal{O}(L^p). \tag{2.43}$$

Hence, we plot $\log(\|u(x,t)\|_2)$ against $\log(L)$ and p is approximated via the slope of the best fit. The results are shown in Figure 2.8(a) for each of the fractional split scheme. The conjectured bound is of $\mathcal{O}(L)$ (see [78] and references therein), i.e., $p = 1$. The value of the slope for each scheme gives a good approximation of this value.

For the fully implicit scheme $p = 1.0047$, for the C-N scheme $p = 1.0074$, for semi-discrete scheme $p = 0.9988$. However, we highlight that the largest deviation is recorded for the NSTG scheme ($p = 0.9767$) which gives a lower bound compared to all the other

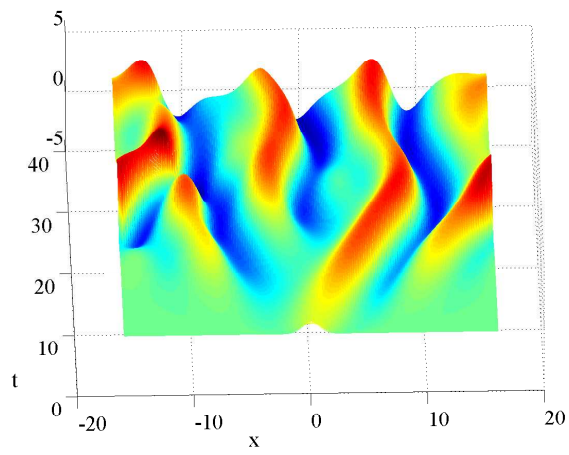

(a) Surface plot on 160 grids

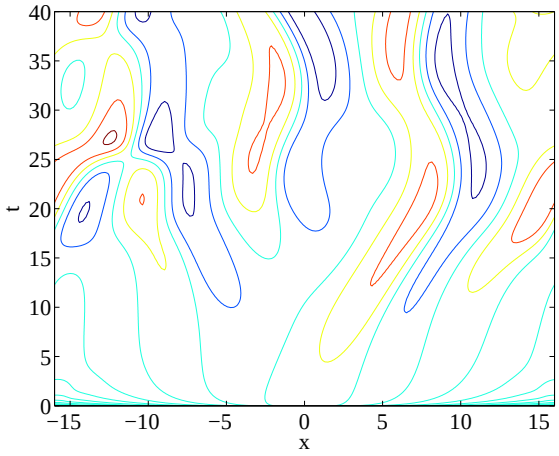

(b) Contour plot showing the peaks (160 grids)

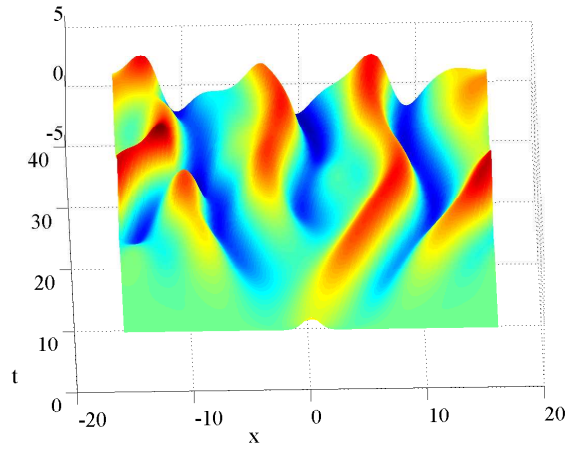

(c) Surface plot on 320 grids

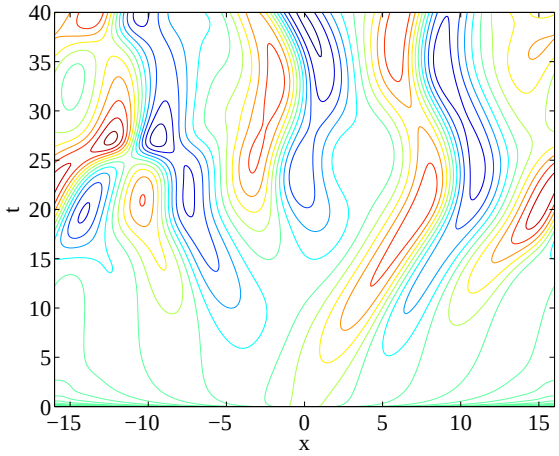

(d) Contour plot showing the peaks (320 grids)

Figure 2.5: The chaotic solution of the K-S equation with Gaussian initial conditions ($\Phi(x) = exp(-x^2)$) up to $T = 40$.

schemes. Figure 2.8(b) shows the system size independence of the quantity

$$\|u_x\|_2^2 = \int_0^L u_x^2 dx, \tag{2.44}$$

as proved theoretically in [63]. Hence, the expression in (2.44) should be of $\mathcal{O}(L^0)$. Our computation reveals that the exponent is -0.02025, 0.0001, 0.0063 and 0.0009 for the NSTG, semi discrete, fully implicit and C-N schemes respectively. It is also evident from Figure 2.8(b) that the NSTG scheme deviates significantly from all other schemes. It is obvious from the Figure that the semi-discrete and the implicit schemes behave equally well unlike the non staggered central scheme.

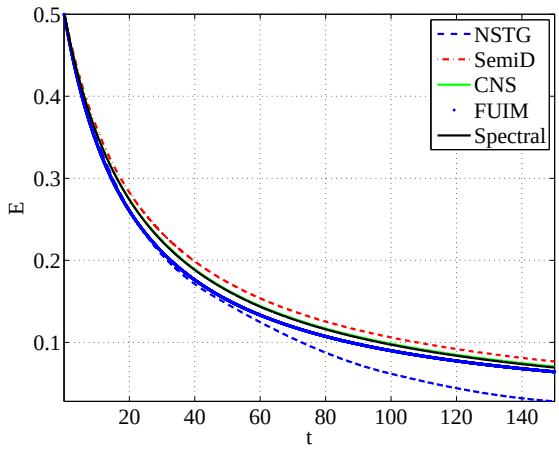

Figure 2.6: Mean energy profiles for the full K-S equation.

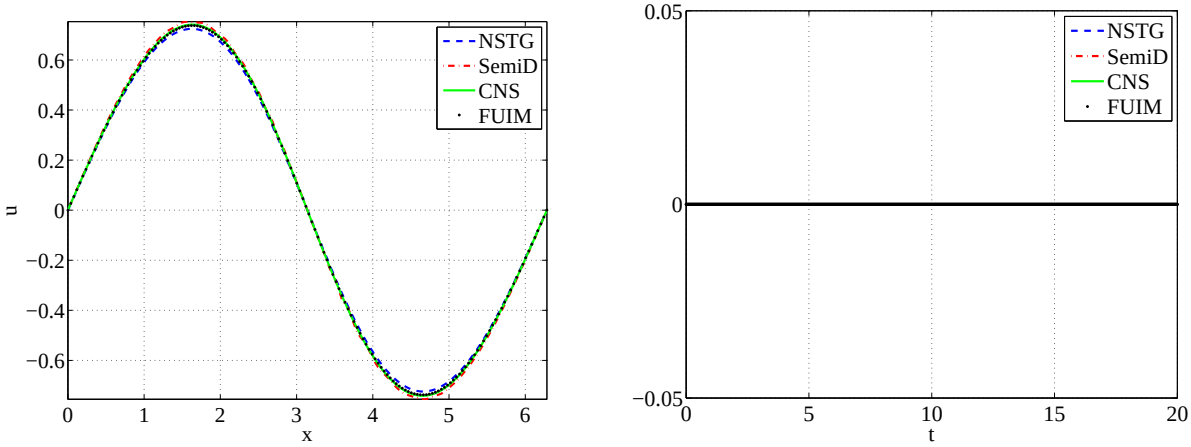

(a) Periodicity (b) Zero average

Figure 2.7: Profile of the K-S equation showing the periodicity and zero average of the solution at $T = 20$ and $L = 2\pi$.

2.3.5 Cahn-Hilliard equation

In this section we apply the fractional splitting method to another relevant equation in physics, the convective Cahn-Hilliard equation (cCH) (2.3). This equation is solved subject to the boundary conditions

$$u_x = \gamma u_{xxx} - \phi(u)_x = 0, \quad (x = a, x = L). \tag{2.45}$$

In particular, we split equation (2.3) using a fractional time step algorithm following the work of, for example, [24, 91]. The stability of the method is guaranteed as long as the properties of each subproblem are preserved, see for example [29]. We split equation (2.3) into three subproblems: the hyperbolic equation

$$u_t - \delta f(u)_x = 0, \tag{2.46}$$

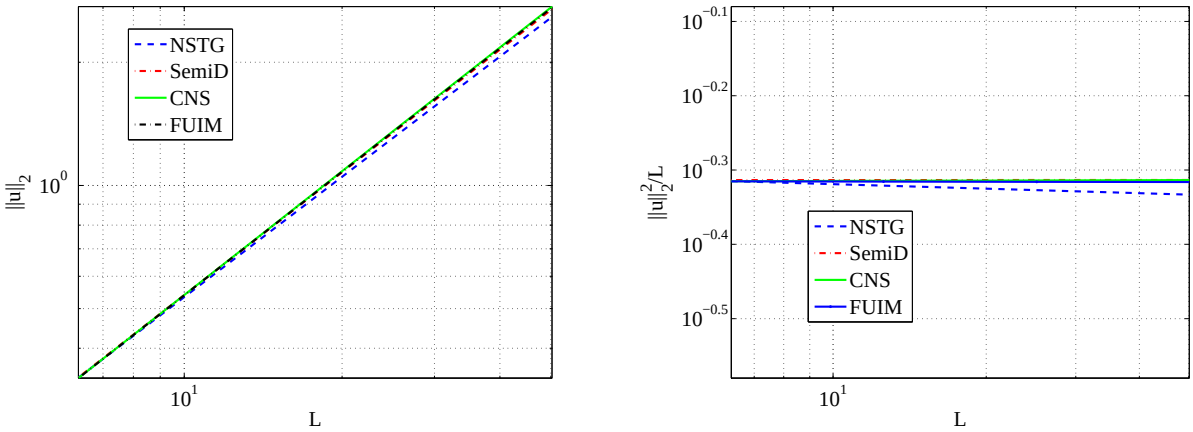

(a) Bound of (2.43) (b) Bound on (2.44)

Figure 2.8: (a) loglog plot of the $\|u\|_2$. (b) loglog plot of $\frac{\|u_x\|_2^2}{L}$.

the linear fourth order equation

$$u_t + \gamma^2 u_{xxxx} + u_{xx} = 0, \tag{2.47}$$

and the nonlinear diffusion equation

$$u_t - \alpha(u^3)_{xx} = 0, \tag{2.48}$$

where $f(u) = u^2/2$.

For $\delta = 0$, equation (2.3) reduces to the traditional Cahn-Hilliard (CH) equation

$$u_t + \gamma^2 u_{xxxx} = \phi(u)_{xx}, \quad x \in \Omega,\ 0 < t, \tag{2.49}$$

which is an equation of conservation of mass with flux

$$J = -\left[\phi(u) - \gamma^2 u_{xx}\right]_x. \tag{2.50}$$

It has been observed that the critical points of the Ginzburg–Landau free energy form

$$\mathcal{E} = \int_0^L \left(F(u) + \frac{\gamma^2}{2} u_x^2\right) dx, \tag{2.51}$$

where F is a Lyapunov functional,

$$F(u) = \int_0^u \phi(s) ds,$$

is a steady state solution of the CH equation (2.49) [19, 62] giving the boundary conditions

$$u_x = \gamma^2 u_{xxx} - \phi(u)_x = 0, \qquad x \in \partial\Omega. \tag{2.52}$$

We believe that this is the first time the equation is handled numerically using a fractional step method of this kind. The hyperbolic subproblem (2.46), and the parabolic subproblems (2.47) and (2.48), being of different natures, can be handled using different efficient numerical schemes.

The convective equation (2.46) will be solved by some of the finite volume schemes designed for hyperbolic conservation laws [51], precisely the NSTG, FD and WENO as outlined in Section 2.2.1 while the linear equation (2.47) will be handled by the second order Diagonally Implicit Runge-Kutta (DIRK) scheme given in Section 2.2.3. Equation (2.48) will be solved by an implicit/explicit conservative/non-conservative scheme, see Section 2.2.2.

We highlight here that the split into (2.47) and (2.48) is motivated by the need to treat linear and nonlinear terms separately. This fractional step scheme converges to the solution of equation (2.3) and this can be shown following a similar analysis as given by Holden et al. [30]. For the specific case when $\delta = 0$, we will combine only equations (2.47) and (2.48) to obtain the solution of the CH equation in (2.49).

First, we discuss the solution of equation (2.3) for the case when $\delta = 0$ for different choices of α. All the simulations were run on a *Windows XP, Intel Core 2 Duo, 2GB RAM* desktop and all the solutions were achieved within 10 seconds of computing time.

Example 2.5 *For the convergence analysis, we consider*

$$\begin{cases} u_t + (\alpha u^3 + u + \gamma^2 u_{xx})_{xx} = 0, \quad x \in (0, 6) \\ u(x, 0) = \cos(\pi x/6), \end{cases} \tag{2.53}$$

and boundary conditions (4.27).

It is obvious that the solution operator of this equation can be split into the solution operator of equation (2.48) and the solution operator of equation (2.47), and the Algorithm in Section 2.2 can be used. We determine the spatial rate of convergence of this scheme for the Cahn-Hilliard equation (4.24) when $\gamma = \alpha = 1$ using the refined grid as the exact solution. The rate of convergence was computed by employing equation (2.32) and the results are presented in Table 2.6.

In addition, we note that the evolution of equation (4.24), for $\alpha = 1/3$ and $\gamma^2 = 0.02$, shown in Figure 2.9 compares well with the work of [18].

2.3.5.1 Solution property of the Cahn-Hilliard equation 4.24

It has been documented that the solution provided by any numerical scheme that solves the Cahn-Hilliard equation must satisfy two main properties [13, 14, 18, 62]:

1. Conservation of mass:

$$\int_\Omega u_0(x)dx = \int_\Omega u dx = ML, \ t > 0,$$

where M is the total mass of the system and

Table 2.6: Convergence rate of the fractional step for the Cahn-Hilliard equation

Grid points	maximum absolute error$\times 10^3$ (p) at T = 1			
	Conservative		Non Conservative Schemes	
	CN	Explicit	CN	Explicit
20	98.8	102	102	101
40	45.9(1.1)	47.5(1.1)	47.5(1.1)	47.2(1.1)
80	19.6(1.21)	20.3(1.2)	20.4(1.2)	20.2(1.2)
160	6.52(1.6)	6.74(1.6)	6.78(1.6)	6.73(1.6)

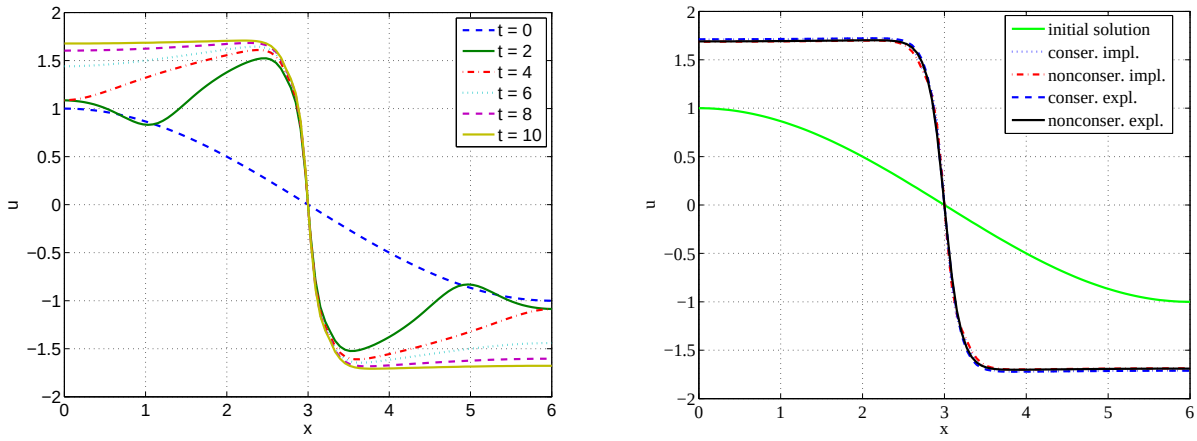

(a) Evolution in time (b) Schemes comparison

Figure 2.9: Solution of the Cahn-Hilliard (4.24) at time $T = 10$. Profiles in (a) are given at equally spaced time intervals.

2. Dissipation of the Ginzburg-Landau free energy functional (equation (2.51)) as time passes.

Hence, this section is dedicated to validate these two main properties using Algorithm 2.9 and Example 2.5. The profiles in Figure 2.10(a) verifies the conservation of mass. We expect change in mass to be zero since $\frac{d}{dt}\int_\Omega u dx = \frac{d}{dt} ML = 0$. The decay in the profiles in Figure 2.10(b) validates the dissipation of energy as expected (see for example, [14, 18]). Note that most of the profiles for the different schemes overlap and hence cannot be distinguished from each other. The mass profile when the conservative implicit scheme is applied to the nonlinear subproblem shows some deviation from the other schemes.

2.3.6 Convective Cahn-Hilliard equation

In this section we give the solution of the cCH equation (2.3) using the splitting Algorithm 2.9.

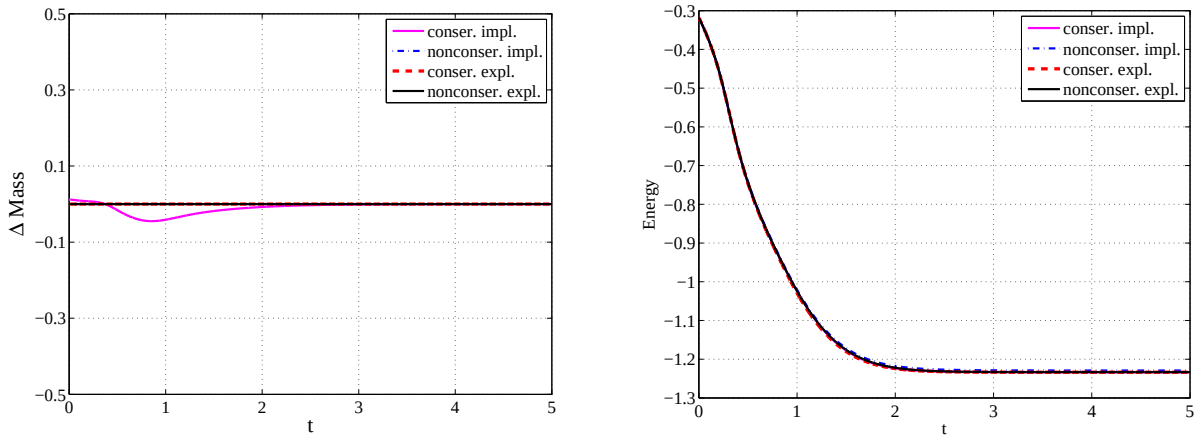

(a) Conservation of Mass $\times 10^{-4}$ (b) Dissipation of Energy

Figure 2.10: Conservation of mass and dissipation of energy.

Example 2.6 *We consider*

$$\begin{cases} u_t - \delta u u_x + (u - \alpha u^3 + \gamma^2 u_{xx})_{xx} = 0, \\ u(x,0) = -\sin(x/6), \end{cases} \tag{2.54}$$

and boundary conditions (2.45).

For the purpose of comparison with results in the literature, we choose $\gamma = \alpha = 1$ and $\delta = 0.1$ – see for example [21, 86]. Following the same refined-grid method as discussed for the Cahn-Hilliard equation, the convergence rate was computed and the results are shown in Tables 2.7 to 2.9. Approximately, all the schemes predict a second order convergence in space.

Table 2.7: Convergence rate of the fractional step for the cCH equation with the NSTG scheme.

Grid points	L^∞ error$\times 10^3$ (convergence rate) at T = 1			
	Conservative		Non Conservative Schemes	
	CN	Explicit	CN	Explicit
20	116	116	116	116
40	53.6 (1.08)	53.5 (1.08)	53.6 (1.07)	53.4 (1.08)
80	22.9 (1.21)	22.8 (1.21)	22.8 (1.21)	22.8 (1.20)
160	7.72 (1.55)	7.70 (1.55)	7.72 (1.55)	7.70 (1.55)

The profiles of the solution as compared with the exact steady state solution are also given in Figures 2.11 and 2.12. For all the schemes, the CFL number is taken between 0.1 and 0.5 which also gives a time step within the stability restriction of the explicit schemes for

Table 2.8: Convergence rate of the fractional step for the cCH equation with the WENO scheme.

Grid points	L^∞ error $\times 10^3$ (convergence rate) at T = 1			
	Conservative		Non Conservative Schemes	
	CN	Explicit	CN	Explicit
20	110	110	110	110
40	51.5 (1.05)	51.4 (1.06)	51.5 (1.05)	51.3 (1.06)
80	22.2 (1.20)	22.1 (1.20)	22.2 (1.20)	22.1 (1.20)
160	7.58 (1.54)	7.55 (1.54)	7.57 (1.54)	7.55 (1.54)

Table 2.9: Convergence rate of the fractional step for the cCH equation with the FD scheme.

Grid points	L^∞ error$\times 10^3$ (convergence rate) at T = 1			
	Conservative		Non Conservative Schemes	
	CN	Explicit	CN	Explicit
20	110	110	110	110
40	51.6 (1.06)	51.5 (1.06)	51.6 (1.05)	51.4 (1.06)
80	22.2 (1.20)	22.1 (1.20)	22.2 (1.19)	22.1 (1.20)
160	7.58 (1.54)	7.56 (1.54)	7.57 (1.54)	7.56 (1.54)

the nonlinear equation. Figures 2.12 highlights the poor performance of explicit schemes (for the nonlinear equation) when coupled with the NSTG scheme (for the advection equation).

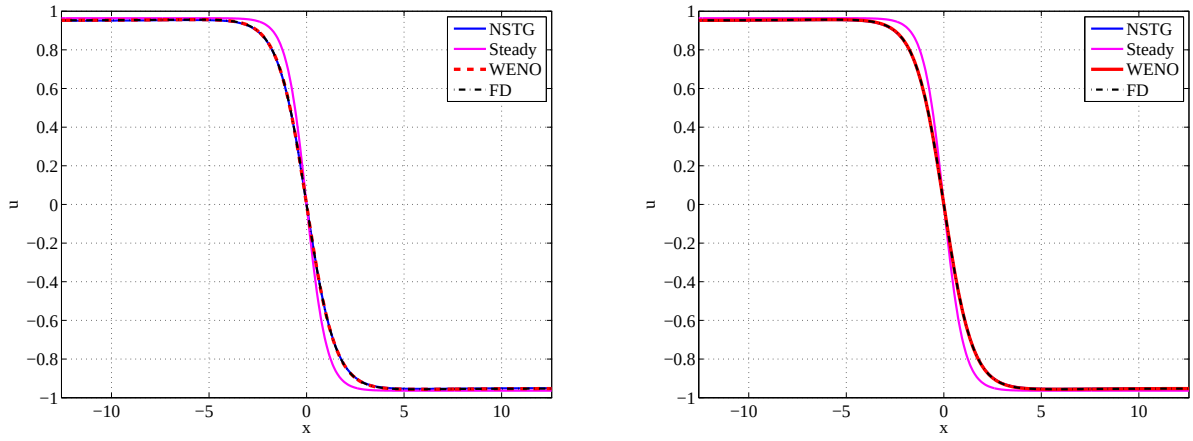

(a) Conservative implicit schemes (b) Non-Conservative implicit schemes

Figure 2.11: Numerical solution of the convective Cahn-Hilliard equation.

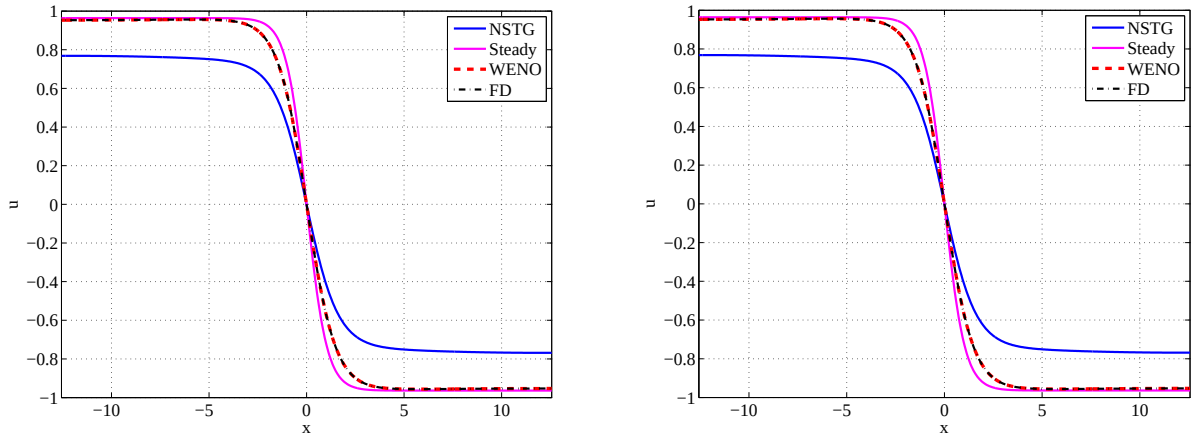

(a) Conservative explicit schemes (b) Non-Conservative explicit schemes

Figure 2.12: Numerical solution of the convective Cahn-Hilliard equation.

2.3.6.1 Solution properties of the convective Cahn-Hilliard equation (4.26)

We will conclude this work by showing the conservation of mass and the coarsening property for the convective Cahn-Hilliard equation (2.3). Coarsening is a major property since it is the behavior of the physical process (spinodal decomposition) that the equation models [25, 69, 86] as time progresses.

Example 2.7 *We solve equation* (4.26) *with* $u(x,0) = 0.5\cos x$ *subject to periodic boundary conditions, for* $\delta = 0.1$ *using* 160 *grid points and Algorithm 2.9 (see for example [17]).*

The integration continues until the solution coarsens and below we present a sequence of figures (i.e., Figures 2.13 and 2.14) showing the behavior of the solution over time.

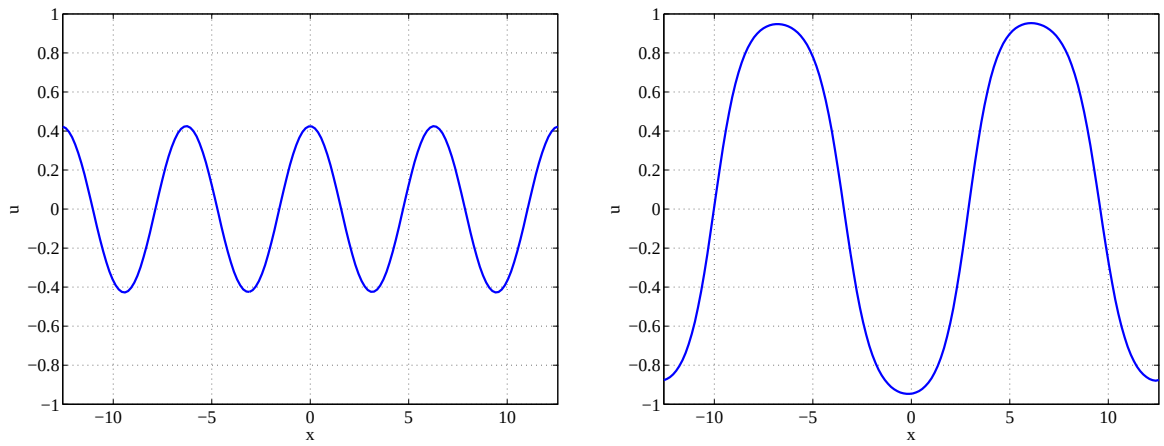

(a) $T = 1$ (Formation of periodic structure) (b) $T = 50$

Figure 2.13: Coarsening process.

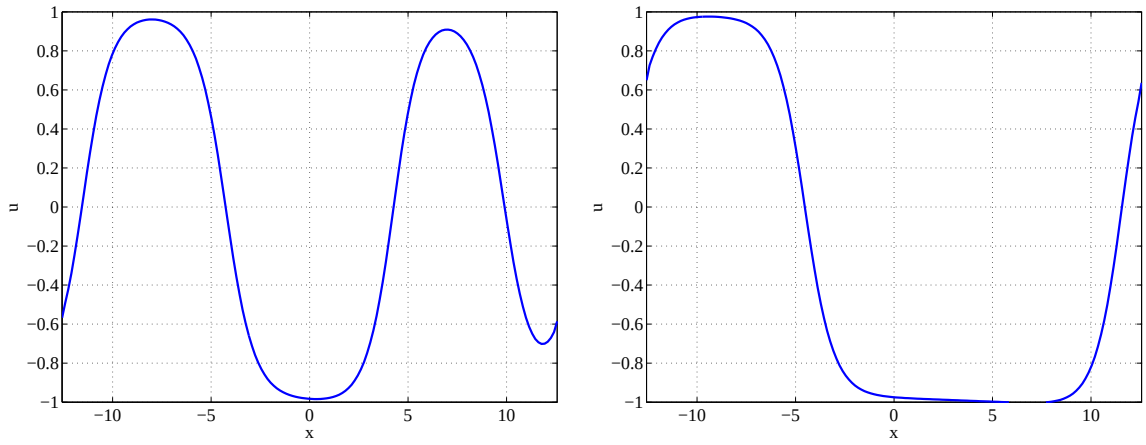

(a) $T = 320$ (b) $T = 640$ (Kink-anti-kink pair)

Figure 2.14: Coarsening process.

For the conservation of mass, we have:

$$\begin{aligned}\frac{d}{dt}\int_{-4\pi}^{4\pi} u dx &= \int_{-4\pi}^{4\pi} u_t dx,\\ &= \int_{-4\pi}^{4\pi} (\delta\frac{u^2}{2} + (-\gamma^2 u_{xx} + \phi(u))_x)_x dx, \\ &= \left(\delta\frac{u^2}{2} + (-\gamma^2 u_{xx} + \phi(u))_x\right)\Big|_{-4\pi}^{4\pi} = 0.\end{aligned} \tag{2.55}$$

The last equality is due to periodicity.

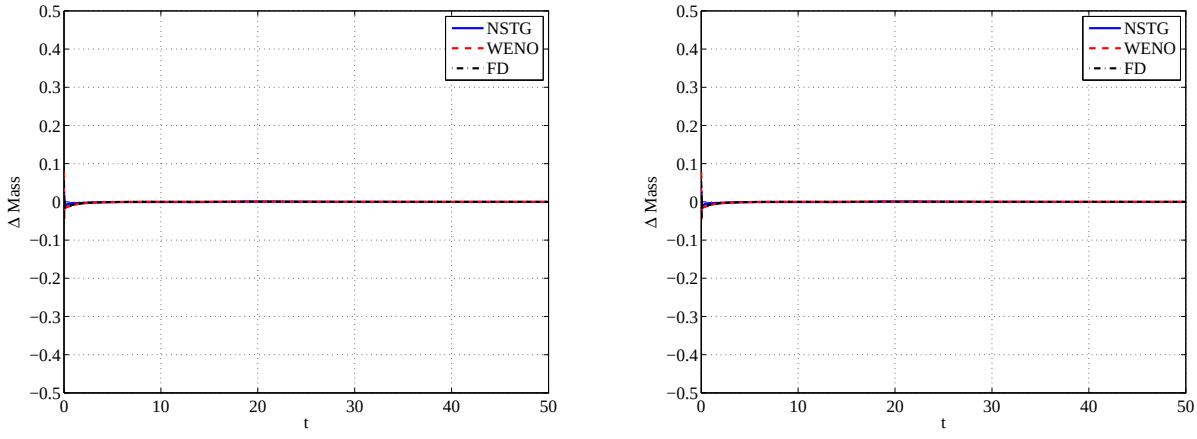

(a) Conservative Implicit Schemes (b) Non-Conservative Implicit Schemes

Figure 2.15: Conservation of mass .

Figures 2.15 and 2.16 shows the conservation of the mass for all the schemes as expected.

Another important property of the cCH equation (2.3) is transition from roughening to an orderless pattern. This is due to the fact that as the value of the driving force, δ, increases,

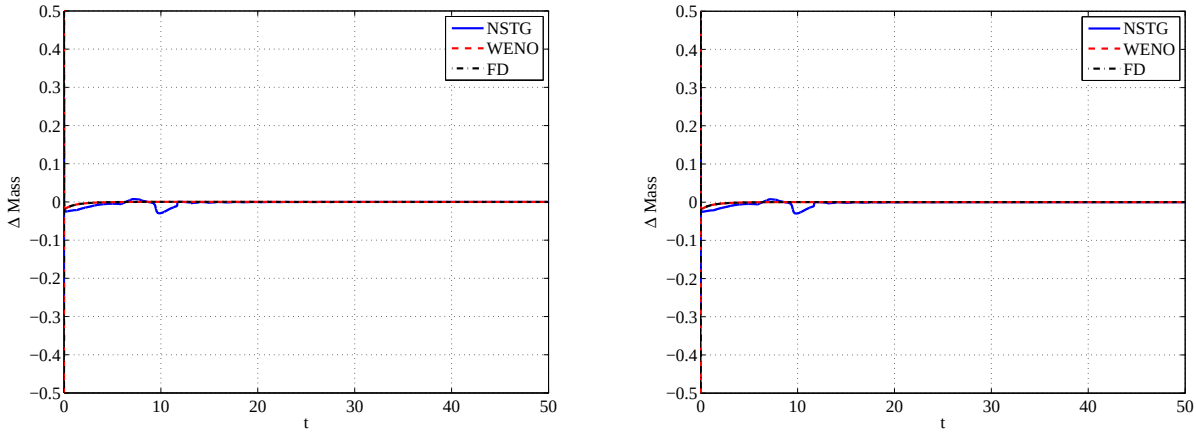

(a) Conservative Explicit Schemes (b) Non-Conservative Explicit Schemes

Figure 2.16: Conservation of mass.

the convective term dominates the equation, consequently it behaves exactly like the famous Kuramoto-Sivashinsky equation. This can be verified by taking $u \to u/\delta$ in equation (2.3), then take $\delta \to \infty$. This was noted by Golovin et al. [26] and Watson [86] among others. The former verified this property using the stationary and the traveling wave solution of equation (2.3) while the latter just remarked this behavior. Here, Figure 2.17, the solution profile of Example 2.7 at final computation time $T = 80$ with $\delta = 5$, clearly shows this behavior.

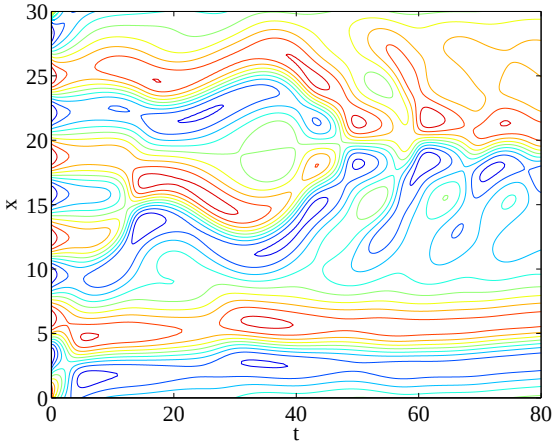

Figure 2.17: Rough behavior of the convective Cahn-Hilliard equation.

2.4 Conclusion

We have employed the fractional time splitting method to approximate the solutions of the K-S and cCH equations through the finite volume discretization. For the K-S equation, the deviation of each of the experimental solvers from the traveling wave solution as shown in

Figure 2.4 reveals that all the schemes approximates the K-S solution. The NSTG is seen to be the closest to the traveling wave solution. The chaotic behaviour of the solution as expected was also replicated through this method (see Figure 2.5) and agrees with the observation of Yan and Chi-Wang [89]. We observed the exponential growth of the mean energy of the linear equation (2.35) in Figure 2.2(b) and the preservation of the mean energy of the hyperbolic equation (2.30) before the onset of shock in Figure 2.1. The poor performance of the Godunov and the implicit schemes are evident here. The performance of the Implicit schemes was also observed also in [91]. The behaviour of the mean energy of these two equations leads to the dissipation of the mean energy of the K-S equation shown in Figure 2.6 [24]. We have shown numerically the observations documented in [24, 63] in Figures 2.6 and 2.8.

Our numerical experiments also reveal that the fractional splitting schemes' approximation of the CH and cCH equations compares well both with existing result in the literatures as well as the exact steady state solution. This is obvious from the Figures 2.9 to 2.12 and Tables 2.6 to 2.9. In all these experiments, the consistency of the WENO scheme in approximating the solution of equation (2.3) is evident. We also validated the dissipation of the Ginzburg Landau energy functional and conservation of mass for the CH equation as well as conservation of mass for the cCH equation, shown in Figures 2.10, 2.15 and 2.16 respectively. In addition to these, Figures 2.13 and 2.14 demonstrates what happens when the mixture of substances in hot temperature is allowed to cool. The solution coarsens because the grains separates. In the presence of high driving force, convection dominates, hence the patterns form becomes rough. This is shown in Figure 2.17. These observations agrees with the physics of the equations as documented in [25].

Chapter 3

Nonclassical methods for singularly perturbed equations

In this chapter, we employ the matched asymptotic expansion method and the nonstandard finite difference method to design two different finite volume schemes for the Schrödinger equation. Results from these schemes are reported in [4].

3.1 Introduction

We investigated second order singularly perturbed equations with the goal of designing accurate numerical schemes. Generally, these are equations of the type

$$-\epsilon^2 u''(x) + b(x)u'(x) + c(x)u(x) = f(x), \tag{3.1}$$

with $\epsilon \ll 1$. Equation (3.1) is a convection-diffusion equation if c = 0 or a diffusion-reaction equation if b = 0. The application of equations of type (3.1) cuts across fluid dynamics, investigating water quality in river networks, oil extraction simulations, thermodynamics, semiconductor device simulation, among others. A quick look at the equation below will open our eyes to what happens with these type of equations. Consider

$$-\epsilon^2 u''(x) + u(x) = 1,\ x \in (0,1),\ u(0) = u(1) = 0. \tag{3.2}$$

Setting $\epsilon = 0$ gives $u(x) = 1$ which completely disagrees with the boundary conditions. The reduced problem therefore has no solution in $C^2[0,1]$. This suggests that the solution of equation (3.2) is not well behaved when ϵ becomes very small. Differential equations depending on small parameters whose solutions approach discontinuous limit as $\epsilon \to 0$ like the one above are termed singularly perturbed equations. Due to their applications, their analysis and numerical solution has attracted the attention of many researchers. As expected,

any discrete model applied to this equation yields ϵ-dependent solution. Hence, classical methods fail to compute the properties of the solution as ϵ approaches some critical value. Of practical interest, their solutions often contain layers; interior or boundary layers. The special case when $b = f = 0$ in equation (3.1) with non-zero Dirichlet boundary condition is of practical interest because of the oscillatory behaviour of the solution. This is evidence from the investigation of the equation of the harmonic oscillator in which c in equation (3.1) is constant. Obviously, the solution of such an equation is trigonometric with wavelength

$$\lambda = 2\pi\sqrt{\frac{\epsilon^2}{c}}.$$

Any difference-type scheme that will well approximate the solution to such an equation therefore, must be with grid size less than the wavelength. Consider a case when the parameter ϵ becomes very small, then such scheme will need much more smaller grid size, consequently it becomes computationally costly. Hence, recent attraction of research activities into providing both analytical and numerical approximation of singularly perturbed equations.

Here, we will focus on the robustness of two schemes discussed in succeeding sections.

3.1.1 Non classical finite volume method

This method combines the knowledge of analytical methods, like perturbation and matched asymptotic expansion, with the strength of numerical approximation. It is referred to as semi-analytical method in [37]. Our discussion here is based on the works of [36, 38, 70]. We will give a detailed description in Section 3.2.2. Jung [36] designed a finite element scheme for singularly perturbed reaction-diffusion equations which has boundary layer elements embedded in it to reduce the effect of the small parameter. Later, Jung and Temam [38] introduced some correctors based on asymptotic expansion into the finite volume scheme to obtain a second order scheme to solve stiff convection-diffusion models. They observed that their finite volume schemes are flexible to incorporate into the finite volume spaces. Recently, Jung and Nguyen [37] introduced some perturbation techniques into the finite volume scheme to resolve the oscillation due to the small parameter in convection-diffusion equations with turning points.

3.1.2 Nonstandard finite difference scheme

Unlike the non classical method, this method derives its strength from the fact that the exact difference scheme of the differential equation is first derived and solved. The idea from the solution of the difference equation is then employed to correct the finite difference scheme of the differential equation. Through this, the denominator is usually changed to a special function of space and/or time step instead of just the grid size or time step. We will follow the results in [53, 54, 57, 58] and the literatures therein. Nonstandard finite difference scheme has been a very useful scheme in investigating differential equations because they

are always designed to give exact schemes of the differential equations. Hence, their design for singularly perturbed equation always incorporate the small parameter into the step size. Mickens [56] applied the nonstandard finite difference scheme to solve the unsteady Schrödinger equation. He gave a comprehensive discussion on the derivation and application including the challenges faced when designing the scheme to solve several models of ordinary and partial differential equations. Recently, Lubuma and Patidar [53] employed the scheme to solve self-adjoint singularly perturbation problems. Later, Patidar and Sharma [65] extended the scheme to handle second order singularly perturbed differential-difference equations with delay. Lubuma and Patidar [54] considered some singularly perturbed problems with oscillatory solutions. They constructed and analysed an exact scheme based on the the works of Mickens. Additional advantages of this method includes preservation of positivity and monotonicity of solutions of differential models with uniform convergence. We will discuss the derivation and application of this method briefly in Section 3.2.3.

3.2 Numerical approach

In this section we design three different finite volume schemes to approximate the solution of the equation

$$\begin{aligned} &\epsilon^2 u'' + \alpha u = 0, x \in (0,1), \\ &u(0) = \alpha_1, \ u(1) = \alpha_2. \end{aligned} \tag{3.3}$$

3.2.1 Classical finite volume scheme

Here we design the traditional classical finite volume (CFV) scheme for equation (3.3). Recall that in finite volume method, given the spatial domain $x \in [0,1]$ with $x_j = jh$, $j = 0, 1, 2, 3, \cdots, m$, $h = \Delta x$ numerical approximations are implemented at cell interfaces $x_{j\pm\frac{1}{2}} = x_j \pm \frac{h}{2}$, $j = 1, 2, 3, \cdots, m-1$, and

$$u_{j\pm\frac{1}{2}} = \frac{u_{j+1} + u_j}{2}.$$

Now, we multiply equation (3.3) by a test function $\chi_{(x_{j-\frac{1}{2}}, x_{j+\frac{1}{2}})}(x)$ and integrate with respect to x. By this we have

$$\epsilon^2 u'\Big|_{x_{j-\frac{1}{2}}}^{x_{j+\frac{1}{2}}} + \alpha \int_{x_{j-\frac{1}{2}}}^{x_{j+\frac{1}{2}}} u\chi_{(x_{j-\frac{1}{2}}, x_{j+\frac{1}{2}})}(x)dx = 0,$$

giving us

$$\epsilon^2 u'\Big|_{x_{j-\frac{1}{2}}}^{x_{j+\frac{1}{2}}} + \alpha h u_j = 0.$$

We employ the interpolation functions [38] for discrete values

$$u_h(x) = \sum_{j=0}^{m} u_j \chi_{(x_{j-\frac{1}{2}}, x_{j+\frac{1}{2}})}(x), \tag{3.4}$$

and

$$u'(x) \sim \nabla_h u_h = \sum_{j=0}^{m} \frac{u_{j+1} - u_j}{h} \chi_{(x_j, x_{j+1})}(x), \tag{3.5}$$

so that

$$u'(x) \sim \frac{u_1 - u_0}{h} \chi_{(x_{\frac{1}{2}}, x_1)}(x) + \sum_{j=1}^{m-1} \frac{u_{j+1} - u_j}{h} \chi_{(x_j, x_{j+1})}(x) + \frac{u_{m+1} - u_m}{h} \chi_{(x_m, x_{m+\frac{1}{2}})}(x).$$

The boundary values of the variable u are approximated and ghost points are eliminated using the given boundary conditions. Bearing these in mind, the equations above can be written as

$$\sigma_{j+1} u_{j+1} + \sigma_j u_j + \sigma_{j-1} u_{j-1} = z_j,$$

where σ_j are some coefficients of discrete unknowns u_j and $z_j = 0$, $j = 1, 2, 3, \cdots, m-1$. Therefore, we have a system of linear equations of the form $\sigma u = Z$ to solve where σ is a tridiagonal matrix with entries

$$\begin{aligned} \sigma_{j-1} &= \tfrac{\epsilon^2}{h}, \\ \sigma_j &= \tfrac{-2\epsilon^2}{h} + \alpha h, \\ \sigma_{j+1} &= \tfrac{\epsilon^2}{h}, \end{aligned} \tag{3.6}$$

and Z is a modification of z_j via the boundary correction.

Remark 3.1 *The boundary correction in the above scheme is direct if the boundary condition is Dirichlet. It becomes much involved when dealing with Neumann boundary condition or mixture of the two type of boundary condition. For the case above* $Z_1 = z_1 - \alpha_1 \frac{\epsilon^2}{h}$ *while* $Z_{m-1} = z_{m-1} - \alpha_2 \frac{\epsilon^2}{h}$.

Remark 3.2 *The above scheme as documented in literatures is deficient in handling singularly perturbed differential equations most especially in the presence of boundary layer, interior layer or when the solution is strongly oscillatory, see [8, 37, 38]. Hence, the introduction of the semi analytical schemes.*

3.2.2 Non classical finite volume method

We discuss the derivation of the non classical finite volume method. Firstly we briefly introduce the known analytical methods for some singularly perturbed differential equations. By so doing we will familiarize ourselves with the tools that are essential for the method under discussion. In particular, we discuss the following:

1. Perturbation method,
2. Matched asymptotic expansion (MAE) and
3. Wentzel-Kramers-Brillouin (WKB) method.

3.2.2.1 Perturbation method

Even though this method is mainly designed for regular perturbation equation, it is a good point to start for better understanding of the new method. Recall that a regular perturbation problem is one in which the solution remains valid even if the small parameter $\epsilon \to 0$. A possible example is the eigenvalue problem for the vertical displacement, $u(x)$, of an elastic string with variable density

$$u'' + \gamma^2[1 + \epsilon\mu]u = 0, \tag{3.7}$$

where $\mu(x)$ is positive and continuous. The solution $u(x)$ and the eigenvalues γ are taken as functions of ϵ. The regular perturbation assumes

$$\begin{aligned} u &\sim u_0 + \epsilon u_1, \\ \gamma &\sim \gamma_0 + \epsilon\gamma_1. \end{aligned}$$

We can put these ansatz into equation (3.7) and equate terms with the same power of ϵ. Inserting the ansatz into the equation, we have

$$u_0'' + \epsilon u_1'' + (\gamma_0^2 + 2\epsilon\gamma_0\gamma_1)(1 + \epsilon\mu(x))(u_0 + \epsilon u_1) = 0,$$

which after expansion and equating the coefficients of the powers of ϵ gives

$$\begin{aligned} O(1) \to &\quad u_0'' + \gamma_0^2 u_0 = 0, \quad u_0(0) = u_0(1) = 0, \\ O(\epsilon) \to &\quad u_1'' + \gamma_0^2 u_1 = 0, \quad u_1(0) = u_1(1) = 0. \end{aligned} \tag{3.8}$$

From the equation above, it is obvious that $u_0 = A\sin(\gamma_0 x)$, $\gamma_0 = j\pi$ where $j \in \mathbb{Z}$.

Remark 3.3 *Regular perturbation technique is not always uniformly valid for singularly perturbed equation most especially near boundary layer regions.*

3.2.2.2 Matched asymptotic expansion

The origin of this method is credited to the works of Prandtl on boundary layer problems, see [33] and the literatures therein. It was a source of breakthrough in the study of singularly perturbed differential equations. The algorithm follows three major steps.

1. Obtain the outer expansion (at least the leading order term).
2. Determine the boundary layer region and obtain the inner expansion.
3. Match the two approximations.

This is illustrated with the following example.

Example 3.1 *Consider the boundary value problem*

$$\begin{aligned} &\epsilon u'' + 2u' + u^3 = 0,\ x \in (0,1),\\ &u(0) = 0,\ u(1) = \tfrac{1}{2}. \end{aligned} \tag{3.9}$$

We will determine the composite expansion of equation (3.9) *by the matched asymptotic expansion method [33].*

In this regard, assume the two term expansion $u = u_0 + \epsilon u_1$ and substitute this into (3.9). This leads to

$$\epsilon(u_0 + \epsilon u_1)'' + 2(u_0 + \epsilon u_1)' + (u_0 + \epsilon u_1)^3 = \epsilon(u_0 + \epsilon u_1)'' + 2(u_0 + \epsilon u_1)' + u_0^3 + 3\epsilon u_0^2 u_1 = 0.$$

This yields,

$$\begin{aligned} O(1) \to &\quad 2u_0' + u_0^3 = 0, && u_0(0) = 0,\ u_0(1) = \tfrac{1}{2},\\ O(\epsilon) \to &\quad 2u_1' + 3\epsilon u_0^2 u_1 = -u_0'', && u_1(0) = 0,\ u_1(1) = 0. \end{aligned} \tag{3.10}$$

Equation $(3.10)_1$ is a first order differential equation which only needs one boundary condition. The fact that we have two boundary conditions means there will be issues (say, boundary layer) at one of the boundaries. We will use the right hand boundary condition and assume there is boundary layer at $x = 0$. With this, the leading order solution is

$$u_0 = \frac{1}{\sqrt{2x+2}}.$$

Since we assumed that there is a boundary layer at $x = 0$, we introduce the transformation $\tilde{x} = \frac{x}{\epsilon^\alpha}$ at this boundary, where $\alpha > 0$ will be determined in the succeeding analysis. The transformation above is referred to as stretching transformation. By this transformation, we have

$$\frac{d}{dx} = \frac{d\tilde{x}}{dx}\frac{d}{d\tilde{x}}.$$

Suppose, $\mathbb{U}(\tilde{x})$ is the solution we sought for at the boundary layer, then we have

$$\epsilon^{1-2\alpha}\mathbb{U}''(\tilde{x}) + 2\epsilon^{-\alpha}\mathbb{U}'(\tilde{x}) + \mathbb{U}^3(\tilde{x}) = 0,\ \mathbb{U}(0) = 0. \tag{3.11}$$

Also, we assume $\mathbb{U} \sim \mathbb{U}_0(\tilde{x}) + \epsilon^\gamma \mathbb{U}_1(\tilde{x}), \cdots$ for $\gamma > 0$. Putting this into equation (3.11) we have

$$\epsilon^{1-2\alpha}(\mathbb{U}_0 + \cdots)'' + 2\epsilon^{-\alpha}(\mathbb{U}_0 + \cdots)' + (\mathbb{U}_0 + \cdots)^3 = 0. \tag{3.12}$$

If we assume that the first and the second term are of the same order of ϵ while the third term is of higher order, then $\alpha = 1$ which implies that the first and the second terms are of order $O(\epsilon^{-1})$ while third term is of order $O(1)$. Hence, we need to solve

$$\begin{aligned} O(\tfrac{1}{\epsilon}) \quad \to \quad &\mathbb{U}_0'' + 2\mathbb{U}_0' = 0,\\ &\mathbb{U}_0(0) = 0. \end{aligned}$$

The solution of this equation is $A(1-\exp(-2\tilde{x}))$ where A is a constant. Before matching these solutions, we need to find the value of A. This is achieved by assuming that the solution of the boundary layer equation outside the layer and the value of the outer solution as one approaches the boundary layer should be equal, i.e. $u_0(0) = \mathbb{U}_0(\infty)$. Hence, $A = \frac{1}{\sqrt{2}}$. Now, we can determine the composite expansion which is the required solution by adding the outer and the inner solution and subtracting the region common to both,

$$u = u_0(x) + \mathbb{U}_0(\tilde{x}) - u_0(0) = \frac{1}{\sqrt{2x+2}} - \frac{1}{\sqrt{2}}\exp\left(-\frac{2x}{\epsilon}\right). \tag{3.13}$$

Even though this method is outlined for a boundary layer problem, it is also applicable to interior layer, boundary layer or corner layer problems.

Remark 3.4 *It is note worthy here that most of the solutions by the match asymptotic expansion method ended up having an exponential dependence on the boundary layer coordinate.*

3.2.2.3 WKB method

This method which supposedly originated from the work of the trio Wentzel, Kramers and Brillouin assumes the exponential dependence on the boundary layer coordinate from the beginning, see [33]. It has been a successful tool in solving problems arising from quantum and solid mechanics, for instance, the Schrödinger equation. As done for the previous methods, we will outline the method by employing it to solve the example below.

Example 3.2 *Approximate the solution of*

$$\epsilon^2 u'' - f(x)u = 0, \tag{3.14}$$

analytically by the WKB method.

Suppose that $f(x) = \tilde{f}$ is a constant function, we know that equation (3.14) will admit a general solution

$$u(x) = \alpha\exp\left(-\frac{1}{\epsilon}\sqrt{\tilde{f}}x\right) + \beta\exp\left(\frac{1}{\epsilon}\sqrt{\tilde{f}}x\right). \tag{3.15}$$

In the WKB method, the solution (3.15) is generalized to solve equation (3.14). The ansatz here is

$$u(x) \sim e^{\frac{\theta(x)}{\epsilon^\alpha}}\left(u_0(x) + \epsilon^\alpha u_1(x) + \cdots\right). \tag{3.16}$$

We will need the second derivative of the assumed solution given above and then substitute it into equation (3.14), equate the coefficients of the powers of ϵ, solve reduced equations and hence, the entire equation. By ideas from calculus,

$$u' \sim e^{\frac{\theta}{\epsilon^\alpha}}\left(\epsilon^{-\alpha}\theta' u_0 + u_0' + \theta' u_1 + \cdots\right), \tag{3.17}$$

and

$$u'' \sim e^{\frac{\theta}{\epsilon^\alpha}}\left(\epsilon^{-2\alpha}\theta'^2 u_0 + e^{-\alpha}(\theta'' u_0 + 2\theta' u_0' + \theta'^2 u_1) + \cdots\right). \tag{3.18}$$

Putting equations (3.16) and (3.18) into equation (3.14) we have

$$\epsilon^2\left(\epsilon^{-2\alpha}\theta'^2u_0+e^{-\alpha}(\theta''u_0+2\theta'u_0'+\theta'^2u_1)+\cdots\right)-f(x)\left(\epsilon^{\alpha}(u_0(x)+\epsilon^{\alpha}u_1(x)+\cdots)\right)=0. \tag{3.19}$$

Interestingly, the exponential term dropped out. Following the same procedure as we did in the last section, we determine that $\alpha = 1$. With this, we have the eikonia equation

$$O(1)\rightarrow \quad (\theta')^2=f(x), \tag{3.20}$$

which have the solution

$$\theta(x)=\pm\int^x\sqrt{f(s)}ds. \tag{3.21}$$

The first term in the expansion is determined by solving the transport equation

$$O(\epsilon)\rightarrow \quad \theta''u_0+2\theta'u_0'+\theta'^2u_1=f(x)u_1. \tag{3.22}$$

Equation (3.21) reduces this to

$$O(\epsilon)\rightarrow \quad \theta''u_0+2\theta'u_0'=0, \tag{3.23}$$

which has the solution

$$u_0(x)=\frac{c}{\sqrt{\theta'}}.$$

Therefore, the solution of equation (3.14) is

$$u\sim f^{-\frac{1}{4}}(x)\left(\alpha\exp\left(-\frac{1}{\epsilon}\int^x\sqrt{f(s)}ds\right)+\beta\exp\left(\frac{1}{\epsilon}\int^x\sqrt{f(s)}ds\right)\right). \tag{3.24}$$

The methods outlined above are all analytical and easy to apply when treating linear equations with $O(\epsilon)$ or greater. A more realistic approximation will be obtained if one can consider terms with $O(\epsilon^2)$ or less. But this may prove really difficult and handling nonlinear equations may present more difficult challenges. This is one of the reasons we may have to appeal to numerical studies of these equations. This is non trivial since, we already know that it is always costly employing standard numerical schemes for this type of equations. Therefore, we will employ our ideas of analytical methods when constructing the numerical schemes, see [37]. To this extent, we will dedicate the next section to the study of corrector methods as introduced and discussed in [70].

The non classical method builds on the idea of the method of matched asymptotic expansion that was explained in Section 3.2.2.2. We will motivate the method by an example also.

Example 3.3 *Investigate the solution of the equation*

$$\mathbb{L}:=-\epsilon u''+b(x)u'+c(x)u=f(x),\ x\in(0,1), \tag{3.25}$$

$$u(0)=u(1)=0, c(x)\geq 0,\ b'(x)\neq 0,\ x\in[0,1], \tag{3.26}$$

given that b, c, f are smooth functions and $0<\epsilon\ll 1$.

It is evident that we can approximate the solution of equations (3.25) and (3.26) by the method of MAE as outlined above in which case we need to first find the outer expansion, say u_{as}. Except in the presence of boundary layer, this will be a well behaved solution of the equation. So let,

$$u_{as} \sim \sum_{i=0}^{m} \epsilon^i u_i(x), \tag{3.27}$$

u_i is to be determined. Following the same procedure as in Section 3.2.2.1 and putting the ansatz (3.27) into (3.25) leads to

$$\begin{aligned} O(1) \rightarrow &\quad bu_0' + cu_0 = f, \\ O(\epsilon^i) \rightarrow &\quad bu_i' + cu_i = u_{i-1}'', \ \ for\ i = 1, \cdots, m. \end{aligned} \tag{3.28}$$

Now, given some other conditions, we will be able to determine the values of the unknowns $[u_0, u_i]$ from these equations. To find u_0 we need only one boundary condition, but we have two, so we are faced with the challenge of choice making. To be able to make the correct choice of the boundary condition, an appeal is made to cancelation law [70].

Remark 3.5 *The location of the boundary layer depends on the behaviour of b. It will be towards the right hand boundary given a positive b and at the left hand boundary otherwise. For our case, because of the definition of the problem, it will be located at $x = 1$. Therefore, we employ only the boundary value at $x = 0$ to define u_0. Hence, u_{as} does not approximate the solution of equation* (3.25) *because it is deficient at $x = 1$.*

Hence we focus on determining the reduced solution, u_0, from the equations

$$\begin{aligned} O(1) \rightarrow &\quad bu_0' + cu_0 = f, && u_0(0) = 0, \\ O(\epsilon^i) \rightarrow &\quad bu_i' + cu_i = u_{i-1}'', \ u_i(0) = 0 && for\ i = 1, \cdots, m. \end{aligned} \tag{3.29}$$

There is need for a local corrector of the solution u_{as} as we approach $x = 1$. To this end, we introduce a stretching transformation at $x = 1$,

$$y = \frac{1 - x}{\delta}, \ 0 < \delta \ll 1.$$

Suppose $\mathbb{L} = \epsilon\mathbb{L}_1 + \mathbb{L}_0$ where $\mathbb{L}_0 v := bv' + cv$, then we want to choose δ so that $\epsilon\mathbb{L}_1$ and $\mathbb{L}_0$ will have the same order with respect to ϵ after transformation from x to y , i.e.,

$$\epsilon\delta^{-2} = \delta^{-1},$$

which gives $\delta = \epsilon$. To continue, we have to expand the functions $b(x) = b(1 - \epsilon y)$ and $c(x) = c(1 - \epsilon y)$ by the Taylor's expansion thus,

$$\sum_{i=0}^{\infty} b_i \epsilon^i y^i, \ \ with, \ \ b_0 = b(1),$$

$$\sum_{i=0}^{\infty} c_i \epsilon^i y^i, \ with, \ c_0 = c(1).$$

Based on these expansions, the boundary layer equation to be solved is

$$-\frac{1}{\epsilon}\frac{d^2u}{dy^2} - \frac{1}{\epsilon}\sum_{i=0}^{\infty} b_i \epsilon^i y^i \frac{du}{dy} + \sum_{i=0}^{\infty} c_i \epsilon^i y^j u = 0. \tag{3.30}$$

Suppose, we have a local expansion for $u(y)$

$$u_{loc}(y) = \sum_{l=0}^{m+1} \epsilon^l \theta_l(y). \tag{3.31}$$

Substituting this into equation (3.30) and equating the powers of ϵ we have

$$\mathcal{T}_0\theta_0 = 0, \tag{3.32}$$

$$\mathcal{T}_0\theta_l = -\sum_{i=1}^{l} \mathcal{T}_i\theta_{l-i}, l = 1, \cdots, m+1, \tag{3.33}$$

where

$$\mathcal{T}_0 := -\frac{d^2}{dy^2} - b_0\frac{d}{dy},$$

$$\mathcal{T}_1 := -b_1 y\frac{d}{dy} + c_0.$$

It appears now that we have to solve second order differential equations which require two boundary conditions each for uniqueness. Since we are focussing on the boundary at $x = 1$, we need a boundary condition here so that the error of our approximation will be zero, then $\theta_l(0) = -u_l(1)$. The second boundary condition will be based on the fact that we need the boundary layer solution localized to this boundary alone, hence we need $\lim_{y\to\infty} \theta_l(y) = 0$. The MAE approximation is

$$u_{as} = \sum_{i=0}^{m} \epsilon^i u_i(x) + \sum_{l=0}^{m} \epsilon^k u_l\left(\frac{1-x}{\epsilon}\right). \tag{3.34}$$

Remark 3.6 *It is the idea of the corrector here that was employed by Jung [36] and Jung and Nguyen [37] in their work. The same procedure will be employed here to solve two equations.*

3.2.3 Non standard finite volume method

In this section we will investigate some singular perturbed second order ordinary differential equations (ODEs) in order to design more accurate scheme to solve them. As stated in Section 3.2, we will investigate equations of the form

$$\begin{cases} -\epsilon^2 u''(x) - g(x)u = 0, \ x \in [0,1], \\ u(0) = \alpha, u(b) = \beta. \end{cases} \tag{3.35}$$

Our discussion in this section is based on the works that were referred to in Section 3.1.2.

3.2.3.1 Nonstandard finite difference schemes for first order differential equations

For better understanding, we derive the scheme for a simple first order decay differential equation

$$\frac{du}{dx} = -\gamma u. \tag{3.36}$$

Integrating equation (3.36), we have its general solution as

$$u = u_0 e^{-\gamma x},\ u_0 = u(0).$$

This means the corresponding difference equation to (3.36) is

$$u_{j+1} = u_j e^{-\gamma h}.$$

Hence,

$$u_{j+1} - u_j = u_j(e^{-\gamma h} - 1),$$

and the nonstandard scheme for (3.36) is

$$\frac{u_{j+1} - u_j}{\phi(h)} = -\gamma u_j,\ \phi(h) = \frac{1 - e^{-\gamma h}}{\gamma}. \tag{3.37}$$

The replacement of the space width h in the denominator of the finite difference scheme by the function $\phi(h)$ as in equation (3.37) such that

$$\lim_{h \to 0} \phi(h) \sim h,$$

gives a significant difference between the classical difference schemes and the NSFD.

3.2.3.2 Nonstandard finite difference schemes for second order differential equations

Here, we derive the denominator function $\phi(h)$ for equation (3.35) in the standard form

$$u'' \pm g(x)_\epsilon u = 0,\ g(x)_\epsilon = \frac{g(x)}{\epsilon^2}. \tag{3.38}$$

Assuming g is constant, for simplicity, we know that the two linearly independent solution of (3.38) are

$$u^1 = \exp(\imath g x),\ \ u^2 = \exp(-\imath g x),\ \imath = \sqrt{-1}. \tag{3.39}$$

$$\begin{vmatrix} \phi_j & \exp(\imath\sqrt{g_\epsilon} h j) & \exp(-\imath\sqrt{g_\epsilon} h j) \\ \phi_{j+1} & \exp(\imath\sqrt{g_\epsilon} h (j+1)) & \exp(-\imath\sqrt{g_\epsilon} h (j+1)) \\ \phi_{j+2} & \exp(\imath\sqrt{g_\epsilon} h (j+2)) & \exp(-\imath\sqrt{g_\epsilon} h (j+2)) \end{vmatrix} = 0. \tag{3.40}$$

From equation (3.40), it is evident that

$$u_j(e^{\imath\sqrt{g_\epsilon}h} - e^{-\imath\sqrt{g_\epsilon}h}) - u_{j+1}(e^{2\imath\sqrt{g_\epsilon}h} - e^{-2\imath\sqrt{g_\epsilon}h}) + u_{j+2}(e^{\imath\sqrt{g_\epsilon}h} - e^{-\imath\sqrt{g_\epsilon}h}) = 0,$$

which by the trigonometric identities

$$2\sin(\theta) = e^{\imath\theta} - e^{-\imath\theta},$$

gives

$$u_j - 2u_{j+1}\cos(\sqrt{g_\epsilon}h) + u_{j+2} = 0. \tag{3.41}$$

The interesting feature here is the common behaviour of the solution $\nu_j = Ae^{\imath\gamma x_j} + Be^{-\imath\gamma x_j}$ of both difference equation (3.41) and the constant coefficient equation (3.38) at the grid point x_j. Recalling that

$$\cos(\theta) = 1 - 2\sin^2\left(\frac{\theta}{2}\right),$$

after an index shift, equation (3.41) finally gives the nonstandard finite difference scheme for the equation (3.39) as

$$\frac{u_{j-1} - 2u_j + u_{j+1}}{\phi(h)^2} + g_\epsilon(x)u_j = 0, \;\; \phi(h) = \frac{2\epsilon}{\sqrt{g}}\sin\left(\frac{\sqrt{g}}{2\epsilon}h\right). \tag{3.42}$$

Now, for $g = g(x)$, equations (3.42) gives

$$\frac{u_{j-1} - 2u_j + u_{j+1}}{\phi(h)^2} + g_\epsilon(x_j)u_j = 0, \;\; \phi(h) = \frac{2\epsilon}{\sqrt{g(x_j)}}\sin\left(\frac{\sqrt{g(x_j)}}{2\epsilon}h\right). \tag{3.43}$$

On a domain discretized into $m+1$ grid points $j = 0, 1, 2, 3, \cdots, m$, the above scheme will result into a system of linear equations of the form

$$\mathbb{A}u = \mathbb{Z}, \tag{3.44}$$

where the sparse matrix $\mathbb{A}$ has the entries

$$\begin{aligned} A_{j-1} &= -\frac{1}{\phi(h)^2}, \\ A_j &= \frac{2}{\phi(h)^2} - g_\epsilon(x_j), \;\; j = 1, 2, \cdots, m, \\ A_{j+1} &= -\frac{1}{\phi(h)^2}, \end{aligned} \tag{3.45}$$

$$\tag{3.46}$$

and

$$\mathbb{Z}_{1,2,\cdots,m} = [-\frac{u_0}{\phi(h)}, 0, 0, 0, \cdots, -\frac{u_m}{\phi(h)}],$$

where u_0 and u_m are boundary values.

It has been shown that the equation (3.64) when solved subject to Dirichlet boundary condition such that $u(0), u(1) \geq 0$ satisfies the maximum principle and that the schemes (3.43) is qualitatively stable [54]. That is, the difference equation or its solution replicates the properties of the original equation.

3.2.3.3 Non standard finite finite volume scheme

The new finite volume scheme to be designed will be an adaptation of the nonstandard finite difference scheme discussed above into the classical finite volume scheme. Comparing the classical finite volume scheme with (3.43), the denominator of the nonstandard finite volume scheme is the function

$$\phi(h) = \frac{2}{\sqrt{f_\epsilon(x_j)}} \sin\left(\frac{\sqrt{f_\epsilon(x_j)}}{2}h\right), \; f_\epsilon = \frac{1}{h\epsilon^2}\int_{x_{j-\frac{1}{2}}}^{x_{j+\frac{1}{2}}} g(x)dx. \tag{3.47}$$

This makes sense since, $\lim_{h\to 0}\phi(h) \sim h$. Then, we will be solving system of linear equations in the form giving in equation (3.44) where

$$\begin{aligned} A_{j,j-1} &= \frac{1}{\phi(h)^2}, \\ A_{j,j} &= -\frac{2}{\phi(h)^2} + f_\epsilon(x_j), \; j = 1, 2, \cdots, m \\ A_{j,j+1} &= \frac{1}{\phi(h)^2}, \end{aligned} \tag{3.48}$$

(3.49)

and

$$\mathbb{Z}_{1,2,\cdots,m} = [-\frac{u_0}{\phi(h)}, 0, 0, 0, \cdots, -\frac{u_{m+1}}{\phi(h)}].$$

We discuss the application of these method to three different problems in the sequel.

3.3 Numerical experiments

Here we apply the three schemes designed above to equation (3.50) below

Example 3.1

$$\begin{aligned} &\epsilon^2 u'' + \alpha u = 0, x \in (0,1), \\ &u(0) = 1, \; u(1) = 0. \end{aligned} \tag{3.50}$$

The boundaries are corrected through

$$u_{\frac{1}{2}} = 1, \; u_{m+\frac{1}{2}} = 0,$$

and the interpolation functions. The numerical approximations are compared with exact solution

$$u(x) = \frac{\sin(\frac{1-x}{\epsilon})}{\sin(\frac{1}{\epsilon})}.$$

The non classical method follows some algorithms to correct the solutions at the points where the classical method fails using the idea of analytical methods. Therefore, we study the formal perturbation approximation of the equation under investigation. Put

$$u_{per} \sim \sum_{i=0}^{\infty} \epsilon^i u_i,$$

into equation (3.50) and equate the orders of powers of ϵ. This leads to the equations

$$O(1) \rightarrow \quad u_0 = 0, \quad u_0(0) = 1, \; u_0(1) = 0, \tag{3.51}$$

$$O(\epsilon) \rightarrow \quad u_1 = 0, \quad u_1(0) = 0, \; u_1(1) = 0, \tag{3.52}$$

$$u_i = -\tfrac{1}{\alpha} u_{i-2}'', \quad u_i(0) = 0, \; u_i(1) = 0. \tag{3.53}$$

Let

$$u \sim \sum_{i=0}^{\infty} \epsilon^i \theta_i(y),$$

then the boundary layer equation is

$$\left(\frac{d^2}{dy^2} + \alpha\right) \sum_{i=0}^{\infty} \epsilon^i \theta_i = 0,$$

with the leading order equation

$$\frac{d^2\theta_0}{dy^2} + \alpha\theta_0 = 0. \tag{3.54}$$

This being a second order equation requires two boundary conditions. As discussed in Section 3.2.2, if $\alpha = 1$, the solution is oscillatory, hence we solve this equation subject to $\theta_0(0) = -1$, $\theta_0(1) = 0$. The solution of equation (3.54) is

$$\theta_0 = \cot\left(\frac{1}{\epsilon}\right) \sin\left(\frac{x}{\epsilon}\right) - \cos\left(\frac{x}{\epsilon}\right). \tag{3.55}$$

Now, we will outline the design of the non-classical finite volume scheme. We seek the solution of the target equation in the form $u = u^c + \gamma\theta_0$, where θ_0 is the corrector just discussed above and u^c will be discretized with finite volumes, while $\gamma \in \mathbb{R}$ will be determined alongside the unknown solution, see [38]. Therefore, the desired solution is

$$\tilde{u} = \gamma\theta_0 + u_h,$$

$$u_h = \sum_{j=1}^{m} u_j \chi_{(x_{j-\frac{1}{2}}, x_{j+\frac{1}{2}})}(x), \tag{3.56}$$

$$\epsilon^2 u^{c''} + \alpha u^c = 0. \tag{3.57}$$

The boundary condition for this new equation is dependent on the original boundary and the behaviour of the corrector at the boundary. Therefore,

$$u^c(0) = u(0) - \gamma\theta_0(0) = 1 + \gamma, \quad u^c(1) = u(1) - \gamma\theta_0(1) = 0. \tag{3.58}$$

Remark 3.1 *It is evident here that if $\gamma = 0$, then we will recover the classical finite volume approximation.*

Obviously, we need an additional equation to cater for the unknown parameter γ for the existence of a unique solution to the expected system of discretized equations. To this extent, we will multiply equation (3.50) by a test function $\theta_0 \chi_{[0,x_{\frac{3}{2}})}$ and integrate by part over $(0,1)$. This leads to

$$\epsilon^2 u^{c'} \theta_0 \Big|_0^{x_{\frac{3}{2}}} - \epsilon^2 \int_0^{x_{\frac{3}{2}}} \theta_0 u^{c'} dx + \alpha \int_0^{x_{\frac{3}{2}}} u^c dx = 0. \tag{3.59}$$

At this point, we introduce the discrete interpolation functions for u and u' as discussed above to replace u^c and recall that by the boundary condition $u_0^c = 1 + \gamma$. Then,

$$u^{c'}(x_{\frac{3}{2}}) = \frac{u_2^c - u_1^c}{h},$$

and

$$u^{c'} = \frac{u_1^c - u_0^c}{h} = \frac{u^c - 1 - \gamma}{h}.$$

Putting all these together we have a system of linear equations

$$\sigma_{0,0}\gamma + \sigma_{0,1} u_1^c + \sigma_{0,2} u_2^c = 0, \tag{3.60}$$

to solve. Here,

$$\begin{aligned}
\sigma_{0,0} &= \frac{\epsilon^2}{h}\left(\theta_0(0) - \int_0^{x_1} \theta_0' dx\right), \\
\sigma_{0,1} &= \frac{\epsilon^2}{h}\left(-(\theta_0(x_{\frac{3}{2}}) + \theta_0(0)) - (\int_0^{x_1} - \int_{x_1}^{x_2})\theta_0' dx\right) + h\alpha, \\
\sigma_{0,2} &= \frac{\epsilon^2}{h}\left(\theta_0(x_{\frac{3}{2}}) + (\int_{x_1}^{x_2} - \int_{x_2}^{x_3})\theta_0' dx\right).
\end{aligned} \tag{3.61}$$

We will move straightforward to design scheme for equations (3.57) putting in mind the interpolation functions earlier discussed. Of course, we will solve a system of linear equations in the form $\sigma u = Z$, where the sparse matrix σ has the entries

$$\begin{aligned}
\sigma_{j,j-1} &= -\frac{\epsilon^2}{h}, \\
\sigma_{j,j} &= \frac{2\epsilon^2}{h} - h\alpha, \ j = 1, \cdots, m, \\
\sigma_{j,j+1} &= -\frac{\epsilon^2}{h},
\end{aligned} \tag{3.62}$$

and $Z_j = 0$ for $j = 2, \cdots, m$ while after boundary correction $Z_1 = -\frac{\epsilon^2}{h}$. Finally, the system to be solved is

$$\begin{aligned}
\sigma_{0,0} &= \frac{\epsilon^2}{h}\left(\theta_0(0) - \int_0^{x_1} \theta_0' dx\right), \\
\sigma_{0,1} &= \frac{\epsilon^2}{h}\left(-(\theta_0(x_{\frac{3}{2}}) + \theta_0(0)) - (\int_0^{x_1} - \int_{x_1}^{x_2})\theta_0' dx\right) + h\alpha, \\
\sigma_{0,2} &= \frac{\epsilon^2}{h}\left(\theta_0(x_{\frac{3}{2}}) + (\int_{x_1}^{x_2} - \int_{x_2}^{x_3})\theta_0' dx\right), \\
\sigma_{j,j-1} &= \frac{\epsilon^2}{h}, \\
\sigma_{j,j} &= -\frac{2\epsilon^2}{h} + h\alpha, \ j = 1, \cdots, m, \\
\sigma_{j,j+1} &= \frac{\epsilon^2}{h},
\end{aligned} \tag{3.63}$$

The performance of the two schemes (3.6) and (3.63) are compared in Figures 3.1 and 3.2.

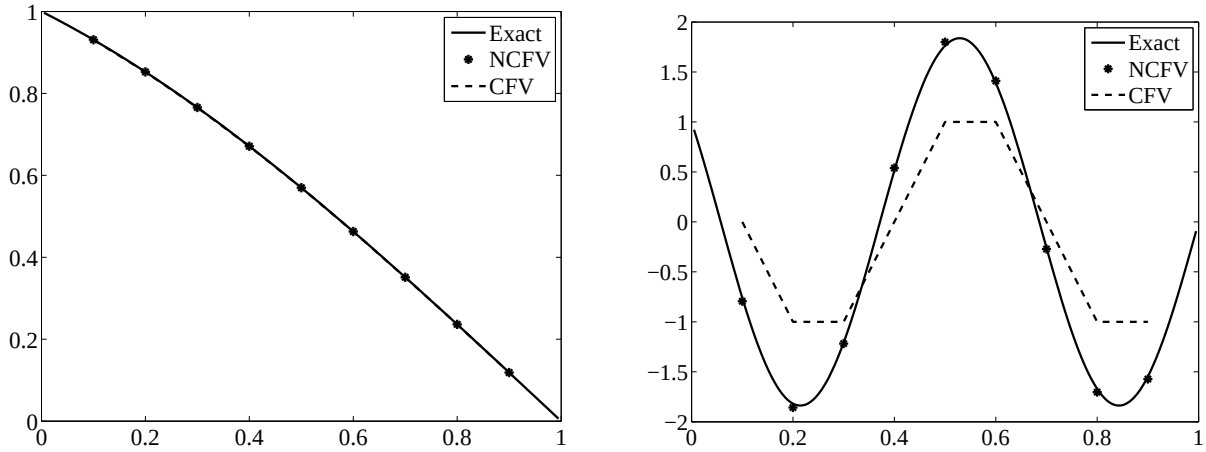

(a) Simulation at $\epsilon = 1$ (b) Simulation at $\epsilon = 0.1$

Figure 3.1: Comparison of the solution of the equation (3.50) as computed by the classical scheme and the new scheme on 10 grids and compared with the exact solution on 200 grids.

We also compare the approximation of the classical and the nonstandard finite volume schemes. The error computations are shown in Tables 3.1 and 3.2. The profile comparison are given in Figures 3.3 and 3.4.

3.3.1 Schrodinger equation

In this section we will apply the three schemes discussed in Section 3.2 to approximate the solution of the Schrodinger equation.

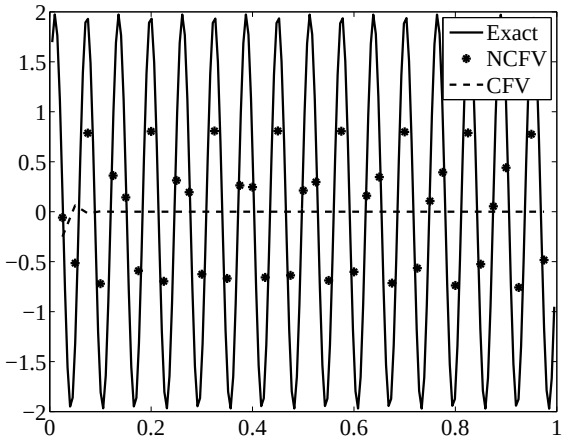

Figure 3.2: Comparison of the solution of the equation (3.50) as computed by the classical scheme and the new scheme on 40 grids and compared with the exact solution on 200 grids when $\epsilon = 0.01$.

Table 3.1: Error values of the nonstandard scheme and the classical scheme for different values of ϵ

Grid points	L_∞ Norm error					
	$\epsilon = 1$		$\epsilon = 0.1$		$\epsilon = 0.01$	
	CFV$\times 10^5$	NSFV$\times 10^{16}$	CFV	NSFV$\times 10^{15}$	CFV	NSFV$\times 10^{13}$
10	6.577	3.330	0.8186	4.4408	1.9626	910.3
20	1.650	5.551	0.2938	3.8580	1.9743	14.21
40	0.412	15.54	0.0806	18.20	1.9743	1.043
80	0.103	18.87	0.0208	37.74	3.0325	22.64

Table 3.2: Error values of the nonstandard scheme for different values of ϵ

Grid points	L_∞ Norm error		
	$\epsilon = 10^{-3}(\times 10^{13})$	$\epsilon = 10^{-4}(\times 10^{12})$	$\epsilon = 10^{-5}(\times 10^{8})$
10	1.165	2.695	1.137
20	1.150	2.819	1.138
40	94.48	2.684	1.137
80	1.066	2.864	1.138

Example 3.2 *Solve the Schrödinger equation*

$$\begin{cases} -\epsilon^2 u''(x) - q(x)u(x) &= 0, \quad 0 < x < 1, \\ \epsilon u'(0) + \imath p(0)u(0) &= 2\imath p(0), \\ \epsilon u'(1) &= \imath p(1)u(1), \end{cases} \tag{3.64}$$

where $p(x) = \sqrt{q(x)} > 0$ *and* $0 < \epsilon \ll 1$.

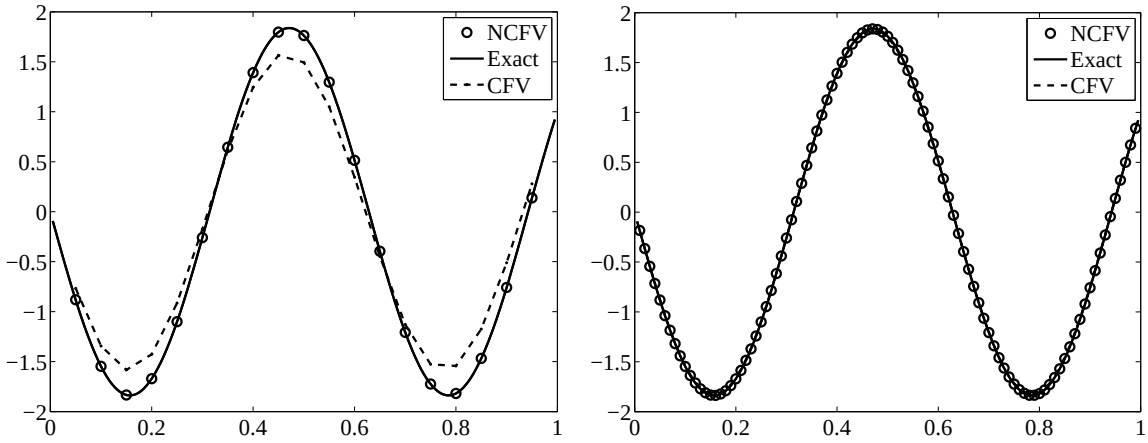

(a) Simulation on 20 grids with $\epsilon = 0.1$ (b) Simulation on 80 grids with $\epsilon = 0.1$

Figure 3.3: Comparison of the solution of equation (3.50) by the schemes (3.6) and (3.47)

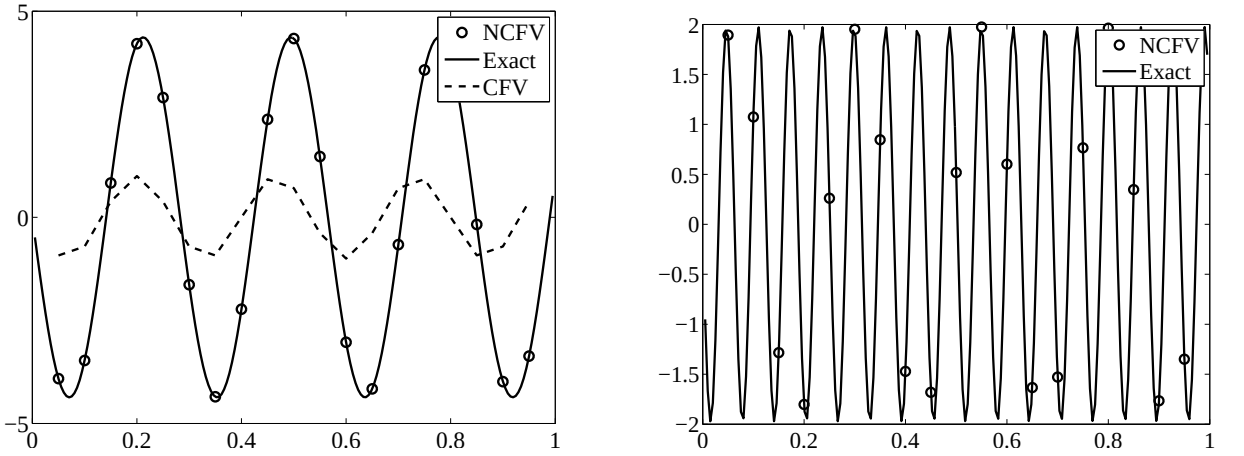

(a) Simulation on 20 grids with $\epsilon = 0.45 \times 10^{-1}$ (b) Simulation on 20 grids with $\epsilon = 1 \times 10^{-2}$

Figure 3.4: Comparison of the solution of equation (3.50) by the schemes (3.6) and (3.47)

It is well known that equation (3.64) is strongly oscillatory and even though appears simple, the presence of the small parameter ϵ has made it a very interesting problem over decades. Also, the relevance of the equation in quantum physics modeling is another reason for gaining attention over the years. Therefore, a lot of numerical analysis and simulation have been done on (3.64) based on finite difference (both classical and adaptive mesh), finite volume, finite element and WKB methods (for example see [8] and literatures therein). Perturbation methods have been very useful in the analysis of equations of this type, most especially, the WKB method, see [33]. Lately, numerical methods have been combined with such perturbation methods. For instance, WKB combined with or used as basis for finite element methods [59, 68]. It should be noted that effort to solve this equation are directed towards the design of cost effective scheme in term of computing memory usage and computing time.

Here, we will employ the classical, non classical and the nonstandard finite volume method as described above to solve (3.64).

3.3.1.1 Classical finite volume scheme for equation (3.64)

We follow the same approach as listed for the classical scheme in Section 3.2. Hence, for all $j's$, the classical scheme for equation (3.81) is

$$-\epsilon\frac{u_{j-1}-2u_j+u_{j+1}}{h}-u_j\int_{x_{j-\frac{1}{2}}}^{x_{j+\frac{1}{2}}}bdx=0. \tag{3.65}$$

The ghost points are taken cared of through the boundary conditions. The discretized form of the boundary conditions are

$$\epsilon(u_{\frac{1}{2}}-u_{-\frac{1}{2}})+\imath p(0)u_0=2\imath p(0), \tag{3.66}$$

at $x=0$ and

$$\epsilon(u_{m+\frac{1}{2}}-u_{m-\frac{1}{2}})-\imath p(1)u_m=0, \tag{3.67}$$

where the cell averages are approximated via the interpolation functions given in Section 3.2.

3.3.1.2 Non classical finite volume scheme for equation (3.64)

In order to resolve the in accurateness in the approximation given by the classical scheme, we design here a non classical scheme. as we did for the first example we appeal to the perturbation analysis of equation (3.64). The formal outer expansion based on the ansatz

$$u=\sum_{l=0}^{\infty}\epsilon^l u_l,$$

gives on substitution into (3.64)

$$\begin{cases} u_0(x)= & 0,\\ q(x)u_l(x)= & -u''_{l-1}(x),\ \ l>0. \end{cases} \tag{3.68}$$

At $x=0$ we have that

$$\sum_{l=0}^{\infty}\epsilon^{l+1}u_l(0)+\imath p(0)\sum_{l=0}^{\infty}\epsilon^l u_l(0)=2\imath p(0),$$

$$\sum_{l=1}^{\infty}\epsilon^l u_{l-1}(0)+\imath p(0)\sum_{l=1}^{\infty}\epsilon^l u_l(0)+\imath p(0)u_0(0)=2\imath p(0),$$

$$\begin{cases} u_0(0)= & 2,\\ u_l(0)= & -\frac{1}{\imath p(0)}u'_{l-1}(0),\ \ l>0. \end{cases} \tag{3.69}$$

Also, at $x = 1$

$$\sum_{l=0}^{\infty} \epsilon^{l+1} u_l(1) - \imath p(1) \sum_{l=0}^{\infty} \epsilon^k u_l(1) = 0,$$

$$\sum_{l=1}^{\infty} \epsilon^l u_{l-1}(1) + \imath p(1) \sum_{l=1}^{\infty} \epsilon^k u_l(1) + \imath p(1) u_0(1) = 0,$$

$$\begin{cases} u_0(1) = & 0, \\ u_l(1) = & \frac{1}{\imath p(1)} u'_{l-1}(1), \quad l > 0. \end{cases} \tag{3.70}$$

From equations (3.68), (3.69) and (3.70) it is observed that u_0 does not agree with the boundary condition $u_0(0) = 2$ while it satisfies $u_0(1) = 0$. This suggests there will be boundary layer issue at the boundary $x = 0$. In order to resolve this, following [38], we carry out an inner expansion at $x = 0$. We employ a formal asymptotic expansion at this boundary layer and Taylor expansion for $q(x)$ at $x = 0$,

$$u(x) \sim \textstyle\sum_{l=0}^{\infty} \epsilon^l \theta_l(\bar{x}), \quad \bar{x} = \frac{x}{\epsilon}, \tag{3.71}$$

and

$$q(x) \sim \sum_{l=0}^{\infty} \frac{q_l \bar{x}^l}{l!}, \tag{3.72}$$

where q_l is the l^{th} order derivative of q. Putting both (3.71) and (3.72) into (3.64), we have the leading order equation as

$$-\theta_0''(\bar{x}) - q_0 \theta_0(\bar{x}) = 0. \tag{3.73}$$

Remark 3.2 *The equation* (3.73) *is also a leading order equation near* $x = 0$ *for*

$$\epsilon^2 \theta''(x) + q_l \theta(x) = 0. \tag{3.74}$$

We now apply the WKB method to obtain the solution of (3.74). Note that our usage of the WKB approximation here is not the same as it was used in [1, 8, 59]. Here, the solution will only be employed as a corrector at the boundary. Using the ideas from [33], the first order WKB approximation to equation (3.74) is

$$\theta(x) \sim -q(x)^{\frac{1}{4}} \left(\alpha_0 e^{-\imath \frac{1}{\epsilon} \int^x \sqrt{q(s)} ds} + \alpha_1 e^{\imath \frac{1}{\epsilon} \int^x \sqrt{q(s)} ds} \right). \tag{3.75}$$

We determine the values of α_0 and α_1 via boundary conditions.

Now, following the same perturbation in the solution as done in the last problem, the boundary conditions of the Schrödinger equation becomes

$$\begin{cases} \epsilon u'(0) + \gamma \theta_x(0) + \imath p(0) u(0) + \imath p(0) \gamma \theta(0) = 2\imath p(0), \\ \epsilon u'(1) + \gamma \theta_x(1) = \imath p(1) u(1) + \imath p(1) \gamma \theta(1). \end{cases} \tag{3.76}$$

Now, we will multiply the Schrödinger equation by the function $\theta\chi[0, x_{\frac{3}{2}}]$ and integrate over $(0, 1)$. This leads to the equation

$$-\epsilon^2 u_x\theta\,|_0^{x_{\frac{3}{2}}} + \epsilon^2\int_0^{x_{\frac{3}{2}}} u_x\theta_x dx - \int_0^{x_{\frac{3}{2}}}\theta q dx = 0, \tag{3.77}$$

which we write in the form

$$\sigma_{00}\gamma + \sigma_{01}u_1 + \sigma_{02}u_2 = 0, \tag{3.78}$$

where, employing interpolation functions (3.4) and (3.5), we have

$$\sigma_{00} = \frac{\epsilon^2}{h}\theta(x_1)\left(\frac{\theta_x(a)h}{\alpha\epsilon} + \frac{\imath p(0)\theta(0)h}{\alpha\epsilon}\right),$$

$$\sigma_{01} = \frac{\epsilon^2}{h}\left(\theta(x_{\frac{3}{2}}) + \theta(x_1)\frac{\alpha\epsilon + 1 + \frac{\imath p(a)h}{2\epsilon}}{\alpha\epsilon}\right) - \int_0^{x_{\frac{3}{2}}} q\theta dx,$$

$$\sigma_{02} = -\frac{\epsilon^2}{h}\Big(\theta(x_{\frac{3}{2}}) - 2\theta(x_2) + \theta(x_1)\Big) - \int_{x_{\frac{3}{2}}}^{x_{\frac{5}{2}}} q\theta dx,$$

where

$$\alpha = \frac{\imath p(a)h}{2\epsilon} - 1.$$

This is done in order to find an extra equation through which the value of the extra parameter γ will be determined. Note that we have made use of the interpolation functions defined earlier in the last problem. Substituting

$$\tilde{u} = u_h + \gamma\theta, \tag{3.79}$$

into the Schrödinger equation (3.64) and integrating over each cell, we have

$$\sigma_{j,j-1}u_{j-1} + \sigma_{j,j}u_j + \sigma_{j,j+1}u_{j+1} = \tilde{Z}_j, \tag{3.80}$$

where $\tilde{Z}$ is zero everywhere except at $j = 1$ with $\tilde{Z}_1 = \frac{2\imath p(0)h\epsilon^2}{h(\frac{\imath p(0)h}{2\epsilon}-1)\epsilon}$ and

$$\begin{aligned}
\sigma_{1,0} &= -\frac{\epsilon^2}{h}\left(\frac{h}{\epsilon}\theta'(0) + \frac{h}{\epsilon}\theta(0)\right), \\
\sigma_{1,1} &= \frac{\epsilon^2}{h}\left(2 + \frac{1 + \frac{\imath p(0)h}{2\epsilon}}{\frac{\imath p(0)h}{2\epsilon} - 1}\right), \\
\sigma_{1,2} &= -\frac{\epsilon^2}{h}, \\
\sigma_{j,j-1} &= -\frac{\epsilon^2}{h}, \\
\sigma_{j,j} &= \frac{2\epsilon^2}{h} - \int_{x_{j-\frac{1}{2}}}^{x_{j+\frac{1}{2}}} q(x), \\
\sigma_{j,j+1} &= -\frac{\epsilon^2}{h}, \\
\sigma_{m,m-1} &= -\frac{\epsilon^2}{h}, \\
\sigma_{m,m} &= \frac{\epsilon^2}{h}\left(2 + \frac{1 + \frac{\imath p(1)h}{2\epsilon}}{\frac{\imath p(1)h}{2\epsilon} - 1}\right).
\end{aligned} \tag{3.81}$$

Finally, we will solve a linear system $\sigma u = \bar{Z}$ for $u = [\gamma, u_1, u_2, \cdots, u_m]$ given $\bar{Z} = [0, \tilde{Z}_j]$, where

$$
\begin{aligned}
\sigma_{00} &= \frac{\epsilon^2}{h}\theta(x_1)\left(\frac{\theta_x(a)h}{\alpha\epsilon} + \frac{ip(0)\theta(0)h}{\alpha\epsilon}\right),\\
\sigma_{01} &= \frac{\epsilon^2}{h}\left(\theta(x_{\frac{3}{2}}) + \theta(x_1)\frac{\alpha\epsilon + 1 + \frac{ip(0)h}{2\epsilon}}{\alpha\epsilon}\right) - \int_0^{x_{\frac{3}{2}}} q\theta dx,\\
\sigma_{02} &= -\frac{\epsilon^2}{h}\left(\theta(x_{\frac{3}{2}}) - 2\theta(x_2) + \theta(x_1)\right) - \int_{x_{\frac{3}{2}}}^{x_{\frac{5}{2}}} q\theta dx,\\
\sigma_{1,0} &= -\frac{\epsilon^2}{h}\left(\frac{h}{\epsilon}\theta'(0) + \frac{h}{\epsilon}\theta(0)\right),\\
\sigma_{1,1} &= \frac{\epsilon^2}{h}\left(2 + \frac{1 + \frac{ip(0)h}{2\epsilon}}{\frac{ip(0)h}{2\epsilon} - 1}\right),\\
\sigma_{1,2} &= -\frac{\epsilon^2}{h},\\
\sigma_{j,j-1} &= -\frac{\epsilon^2}{h},\\
\sigma_{j,j} &= \frac{2\epsilon^2}{h} - \int_{x_{j-\frac{1}{2}}}^{x_{j+\frac{1}{2}}} q(x),\\
\sigma_{j,j+1} &= -\frac{\epsilon^2}{h},\\
\sigma_{m,m-1} &= -\frac{\epsilon^2}{h},\\
\sigma_{m,m} &= \frac{\epsilon^2}{h}\left(2 + \frac{1 + \frac{ip(1)h}{2\epsilon}}{\frac{ip(1)h}{2\epsilon} - 1}\right).
\end{aligned}
\tag{3.82}
$$

Remark 3.3 *The Scheme* (3.81) *gives the classical finite volume when* $\gamma = 0$ *otherwise, NCFV scheme.*

We ran the numerical experiment on this with $q(x) = (x+1/2)^2\ \forall x \in [0,1]$. The convergence and the behavior of the solution for different values of ϵ are shown in the Figures 3.5 and 3.6.

Remark 3.4 *The rate of convergence is* $\sim O(h^{1.56})$ *for both schemes. When* $\epsilon \leq 0.02$ *error due to the classical scheme becomes significant and the rate of convergence becomes non-uniform.*

Remark 3.5 *We observe uniform convergence rate of* $O(h^{1.56})$ *with the new scheme while the convergence rate due to the classical scheme is not uniform, in fact it is* $\epsilon-$*dependent.*

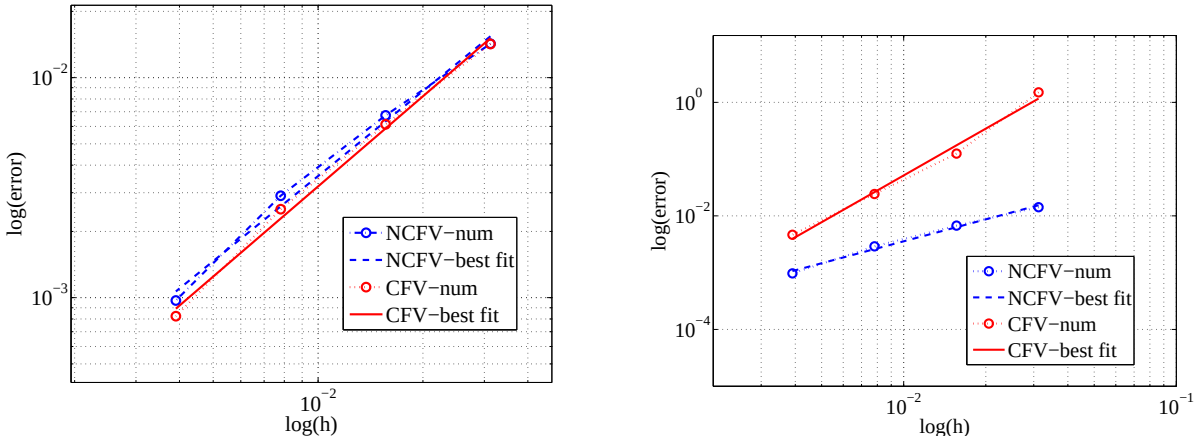

(a) Simulation at $\epsilon = 2 \times 10^{-1}$ (b) Simulation at $\epsilon = 2 \times 10^{-2}$

Figure 3.5: The slope of the lines say $r = \frac{\Delta(\log(error))}{\Delta(\log(h))}$ represents the convergence rate due to each scheme. The approximation on $32, 64, 128, 256$ elements grid are compared with a reference solution on 512 element grid.

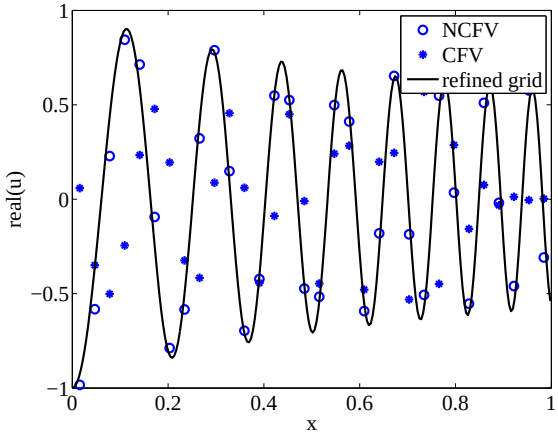

Figure 3.6: Comparison of the solution of the equation (3.64) between the classical scheme and the new scheme. Solution was computed with $\epsilon = 2 \times 10^{-2}$ on 32 element grid.

3.3.1.3 Nonstandard finite volume scheme for equation (3.64)

Here, we design the nonstandard finite volume schemes designed in the previous section to equation (3.64). We need to derive an exact scheme to handle the boundary equations. We therefore, follow the same procedure that was highlighted above for first order equations at the boundary. At the boundary $x = 0$,

$$u' + \frac{\imath p(0)}{\epsilon} u = \frac{2\imath p(0)}{\epsilon}. \tag{3.83}$$

Multiply by the integrating factor, $\exp(\frac{\imath p(0)}{\epsilon}x)$, and integrate. This yields

$$\frac{d}{dx}\left(u\exp(\frac{\imath p(0)}{\epsilon}x)\right) = \frac{2\imath p(0)}{\epsilon}\exp(\frac{\imath p(0)}{\epsilon}x),$$

$$u\exp(\frac{\imath p(0)}{\epsilon}x) = 2\exp(\frac{\imath p(0)}{\epsilon}x) + c,$$

where c is an arbitrary constant of integration. This gives

$$u = 2 + c\exp(-\frac{\imath p(0)}{\epsilon}x).$$

$c = \phi(0) - 2$ given that $\phi(0)$ is the initial condition. By this, the difference scheme will be

$$u_j = 2 + (u_{j-1} - 2)\exp(-\frac{\imath p(0)}{\epsilon}h).$$

Then,

$$u_j - u_{j-1} = 2 + (u_{j-1} - 2)\exp(-\frac{\imath p(0)}{\epsilon}h) - u_{j-1},$$

$$u_j - u_{j-1} = 2(1 - \exp(-\frac{\imath p(0)}{\epsilon}h)) - u_{j-1}(1 - \exp(-\frac{\imath p(0)}{\epsilon}h)).$$

Hence, the scheme at the boundary $x = 0$ is,

$$\epsilon\frac{u_j - u_{j-1}}{\frac{\epsilon}{\imath p(0)}(1 - \exp(-\frac{\imath p(0)}{\epsilon}h))} + \imath p(0)u_{j-1} = 2\imath p(0). \tag{3.84}$$

Following the same procedure at the boundary $x = 1$, we have

$$\frac{u'}{u} = \frac{\imath p(1)}{\epsilon},$$

$$\ln(u) = \frac{\imath p(1)}{\epsilon}x + c,$$

c is just an arbitrary constant of integration. This gives

$$u = Ae^{\frac{\imath p(1)x}{\epsilon}},$$

A is determined through the initial condition and we have

$$u = u_0 e^{\frac{\imath p(1)x}{\epsilon}}.$$

Therefore, a corresponding general difference solution at this boundary will be

$$u_{j+1} = u_k e^{\frac{\imath p(1)h}{\epsilon}}.$$

Then,

$$u_{j+1} - u_j = u_j(e^{\frac{\imath p(1)h}{\epsilon}} - 1),$$

and exact difference scheme for the boundary condition at $x = 1$ is

$$\epsilon \frac{u_{j+1} - u_j}{\frac{\epsilon}{\imath p(1)}(e^{\frac{\imath p(1)h}{\epsilon}} - 1)} = \imath p(1) u_j. \tag{3.85}$$

From the equation (3.84) and (3.85) the values of u_{-1} and u_{m+1} are estimated.

Now we design the scheme for $x \in (0, 1)$. If we integrate the Schrödinger equation (3.64) and let

$$\mathbb{F}_j = \int_{x_{j-\frac{1}{2}}}^{x_{j+\frac{1}{2}}} q(x)dx,$$

then the nonstandard finite volume scheme follows directly from Section 3.2. The entire scheme results into solving system of linear algebraic equations. The entries of the sparse tridiagonal matrix constructed is given below:

$$\begin{aligned}
A_{1,1} &= \frac{2}{\tilde{\phi}_1^2} - \frac{\exp(\frac{\imath p(a)}{\epsilon}h)}{\tilde{\phi}_1} + \mathbb{F}_1, \\
A_{1,2} &= -\frac{1}{\tilde{\phi}_1^2}, \\
A_{j,j-1} &= -\frac{1}{\tilde{\phi}_{j-1}^2}, \\
A_{j,j} &= \frac{2}{\tilde{\phi}_j^2} - \mathbb{F}_j, \\
A_{j,j+1} &= -\frac{1}{\tilde{\phi}_{j+1}^2}, \\
A_{m,m-1} &= -\frac{1}{\tilde{\phi}_m^2}, \\
A_{m,m} &= \frac{2}{\tilde{\phi}_m^2} - \frac{\exp(\frac{\imath p(b)}{\epsilon}h)}{\tilde{\phi}_m} + \mathbb{F}_m,
\end{aligned} \tag{3.86}$$

(3.87)

where,

$$\tilde{\phi}_j = \frac{2\epsilon}{\sqrt{\mathbb{F}_j}} \sin\left(h\sqrt{\frac{\mathbb{F}_j}{4\epsilon^2}}\right).$$

Our numerical experiments and observations are shown in Table 3.3 and Figures 3.7 to 3.8.

3.4 Conclusion

We investigated singularly perturbed second order ordinary differential equations via two different methods. Firstly, we employed the semi-analytical method as proposed in [37, 70]

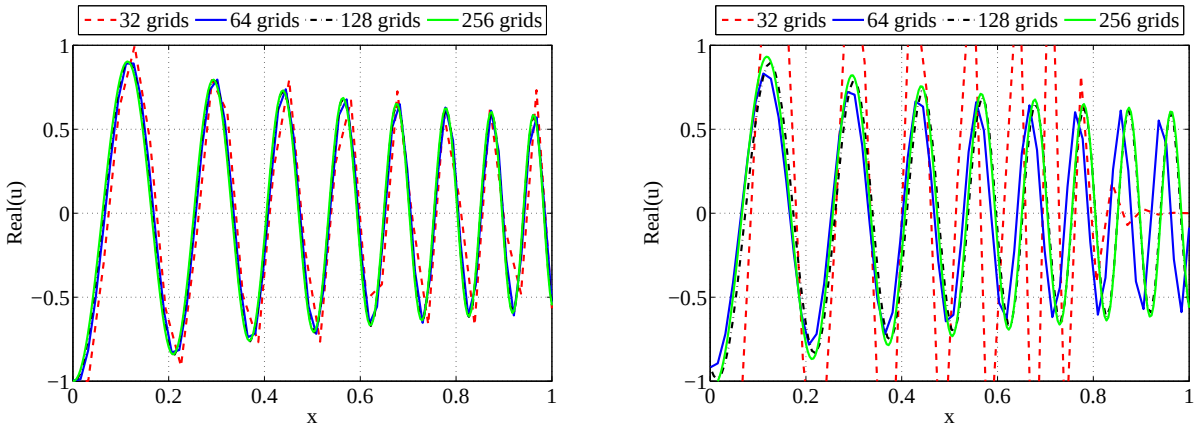

(a) NSFD Simulation (b) Classical Simulation

Figure 3.7: Convergence of the simulations with, $\epsilon = 1 \times 10^{-2}$ and several grid choices.

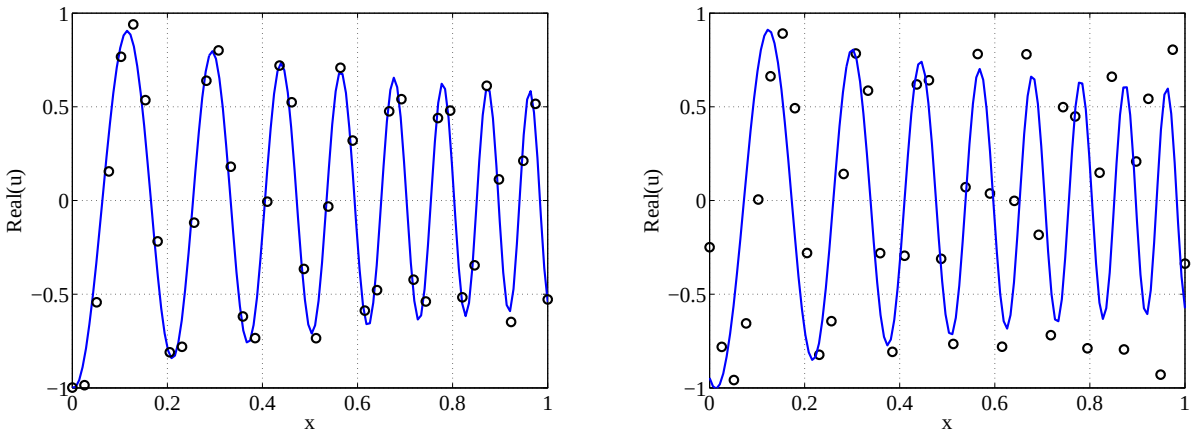

(a) NSFD Simulation (b) Classical Simulation

Figure 3.8: Comparison of the solution of the Schrödinger equation (3.64) on 40 grid nodes (dots) and 512 grid nodes (solid line) with $\epsilon = 2 \times 10^{-2}$.

Table 3.3: Error between the solution at different grid points as compared with a reference solution at 256 grid points

Grid points	L_∞ Norm error					
	$\epsilon = 0.2$		$\epsilon = 0.1$		$\epsilon = 0.02$	
	CFV	NSFV	CFV	NSFV	CFV	NSFV
16	0.1702	0.0407	0.4025	0.0412	2.2942	1.9891
32	0.0814	0.0204	0.2213	0.0278	1.5878	0.1154
64	0.0343	0.0091	0.1104	0.0151	0.1578	0.0146
128	0.0100	0.0031	0.0441	0.0056	0.0207	0.0037

to solve equation (3.50). Figures 3.1 and 3.2 show the better performance of the non classical schemes even when ϵ is small with relatively small number of grids. This motivates us to extend the scheme to approximate the Schrödinger equation which is more complicated because the boundary condition is defined on a complex plane. Figure 3.5 shows the convergence rate obtained for different grids when $\epsilon = 0.2$ and 0.02 using the solution at 128 grid points as reference solution. It is clearly seen that the new scheme converges better than the classical scheme. Also, the approximation at 16 grids compared with the reference solution when $\epsilon = 0.02$ proves a better performance of the new scheme as shown in Figure 3.6.

The second part of the chapter employed a non standard finite volume scheme to the same equations as above. The table of errors, Tables 3.1 and 3.2, reveals a better performance of this new scheme as compared with the classical scheme for very small ϵ. This is also verified in Figures 3.3 and 3.4. This non standard scheme approximates the solution almost exactly. When this scheme is applied to the Schrödinger equation, Figure 3.7 shows the convergence of approximations at different grid points to a reference solution. The new scheme is shown to perform better at less number of grids than the classical one. This is also justified in table of errors, Table 3.3.

Chapter 4

Nonclassical methods for higher order equations

In this chapter, we design a nonstandard finite volume scheme for fourth order equations and test the application of the schemes by seeking numerical solution of the Kuramoto-Sivashinsky (K-S) and the Cahn-Hilliard (CH) equations.

4.1 Introduction

We design an explicit nonstandard finite volume (NSFV) schemes each for the K-S and CH equations investigated in Chapter 2 by the fractional splitting method. The schemes follow the idea of nonstandard finite volume method discussed in Chapter 3. Our numerical algorithm makes use of the a finite volume scheme for the hyperbolic equation and nonstandard schemes for the nonlinear diffusion and the fourth order linear equations. The nonstandard schemes were designed following the rules in [57].

As discussed in Chapter 3, the nonstandard finite difference methods has the advantage of preserving the properties of the physical models in that it preserves positivity and monotonicity of the solution. It has been employed in approximating various differential equations of orders not more than 3. Here, we extend it to approximate the solution of fourth order PDEs. We achieve this by designing nonstandard schemes for the sub-equations that make up these higher order equations. This idea was employed earlier in solving the viscous Burger's equation and advection-logistic equation among others, see [57]. The sub-equations of the CH and K-S equations are the inviscid Burger's equation , the porous media equation and the linear fourth order equation. Therefore, we design nonstandard schemes for each of these equations.

Denoting the solution operators $\mathcal{H}_k$, $\mathcal{N}_k$ and $\mathcal{L}_k$ for the inviscid Burger's, porous media and the linear fourth order equations respectively, we apply the fractional time splitting algorithm to approximate the solution of the K-S and the CH equations. Giving $v^0 = u_0$ for

$n = 0$; for $n > 0$, we obtain v^{n+1} from v^n via the solution of

$$v_k(x, nk) = [\mathcal{L}_k \circ \mathcal{H}_k]^n v_0(x), \tag{4.1}$$

for the K-S equation,

$$v_k(x, nk) = [\mathcal{L}_k \circ \mathcal{N}_k]^n v_0(x), \tag{4.2}$$

for the CH equation and

$$v_k(x, nk) = [\mathcal{L}_k \circ \mathcal{N}_k \circ \mathcal{H}_k]^n v_0(x), \tag{4.3}$$

convective CH equation. In Section 4.2, we use the subequation approach to design the NSFV scheme for each of the equations and in Section 4.3, the performance of all the schemes were tested and our observations were discussed in Section 4.4.

4.2 Numerical approach

We are interested in designing nonstandard finite volume schemes for the inviscid Burger's equation, porous media equation (PME) and the linear fourth equations which are components of either the K-S or CH equations. Recall that for $h = \Delta x = x_{j+\frac{1}{2}} - x_{j-\frac{1}{2}}$, $j = 0, 1, \cdots, m$ and $k = t^n - t^{n-1}$, $n = 1, 23, \cdots$, the intercell average

$$v^n \sim \frac{1}{\Delta x} \int_{x_{j-\frac{1}{2}}}^{x_{j+\frac{1}{2}}} u(x, t^n) dx.$$

4.2.1 The inviscid Burger's equation

In this section, we present the nonstandard scheme for the inviscid Burger's equation

$$u_t + \delta \left(\frac{u^2}{2} \right)_x = 0. \tag{4.4}$$

Integrating this first, with respect to x in $I = [x_{j-\frac{1}{2}}, x_{j+\frac{1}{2}}]$ and later with respect to time and employing the interpolation functions discussed in preceding chapters, we have

$$\frac{v_j^{n+1} - v_j^n}{\Delta t} + \delta \frac{v_{j+1}^n + v_{j-1}^n}{2} \left(\frac{v_{j+1}^n - v_{j-1}^n}{2\Delta x} \right) = 0. \tag{4.5}$$

An alternative approximation is the 3-point averaging used in [92] for the numerical approx of the KdV equation. Here the schemes is given by

$$\frac{v_j^{n+1} - v_j^n}{\Delta t} + \delta \frac{v_{j+1}^n + v_j^n + v_{j-1}^n}{3} \left(\frac{v_{j+1}^n - v_{j-1}^n}{2\Delta x} \right) = 0. \tag{4.6}$$

4.2.2 The porous media equation

Here, we design a nonstandard scheme for the porous media equation

$$u_t = \alpha(u^p)_{xx}$$

in one-dimension.The nonstandard scheme for this equation is given as

$$\frac{v_j^{n+1} - v_j^n}{\Delta t} = r\alpha \frac{1}{\Delta x^2}\left(f^n_{j+\frac{1}{2}} v^n_{j+1} - (f^n_{j+\frac{1}{2}} + f^n_{j-\frac{1}{2}})v_j^{n+1} + f^n_{j-\frac{1}{2}} v^n_{j-1}\right), \tag{4.7}$$

where the average

$$f_{j+\frac{1}{2}} = \frac{f_{j+1} + f_j}{2},$$

and $f_j^n = (u_j^n)^{r-1}$. The scheme (4.7) is non consistent but can be made conditionally consistent. This is achieved as

$$\frac{v_j^{n+1} - v_j^n}{\Delta t} = \frac{r\alpha}{\Delta x^2}\left(f^n_{j+\frac{1}{2}} v^n_{j+1} - (f^n_{j+\frac{1}{2}} + f^n_{j-\frac{1}{2}})v_j^{n+1} + f^n_{j-\frac{1}{2}} v^n_{j-1}\right) + \frac{r\alpha}{\Delta x^2}(f^n_{j+\frac{1}{2}} + f^n_{j-\frac{1}{2}})(v_j^{n+1} - v_j^n),$$

which implies that

$$\left(1 - r\alpha\lambda(f^n_{j+\frac{1}{2}} + f^n_{j-\frac{1}{2}})\right)(v_j^{n+1} - v_j^n) = r\alpha\lambda\left(f^n_{j+\frac{1}{2}} v^n_{j+1} - (f^n_{j+\frac{1}{2}} + f^n_{j-\frac{1}{2}})v_j^{n+1} + f^n_{j-\frac{1}{2}} v^n_{j-1}\right), \tag{4.8}$$

which gives

$$v_j^{n+1} = v_j^n + r\alpha\lambda\left(f^n_{j+\frac{1}{2}} v^n_{j+1} + (f^n_{j+\frac{1}{2}} + f^n_{j-\frac{1}{2}})v_j^n + f^n_{j-\frac{1}{2}} v^n_{j-1}\right),$$

where $\lambda = \frac{\Delta t}{\Delta x^2}$. By this, we have to re-scale the time derivative of the target equation by

$$1 - r\alpha\lambda(f^n_{j+\frac{1}{2}} + f^n_{j-\frac{1}{2}}),$$

for consistency. We employ this scheme to solve porous media equation when $r = 3$,

$$u_t = \alpha(u^3)_{xx} = 3\alpha(u^2 u_x)_x = 3\alpha(f(u)u_x)_x = 0. \tag{4.9}$$

4.2.3 The linear fourth order equation

Our focus here is to derive a nonstandard scheme for the equation

$$u_t(x,t) + (u(x,t) + u(x,t)_{xx})_{xx} = 0, \quad u(x,0) = u_0(x). \tag{4.10}$$

In doing this we will follow the rules and the procedures highlighted in [57, 58]. The steady state of equation (4.10) is the linear homogeneous equation

$$(u + \gamma^2 u_{xx})_{xx} = 0, \tag{4.11}$$

which admits four linearly independent solutions γ, $\frac{x}{\gamma}$, $e^{\imath h\frac{x}{\gamma}}$ and $e^{-\imath h\frac{x}{\gamma}}$. From this we know that

$$\begin{vmatrix} u_j & 1 & hj & e^{\imath j\frac{h}{\gamma}} & e^{-\imath j\frac{h}{\gamma}} \\ u_{j+1} & 1 & h(j+1) & e^{\imath\frac{h}{\gamma}(j+1)} & e^{-\imath\frac{h}{\gamma}(j+1)} \\ u_{j+2} & 1 & h(j+2) & e^{\imath\frac{h}{\gamma}(j+2)} & e^{-\imath\frac{h}{\gamma}(j+2)} \\ u_{j+3} & 1 & h(j+3) & e^{\imath\frac{h}{\gamma}(j+3)} & e^{-\imath\frac{h}{\gamma}(j+3)} \\ u_{j+4} & 1 & h(j+4) & e^{\imath\frac{h}{\gamma}(j+4)} & e^{-\imath\frac{h}{\gamma}(j+4)} \end{vmatrix} = 0. \tag{4.12}$$

This simplifies to give

$$h\begin{vmatrix} u_j & 1 & j & 1 & 1 \\ u_{j+1} & 1 & j+1 & e^{\imath\frac{h}{\gamma}} & e^{-\imath\frac{h}{\gamma}} \\ u_{j+2} & 1 & j+2 & e^{2\imath\frac{h}{\gamma}} & e^{-2\imath\frac{h}{\gamma}} \\ u_{j+3} & 1 & j+3 & e^{3\imath\frac{h}{\gamma}} & e^{-3\imath\frac{h}{\gamma}} \\ u_{j+4} & 1 & j+4 & e^{4\imath\frac{h}{\gamma}} & e^{-4\imath\frac{h}{\gamma}} \end{vmatrix} = 0.$$

This can be written as

$$\begin{vmatrix} 1 & u_j & j & 1 & 1 \\ 1 & u_{j+1} & j+1 & e^{\imath\frac{h}{\gamma}} & e^{-\imath\frac{h}{\gamma}} \\ 1 & u_{j+2} & j+2 & e^{2\imath\frac{h}{\gamma}} & e^{-2\imath\frac{h}{\gamma}} \\ 1 & u_{j+3} & j+3 & e^{3\imath\frac{h}{\gamma}} & e^{-3\imath\frac{h}{\gamma}} \\ 1 & u_{j+4} & j+4 & e^{4\imath\frac{h}{\gamma}} & e^{-4\imath\frac{h}{\gamma}} \end{vmatrix} = 0.$$

Factorization leads to

$$-\begin{vmatrix} 2u_{j+1}-u_{j+2}-u_j & 2e^{\imath\frac{h}{\gamma}}-e^{2\imath\frac{h}{\gamma}}-1 & 2e^{-\imath\frac{h}{\gamma}}-e^{-2\imath\frac{h}{\gamma}}-1 \\ 3u_{j+1}-u_{j+3}-2u_j & 3e^{\imath\frac{h}{\gamma}}-e^{3\imath\frac{h}{\gamma}}-2 & 3e^{-\imath\frac{h}{\gamma}}-e^{-3\imath\frac{h}{\gamma}}-2 \\ 4u_{j+1}-u_{j+4}-3u_j & 4e^{\imath\frac{h}{\gamma}}-e^{4\imath\frac{h}{\gamma}}-3 & 4e^{-\imath\frac{h}{\gamma}}-e^{-4\imath\frac{h}{\gamma}}-3 \end{vmatrix} = 0.$$

The determinant can be simplified to

$$\begin{aligned} &(2u_{j+1}-u_{j+2}-u_j)(3e^{\imath\frac{h}{\gamma}}-e^{3\imath\frac{h}{\gamma}}-2)(4e^{-\imath\frac{h}{\gamma}}-e^{-4\imath\frac{h}{\gamma}}-3) \\ &-(2u_{j+1}-u_{j+2}-u_j)(3e^{-\imath\frac{h}{\gamma}}-e^{-3\imath\frac{h}{\gamma}}-2)(4e^{\imath\frac{h}{\gamma}}-e^{4\imath\frac{h}{\gamma}}-3) \\ &+(3u_{j+1}-u_{j+3}-2u_j)(2e^{-\imath\frac{h}{\gamma}}-e^{-2\imath\frac{h}{\gamma}}-1)(4e^{\imath\frac{h}{\gamma}}-e^{4\imath\frac{h}{\gamma}}-3) \\ &-(3u_{j+1}-u_{j+3}-2u_j)(2e^{\imath\frac{h}{\gamma}}-e^{2\imath\frac{h}{\gamma}}-1)(4e^{-\imath\frac{h}{\gamma}}-e^{-4\imath\frac{h}{\gamma}}-3) \\ &+(4u_{j+1}-u_{j+4}-3u_j)(2e^{\imath\frac{h}{\gamma}}-e^{2\imath\frac{h}{\gamma}}-1)(3e^{-\imath\frac{h}{\gamma}}-e^{-3\imath\frac{h}{\gamma}}-2) \\ &-(4u_{j+1}-u_{j+4}-3u_j)(2e^{-\imath\frac{h}{\gamma}}-e^{-2\imath\frac{h}{\gamma}}-1)(3e^{\imath\frac{h}{\gamma}}-e^{3\imath\frac{h}{\gamma}}-2). \end{aligned}$$

Appealing to the identity

$$\sin(\theta) = \frac{e^{\imath\theta}-e^{-\imath\theta}}{2\imath},$$

the equation when simplified, after shifting the index j, gives

$$\frac{u_{j-2}-4u_{j-1}+6u_j-4u_{j+1}+u_{j+2}}{\phi(h)^4} + \frac{u_{j-1}-2u_j+u_{j+1}}{\phi(h)^2} = 0, \tag{4.13}$$

where

$$\phi(h) = 2\gamma \sin\left(\frac{h}{2\gamma}\right).$$

Equation (4.13) is the nonstandard finite difference scheme for equation (4.11). The nonstandard scheme for the fourth order time dependent equation (4.10) is therefore, using Euler method to integrate with respect to time

$$\frac{u_j^{n+1} - u_j^n}{\Delta t} + \gamma^2 \frac{u_{j-2}^n - 4u_{j-1}^n + 6u_j^n - 4u_{j+1}^n + u_{j+2}^n}{\phi(h)^4} + \frac{u_{j-1}^n - 2u_j^n + u_{j+1}^n}{\phi(h)^2} = 0. \tag{4.14}$$

Equation (4.14), leads to an explicit scheme

$$u_j^{n+1} = u_j^n - \frac{\gamma^2 \Delta t}{\phi(h)^4}\left(u_{j-2}^n - 4u_{j-1}^n + 6u_j^n - 4u_{j+1}^n + u_{j+2}^n\right) - \frac{\Delta t}{\phi(h)^2}\left(u_{j-1}^n - 2u_j^n + u_{j+1}^n\right). \tag{4.15}$$

Now, we will adapt the NSFD scheme discussed above to a finite volume scheme for equation (4.10). As usual, we multiply equation (4.10) by a characteristic function $\chi_{(x_{j-\frac{1}{2}}, x_{j+\frac{1}{2}})}(x)$ and then integrate within each cell. This gives us

$$\frac{v_j^{n+1} - v_j^n}{\Delta t} + \gamma^2 \frac{v_{j-2}^n - 4v_{j-1}^n + 6v_j^n - 4v_{j+1}^n + v_{j+2}^n}{\phi(h)^3} + \frac{v_{j-1}^n - 2v_j^n + v_{j+1}^n}{\phi(h)} = 0, \tag{4.16}$$

for $j = 2, 3, \cdots, m-2$, where we have used the interpolation functions

$$u \sim u_h = \sum_{j=0}^{m} u_j \chi_{(x_{j-\frac{1}{2}}, x_{j+\frac{1}{2}})}(x),$$

$$u_x \sim \nabla u_h = \sum_{j=0}^{m} \frac{u_{j+1} - u_j}{h} \chi_{(x_{j-\frac{1}{2}}, x_{j+\frac{1}{2}})}(x),$$

and

$$u_{xxx} \sim \nabla^3 u_h = \sum_{j=0}^{m} \frac{-u_{j-1} + 3u_j - 3u_{j+1} + u_{j+2}}{h^3} \chi_{(x_{j-\frac{1}{2}}, x_{j+\frac{1}{2}})}(x).$$

The solution approximations at $j = 0, 1$ and $j = m-1, m$ are addressed by employing the given boundary conditions. The replacement of h by $\phi(h)$ makes sense since $\lim_{h\to 0} \phi(h) \to h$.

4.3 Numerical experiments

We will demonstrate the performance of all the schemes designed and discussed above. We will start with the nonlinear porous media, the linear fourth order, the K-S, the CH and the convective CH equations.

4.3.1 The porous media equation

We carried out the following experiment in order to test the performance of the scheme (4.7).

Example 4.1 *Solve the porous media equation*

$$\begin{cases} u_t = (u^3)_{xx}, \ x \in [-6, 6], \\ u(-6, t) = u(6, t) = 0, \\ u(x, 1) = u_0(x). \end{cases} \tag{4.17}$$

We compare our results with the famous Barenblatt solution of the porous media equation

$$u_3(x, t) = t^{\frac{1}{4}} \sqrt{[1 - \frac{|x|^2}{12\sqrt{t}}]_+}, \ t > 0,$$

at time $T = 2$, where $[.]_+ = \max(., 0)$. Taking $\lambda = \frac{k}{h^2}$, Figure 4.1 shows the convergence of the scheme (4.7) as $k \to 0$.

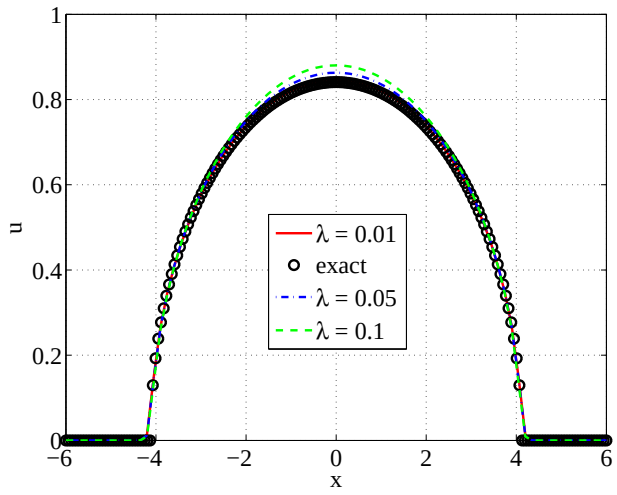

Figure 4.1: Solution profile of equation (4.17)

Remark 4.1 *Here, we did not solve Example 4.1 by* (4.8). *We observe that as long as* $0 < u_j^n < 1$, *then* $f_j^n \ll 1$ *by which it is obvious that equation* (4.7)∼(4.8). *Also, we note that the solution profile when* $\lambda = 0.01$ *coincides with the exact solution profile.*

4.3.2 The linear fourth order equation

In order for us to check the efficiency of the scheme (4.16) we perform the experiment below.

Example 4.2 *Solve the equation*

$$\begin{cases} u_t(x,t) + (u(x,t) + \gamma^2 u_{xx}(x,t))_{xx} &= 0, \\ u(x+L,t) &= u(x,t), \\ u(x,0) &= \sin(x), \end{cases} \tag{4.18}$$

where we have chosen $\gamma = 1$.

The error computation for the classical finite volume (where ϕ is replaced by h), the BDF2 and nonstandard schemes (4.16) are compared in Table 4.1. The numerical solution is compared with the steady state exact solution $u(x,t) = \sin(x)$.

Table 4.1: Error computations for Example 4.2

Grid points	L_∞ Norm error		
	Classical ($error \times 10^4$)	NSFV ($error \times 10^{16}$)	BDF ($error \times 10^2$)
10	150.1	2.220	
20	40.71	1.665	15.91
40	10.26	6.661	7.923
80	2.568	4.441	3.951

Example 4.3 *Apply the scheme* (4.16) *to approximate the solution of*

$$\begin{cases} u_t(x,t) + (u(x,t) + \gamma^2 u_{xx}(x,t))_{xx} &= 0, \\ u(x+L,t) &= u(x,t), \\ u(x,0) &= \exp(-x^2), \end{cases} \tag{4.19}$$

and show the behaviour of the mean energy

$$\mathcal{E}(t) = \frac{1}{L}\int_0^L u(x,t)^2 dx, \tag{4.20}$$

in time.

Solving the above problem, we observe the exponential growth of the mean energy in time as expected [24]. This is shown in Figure 4.3(a).

4.3.3 Kuramoto-Sivashinsky equation

In this section we consider the Kuramoto-Sivashinsky equation

$$\begin{cases} u_t + uu_x + u_{xx} + u_{xxxx} = 0, \quad \forall\ (x,t) \in (-L,L) \times (0,T], \\ u(x,0) = g(x,0). \end{cases} \tag{4.21}$$

Throughout this section, we employ the fractional splitting scheme (4.1) and use schemes (4.6) and (4.16) to approximate the solutions of the inviscid Burger's and the linear sub-problems respectively.

Example 4.4 *Solve equation* (4.21) *by the fractional splitting scheme* (4.1).

1.
$$u(-L,t)=g(-L,t),\quad u(L,t)=g(L,t),\quad u_x(-L,t)=g_x(-L,t),\quad u_x(L,t)=g_x(L,t), \tag{4.22}$$
where $g(x,t)$ *is the exact solution given by*
$$g(x,t)=c+\frac{15}{19}\sqrt{\frac{11}{19}}(-9\tanh[l(x-ct-x_0)]+11\tanh^3[l(x-ct-x_0)]), \tag{4.23}$$
and c, l *and* x_0 *are constants. In the computations we take* $L=30$, $x_0=-12$, $c=5$ *and* $l=\sqrt{11/19}/2$ *as documented in [7, 89].*

2. *periodic boundary condition and initial condition*
$$u(x,0)=\exp(-x^2).$$

The errors due to the scheme (4.1) are shown in Table 4.2 while the solution profile for the boundary condition (4.22) and the chaotic property of equation (4.21) due to periodic boundary condition are shown in Figures 4.2(a) and 4.2(b) respectively.

Table 4.2: Error computations for Example 4.4_1

Grids	Errors$\times 10^2$	rate of convergence
40	474.3	
80	99.87	2.2
160	12.84	2.9
320	2.891	2.1

Remark 4.2 *The major contribution to this error is coming from the solver for the hyperbolic sub-problem. The error due to the scheme for the linear equation is shown in Table 4.1.*

Example 4.5 *Solve equation* (4.21) *subject to periodic boundary condition and initial condition* $u(x,0)=\sin(x)$ *by the fractional splitting scheme* (4.1).

Here, we verify the bounds on the mean energy $(L\mathcal{E})^{\frac{1}{2}}$ as was done in Chapter 2. The scheme reproduces the bound that has been established in the literatures on the Kuramoto-Sivashinsky equation (4.21) as discussed in Chapter 2, this is shown in Figure 4.3(b). We note that the slope of this graph is 0.978.

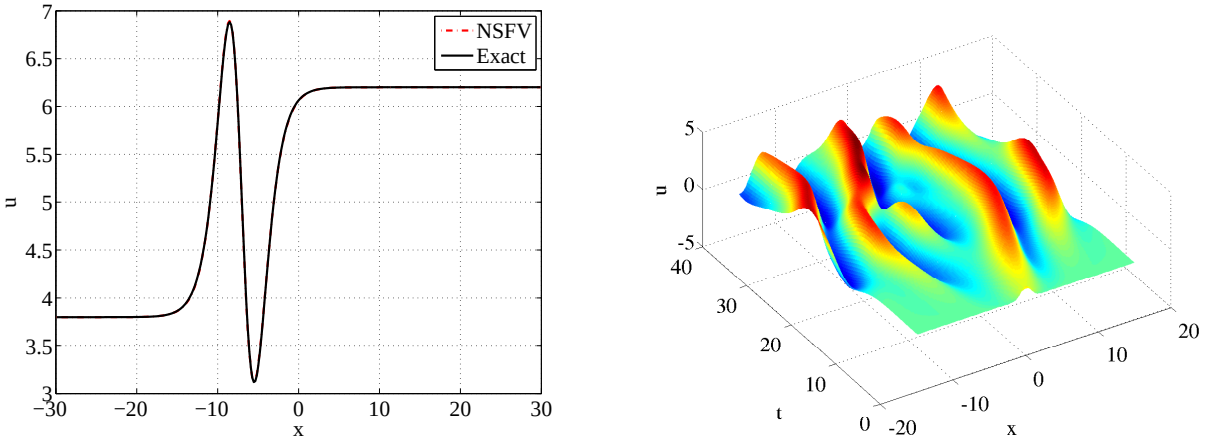

(a) Solution on a non periodic domain (b) Chaotic Solution on a periodic domain

Figure 4.2: Solution of the Kuramoto-Sivashinsky equation by the NSFV scheme.

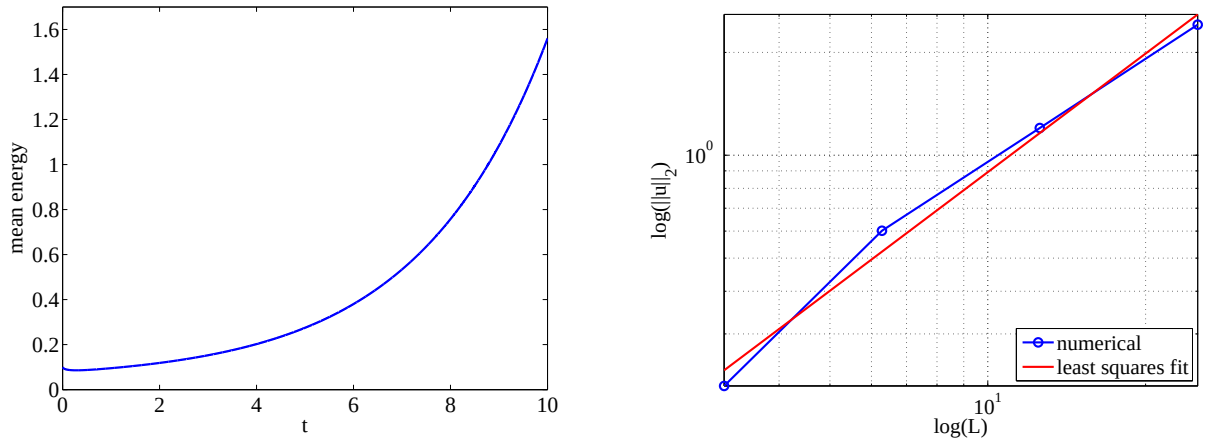

(a) Mean energy bound of equation (4.10) (b) Energy bound of the K-S equation.

Figure 4.3: Bounds verified for the linear and the Kuramoto-Sivasinsky (K-S) equation by the NSFV scheme.

4.3.4 Cahn-Hilliard equation

In this section we approximate the solution of the Cahn-Hilliard equation by the fractional step scheme (4.2) employing the nonstandard solution operators for each of the subproblems involved. That is, we make use of the schemes (4.7) and (4.16) for the Cahn-Hilliard equation.

Example 4.6 *Solve the CH equation*

$$\begin{cases} u_t + (\alpha u^3 + u + \gamma^2 u_{xx})_{xx} = 0, \quad x \in (0,6) \\ u(x,0) = \cos(\pi x/6), \end{cases} \tag{4.24}$$

subject to boundary conditions

$$u_x = \gamma^2 u_{xxx} - \phi(u)_x = 0, \qquad x \in \partial\Omega. \tag{4.25}$$

We highlight here that these schemes perform comparably well with the schemes discussed in Chapter 2. The evolution of the solution of the Cahn-Hilliard equation is shown in Figure 4.5(a). We also solve Example 4.6 and demonstrate the conservation of mass and the dissipation of the Ginzburg-Landau energy as expected. Figure 4.4 shows that the new schemes preserves these properties.

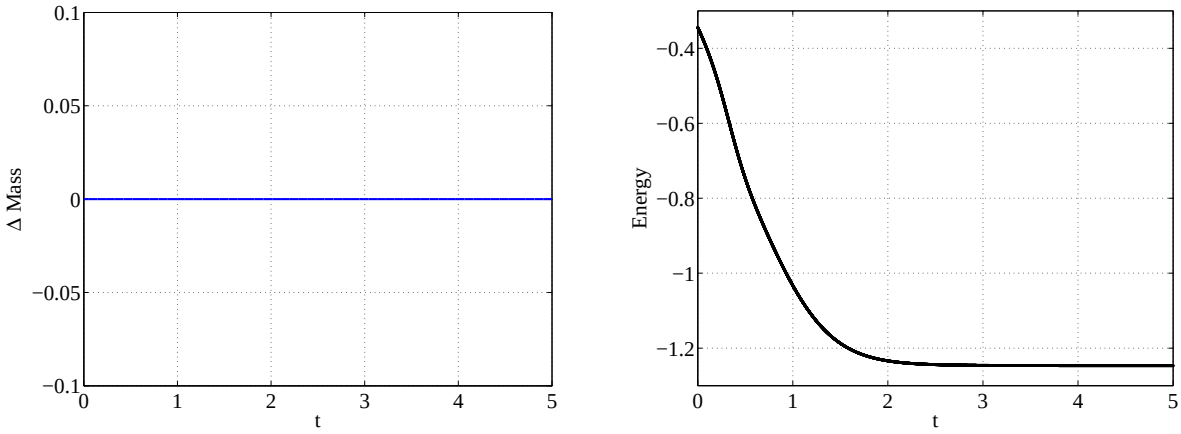

(a) Conservation of mass (b) Dissipation of the Ginzburg Landau energy

Figure 4.4: Properties of the Cahn-Hilliard equation verified by the nonstandard schemes with $\gamma^2 = 0.03$

Remark 4.3 *We highlight that this properties are resolved better here when compared with the standard schemes discussed in Chapter 2.*

4.3.5 Convective Cahn-Hilliard equation

In this section we approximate the solution of the convective Cahn-Hilliard equation by the fractional step scheme (4.3) employing the nonstandard solution operators for each of the subproblems involved. That is, we make use of the schemes (4.6), (4.7) and (4.16) for the Burger's, porous media and the linear sub-problems respectively. We solve the problems given below.

Example 4.7 *Solve*

$$\begin{cases} u_t - \delta u u_x + (u + \alpha u^3 + \gamma^2 u_{xx})_{xx} = 0, \\ u(x,0) = -\sin(x/6), \end{cases} \tag{4.26}$$

subject to boundary conditions

$$u_x = \gamma^2 u_{xxx} - \phi(u)_x = 0, \qquad x \in \partial\Omega. \tag{4.27}$$

The comparison of the numerical solution with the steady state solution for the convective Cahn-Hilliard equation is shown in Figure 4.5(b). These nonstandard schemes are employed

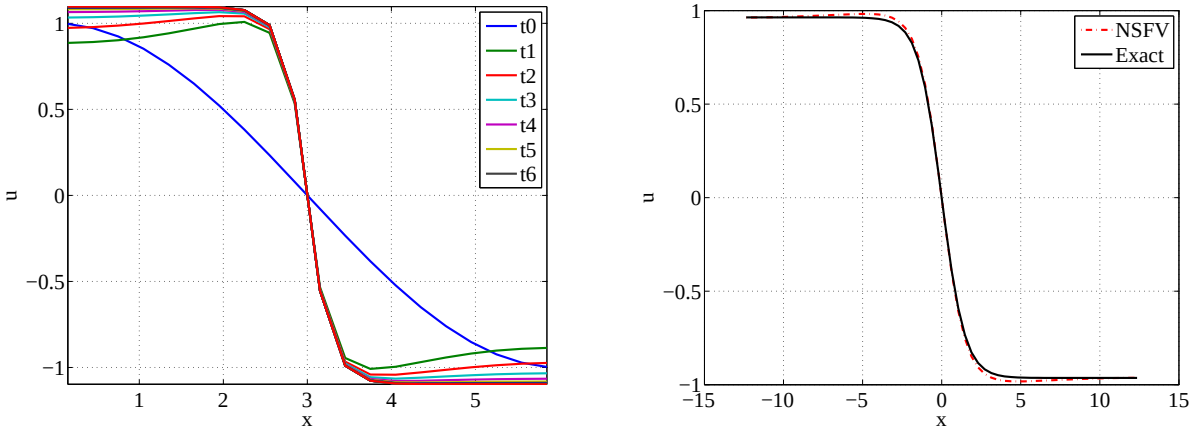

(a) Evolution of the CH equation (b) Solution of the cCH equation

Figure 4.5: Solutions of the Cahn-Hilliard and the convective Cahn-Hilliard equation by the nonstandard schemes. (a)$\gamma^2 = 0.02$, (b) $\gamma = 1$.

to solve Example 4.7 subject to periodic boundary condition and initial condition $0.5\cos(x)$ for all $x \in [-4\pi, 4\pi]$. The conservation of mass is shown in Figure 4.6.

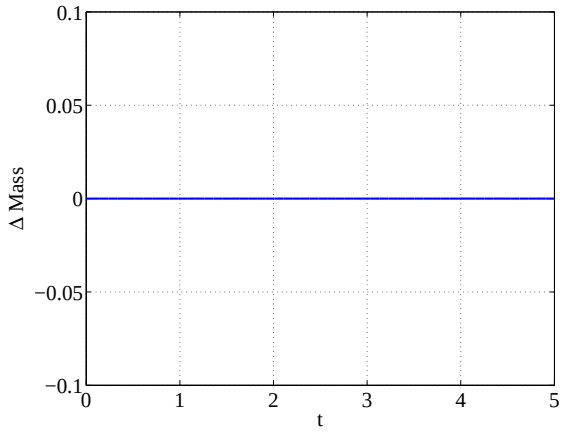

Figure 4.6: Conservation of Mass of the cCH equation

We also verify the coarsening process of the cCH equation. To achieve this, we investigate the problem below.

Example 4.8 *Solve the Example 4.7 subject to periodic boundary condition and initial condition* $0.5\cos(x)$ *for all* $x \in [-4\pi, 4\pi]$ *by the fractional splitting scheme* (4.3).

Figure 4.8 shows that the solution coarsens as we advance in time from integration time $T = 1$ to $T = 640$. We have taken the value of $\gamma = 1$ in this experiment.

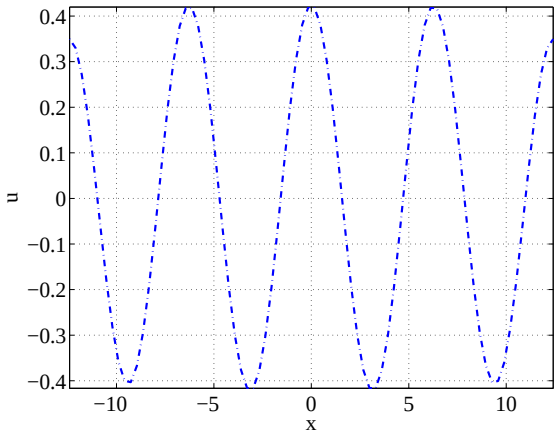

(a) Formation of periodic structure, $T = 1$

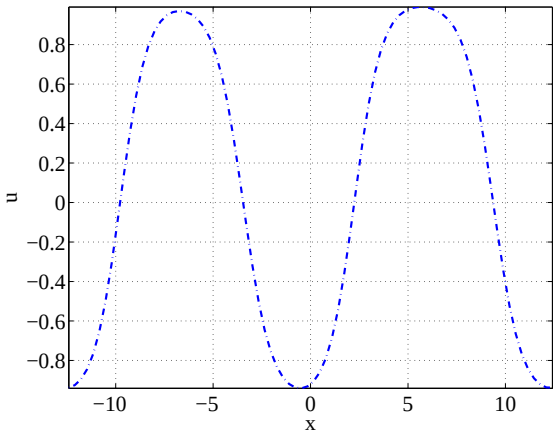

(b) Coarsening process, $T = 50$

Figure 4.7: Coarsening properties of the convective Cahn-Hilliard equation verified by the nonstandard schemes

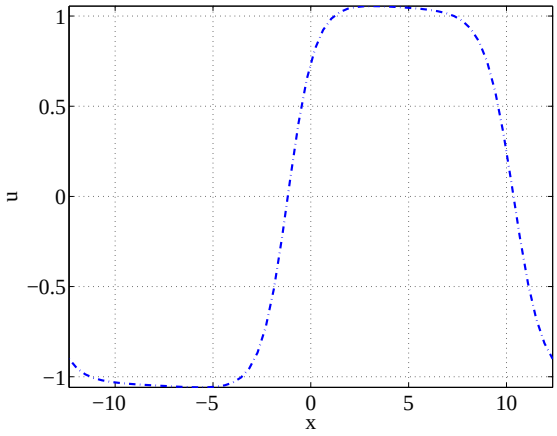

Figure 4.8: Coarsening process $T = 640$

4.4 Conclusion

We have proposed a fractional splitting scheme each for the the K-S and the CH equations where each of the sub equations are approximated by nonstandard schemes. Hence, the schemes are explicit. The nonstandard finite volume scheme (4.16) approximates the solution of the fourth order time dependent equation more accurate that the classical scheme as shown in Table 4.1. The exponential growth of the mean energy of its solution as expected is shown in Figure 4.3(a).

All the properties of the K-S equation were reproduced when this scheme is combined with the NSFV scheme (4.6) by the fractional step method. The chaotic behaviour of the solution on a periodic domain is shown in Figure 4.2(b) while the profile for the mean energy bound is shown in Figure 4.3(b).

Of particular significance, almost all the properties of the solution of the CH and cCH

equations are reproduced by these new schemes. The dissipation of the Ginzburg-Landau energy and the conservation of mass of the CH equation are shown in Figure 4.4. The conservation of mass of the cCH equation is observed in Figure 4.6. The coarsening progress are shown in Figure 4.7 and 4.8.

Chapter 5

Conclusion and future perspective

This thesis is dedicated to the design and implementation of finite volume schemes to differential equations arising in mathematical physics. In Chapter 1 we introduced the equations under investigation, i.e. the K-S equation, the CH equation and the Schrödinger equation. We also introduced the numerical recipes used throughout this work. Our observations and conclusions are highlighted below.

In Chapter 2, we proposed a fractional splitting method for each of the K-S and CH equations. The hyperbolic sub-equation was handled by the shock capturing schemes. We have compared the performance of some of the explicit schemes such as the semi-discrete, the fully discrete, the non-staggered finite difference scheme and the WENO scheme for this equation. The nonlinear diffusion equation was handled by a θ-method while the linear fourth order by either of the backward differentiation formula or the diagonally implicit Runge-Kutta scheme. This relaxes the stability restriction since the explicit schemes were employed only for the hyperbolic equation and the schemes for the fourth order equation are A-stable. The solution of the simplified equation are combined by the fractional step splitting method. The complexity in the two equations were simplified without losing the physical properties of the equations. We observed that all the known solution properties of these two equations are reproduced. For the K-S equation, the traveling wave solution, chaotic behaviour, preservation of periodicity, energy bounds are shown in Figures 2.4, 2.5, 2.7, 2.6 and 2.8 respectively. For the CH and cCH equation, the dissipation of the Ginzburg-Landau energy, the conservation of mass, the coarsening process and the transition from coarsening to roughening of the cCH equation are respectively observed in Figures 2.10, 2.13 and 2.14 and 2.17.

In Chapter 3, our quest for optimal schemes to handle singularly perturbed fourth order equation encountered in Chapter 2 led us to the study of singularly perturbed second order ordinary differential equations. One of the interesting example of these types of equations is the Schrödinger equation. The complex boundary condition of the Schrödinger equation makes its approximation by these two schemes non trivial. We proposed two new schemes for the Schrödinger equation. The semi-analytical scheme is based on some perturbation

technique while the nonstandard finite volume scheme is based on the existing nonstandard finite difference scheme.

The semi-analytical scheme followed three main steps namely,

- perturbation analysis of the given equation which leads to
- boundary layer analysis through which boundary layer equations are derived, solved and employed and lastly
- correcting of classical schemes.

The nonstandard finite volume scheme follows from deriving an exact scheme by the idea of the difference equation of the given equation. The merit of this method is that it preserves positivity, monotonicity and in fact the properties of the physical model. We design this nonstandard scheme both for the equation and its complicated boundary conditions.

To test the performance of these schemes, they were employed to solve some singularly perturbed equations. The approximation compares well with the exact solution of the tested equations. This can be seen in Tables 3.1 to 3.2 and Figures 3.3 to 3.4. The two methods reduce the computational cost known with classical approximation of singularly perturbed equations. In addition, these two schemes reproduces the the expected oscillatory behaviour of the Schrödinger equation with relatively little numbers of grids. Figures 3.5, 3.6, 3.7, 3.8 and Table 3.3 attests to the optimal performance of these new schemes as compared with classical schemes.

In Chapter 4, we employed the nonstandard finite volume scheme discussed in Chapter 3 to design robust schemes for the singularly perturbed fourth order equation. We design nonstandard schemes for the hyperbolic equation, the nonlinear diffusion equation and the linear fourth order parabolic equation. We showed that the scheme gave a better approximation of the linear fourth order PDE than any classical scheme. This is shown in Table 4.1. The exponential growth of the mean energy of its solution as expected is shown in Figure 4.3(a). The nonstandard scheme for each of the sub-equations are combined via the fractional splitting algorithm to yield nonstandard schemes for each of the K-S equation, the CH equation and the cCH equation. We highlight here, that this is the first time such a nonstandard scheme is designed for a higher order equation and suggest that this can be extended to other higher order equations.

For the K-S equation, Figures 4.2(b) and 4.3(b) shows the chaotic behaviour and the profile for the mean energy bound respectively. For the CH and cCH equations, the dissipation of the Ginzburg-Landau energy and the conservation of mass of the CH equation are shown in Figure 4.4. The conservation of mass of the cCH equation is observed in Figure 4.6 while the coarsening progress is shown in Figure 4.8.

The results in this work can be employed as tools to investigate many other practically relevant models. Some of the obvious area of further research from this thesis are listed below.

1. Numerical analysis of the schemes is possible even though non trivial. It is interesting to investigate the convergence of operator splitting schemes to fourth order equations [32].

2. Extension to higher order splitting is non-trivial but it is also a possible area of research focus.

3. Simulation of these equations in higher dimension by the Alternating Direction Method is an interesting area of research. In this case, one may need to employ other programming environment than MATLAB for the computation.

4. The scheme employed for the Schrödinger equation in this work can be extended to simulate the Schrödinger-Poison equation with better convergence and accuracy.

Bibliography

[1] N. B. Abdallah and O. Pinaud. Multiscale simulation of transport in an open quantum system: Resonances and WKB interpolation. *J. Comput. Phys.*, 213(1):288–310, 2006.

[2] A. A. Aderogba, M. Chapwanya, and J. K. Djoko. Travelling wave solution of the Kuramoto-Sivashinsky equation: A computational study. In *AIP Conf. Proc.*, volume 1479, page 777, 2012.

[3] A. A. Aderogba, M. Chapwanya, and J. K. Djoko. On a fractional step-splitting scheme for the Cahn-Hilliard equation. *Eng. Computation.*, (To appear), 2014.

[4] A. A. Aderogba, M. Chapwanya, and J. K. Djoko. Numerical approach for the solution of oscillatory 1d Schrödinger equation. In *9th SACAM Conf. Proc.*, 2014.

[5] K. Alexander and E. Tadmor. New high-resolution central schemes for nonlinear conservation laws and convection-diffusion equations. *J. Comput. Phys.*, 160:241–282, 2000.

[6] K. Alexander, N. Sebastian, and P. Guergana. Semidiscrete central-upwind schemes for hyperbolic conservation laws and Hamilton-Jacobi equations. *SIAM J. Sci. Comput.*, 23(3):707–740, 2001.

[7] D. Anders, M. Dittmann, and K. Weinberg. A higher-order finite element approach to the Kuramoto-Sivashinsky equation. *J. Appl. Math. Mech.*, 92(8):599–607, 2012.

[8] A. Arnold, N. B. Abdallah, and C. Negulescu. WKB-based schemes for the oscillatory 1d Schrödinger equation in the semiclassical limit. *SIAM J. Numer. Anal.*, 49(4):1436–1460, 2011.

[9] J. C. Bronski and T. N. Gambill. Uncertainty estimates and L^2 bounds for the Kuramoto-Sivashinsky equation. *Nonlinearity*, 19(9):2023, 2006.

[10] P. Collet, J-P Eckmann, H. Epstein, and J. Stubbe. A global attracting set for the Kuramoto-Sivashinsky equation. *Commun. Pure Appl. Math.*, 152(1):203–214, 1993.

[11] M. Crandall and A. Majda. The method of fractional steps for conservation laws. *Numer. Math.*, 34:285–314, 1980.

[12] L. Cueto-Felgueroso and J. Peraire. A time-adaptive finite volume method for the Cahn-Hilliard and Kuramoto-Sivashinsky equations. *J. Comput. Phys.*, 227(24):9985–10017, 2008.

[13] E. V. L. De Mello and O. Teixeira da Silveira Filho. Numerical study of the Cahn–Hilliard equation in one, two and three dimensions. *Physica A*, 347:429–443, 2005.

[14] M. Dehghan and D. Mirzaei. A numerical method based on the boundary integral equation and dual reciprocity methods for one-dimensional Cahn-Hilliard equation. *Eng. Anal. Boundary Elem.*, 33(4):522–528, 2009.

[15] J. Douglas and H. Rachford. On the numerical solution of heat conduction problem in two and three space variables. *Trans. Amer. Math. Soc.*, 82(2):421–439, 1956.

[16] Q. Du and R. A. Nicolaides. Numerical analysis of a continuum model of phase transition. *SIAM J. Numer. Anal.*, 28(5):1310–1322, 1991.

[17] A. Eden and V. K. Kalantarov. The convective Cahn–Hilliard equation. *Appl. Math. Lett.*, 20(4):455–461, 2007.

[18] C. M. Elliott and D. A. French. Numerical studies of the Cahn-Hilliard equation for phase separation. *IMA J. Appl. Math.*, 38:97–128, 1987.

[19] C. M. Elliott and Z. Songmu. On the Cahn-Hilliard equation. *Arch. Rat. Mech. Anal.*, 96(4):339–357, 1986.

[20] C. M. Elliott, D. A. French, and F. A. Milner. A second order splitting method for the Cahn-Hilliard equation. *Numer. Math.*, 54(5):575–590, 1989.

[21] C. L. Emmott and Bray A. J. Coarsening dynamics of a one dimensional driven Cahn-Hilliard equation. *Phys. Rev. E*, 54(5):4568–4575, 1996.

[22] D. J. Eyre. Unconditionally gradient stable time marching the Cahn-Hilliard equation. In *MRS Proceedings*, volume 529. Cambridge Univ Press, 1998.

[23] E. K. George, I. Moshe, and A. O. Steven. High-order splitting methods for the incompressible Navier-Stokes equations. *J. Comput. Phys.*, 97:414–443, 1991.

[24] L. Giacomelli and F. Otto. New bounds for the Kuramoto-Sivashinsky equation. *Commun. Pure Appl. Math.*, 58(3):297–318, 2005.

[25] A. A. Golovin, S. H. Davis, and A. A. Nepomnyashchy. A convective Cahn-Hilliard model for the formation of facets and corners in crystal growth. *Physica D*, 122(1-4): 202–230, 1998.

[26] A. A. Golovin, A. A. Nepomnyashchy, S. H. Davis, and Zaks M. A. Convective Cahn-Hilliard models: From coarsening to roughening. *Phys. Rev. Lett.*, 86(8):1550–1553, 2001.

[27] J. Goodman. Stability of the Kuramoto-Sivashinsky and related systems. *Commun. Pure Appl. Math.*, 47(3):293–306, 1994.

[28] S. Haq, N. Bibi, S. I. A. Tirmizi, and M. Usman. Meshless method of lines for the numerical solution of generalized Kuramoto-Sivashinsky equation. *Appl. Math. Comput.*, 217:2404–2413, 2010.

[29] H. Holden. *Splitting methods for partial differential equations with rough solutions: Analysis and MATLAB programs*. Amer Mathematical Society, 2010.

[30] H. Holden, K. H. Karlsen, and N. H. Risebro. Operator splitting methods for generalized Korteweg-de Vries equations. *J. Comput. Phys.*, 153(1):203–222, 1999.

[31] H. Holden, K. H. Karlsen, and K-A Lie. Operator splitting methods for degenerate convection-diffusion equations I: convergence and entropy estimates. In *Stochastic Processes, Physics and Geometry: New Interplays. II A Volume in Honor of Sergio Albeverio*, pages 293–316, 2000.

[32] H. Holden, K. Karlsen, N. Risebro, and T. Tao. Operator splitting for the KdV equation. *Math. Comput.*, 80(274):821–846, 2011.

[33] M. H Holmes. *Introduction to perturbation methods*, volume 20. Springer-Verlag New York, 2013.

[34] A. P. Hooper and R. Grimshaw. Traveling wave solutions of the Kuramoto-Sivashinsky equation. *Wave Motion*, 10:405–420, 1988.

[35] K. Inoue, H. Sakaki, J. Yoshino, and T. Hotta. Self-consistent calculation of electronic states in AlGaAs/GaAs/AlGaAs selectively doped double-heterojunction systems under electric fields. *J. Appl. Phys.*, 58(11):4277–4281, 1985.

[36] C-Y Jung. Finite elements scheme in enriched subspaces for singularly perturbed reaction–diffusion problems on a square domain. *Asymptotic Anal.*, 57(1):41–69, 2008.

[37] C-Y Jung and T. B. Nguyen. Semi-analytical numerical methods for convection-dominated problems with turning points. *Int. J. Numer. Anal. Model.*, 10(2):314–332, 2013.

[38] C-Y Jung and R. Temam. Finite volume approximation of one-dimensional stiff convection-diffusion equations. *J. Sci. Comput.*, 41(3):384–410, 2009.

[39] K. H. Karlsen and N. H. Risebro. An operator splitting method for nonlinear convection-diffusion equations. *Numer. Math.*, 77(3):365–382, 1997.

[40] K. H. Karlsen and N. H. Risebro. Corrected operator splitting for nonlinear parabolic equations. *SIAM J. Numer. Anal.*, 37(3):980–1003, 2000.

[41] K. Kassner, A. K. Hobbs, and P. Metzener. Dynamical patterns in directional solidification. *Physica D*, 93(23), 1996.

[42] L. A. Khan and P. L-F Liu. Intermediate Dirichlet boundary conditions for operator splitting algorithms for the advection-diffusion equation. *Comput. Fluids*, 24(4):447–458, 1995.

[43] A. H. Khater and R. S. Temsah. Numerical solutions of the generalized Kuramoto-Sivashinsky equation by Chebyshev spectral collocation methods. *Comp. Math. Appl.*, 56:1465–1472, 2008.

[44] Y. Kuramoto and T. Tsuzuki. Persistent propagation of concentration waves in dissipative media far from thermal equilibrium. *Prog. Theor. Phys.*, 55:356–369, 1976.

[45] T. Ladics. Application of operator splitting to solve reaction-diffusion equations. *Proc. 9th Coll. QTDE*, (9):1–20, 2012.

[46] M. Lakestani and M. Dehghan. Numerical solutions of the generalized Kuramoto-Sivashinsky equation using B-spline functions. *Appl. Math. Modelling*, 36:605–617, 2012.

[47] S. E. Laux and F. Stern. Electron states in narrow gate-induced channels in Si. *Appl. Phys. Lett.*, 49(2):91–93, 1986.

[48] H. G. Lee, J. W. Choi, and J. Kim. A practically unconditionally gradient stable scheme for the N-component Cahn–Hilliard system. *Physica A*, 2011.

[49] K. Leung. Theory on morphological instability in driven systems. *J. Stat. Phys.*, 61(1): 345–364, 1990.

[50] R. J. LeVeque. High-resolution conservative algorithms for advection in incompressible flow. *SIAM J. Numer. Anal.*, 33:627–665, 1996.

[51] R. J. LeVeque. Finite-volume methods for hyperbolic problems. *Cambridge University Press*, 2004.

[52] Randall J LeVeque. *Finite difference methods for ordinary and partial differential equations: steady-state and time-dependent problems*, volume 98. Siam, 2007.

[53] J. M-S Lubuma and K. C. Patidar. Uniformly convergent non-standard finite difference methods for self-adjoint singular perturbation problems. *J. Comput. Appl. Math.*, 191 (2):228–238, 2006.

[54] J. M-S Lubuma and K. C. Patidar. Non-standard methods for singularly perturbed problems possessing oscillatory/layer solutions. *Appl. Math. Comput.*, 187(2):1147–1160, 2007.

[55] D. Michelson. Steady solutions of the Kuramoto-Sivashinsky equation. *Physica D*, 19 (1):89–111, 1986.

[56] R. E Mickens. Novel explicit finite-difference schemes for time-dependent Schrödinger equations. *Comput. Phys. Commun.*, 63(1):203–208, 1991.

[57] R. E Mickens. *Nonstandard finite difference models of differential equations.* World Scientific, 1994.

[58] R. E Mickens. Nonstandard finite difference schemes for differential equations. *J Differ. Equ. Appl.*, 8(9):823–847, 2002.

[59] C. Negulescu. Numerical analysis of a multiscale finite element scheme for the resolution of the stationary Schrödinger equation. *Numer. Math.*, 108(4):625–652, 2008.

[60] J. Nickel. Travelling wave solutions to the Kuramoto-Sivashinsky equation. *Chaos Soliton. Fract.*, 33:1376–1382, 2007.

[61] B. Nicolaenko, B. Scheurer, and R.r Temam. Some global dynamical properties of the Kuramoto-Sivashinsky equations: nonlinear stability and attractors. *Physica D*, 16(2): 155–183, 1985.

[62] A. Novick-Cohen and L. A. Segel. Nonlinear aspects of the Cahn-Hilliard equation. *Physica D*, 10(3):277–298, 1984.

[63] F. Otto. Optimal bounds on the Kuramoto–Sivashinsky equation. *J. Funct. Anal.*, 257 (7):2188–2245, 2009.

[64] E. J. Parkes and B. R. Duffy. An automated tanh-function method for finding solitary wave solutions to non-linear evolution equations. *Comput. Phys. Commun.*, 98:288, 1996.

[65] K. C. Patidar and K. K. Sharma. Uniformly convergent non-standard finite difference methods for singularly perturbed differential-difference equations with delay and advance. *Int. J. Numer. Meth. Eng.*, 66(2):272–296, 2006.

[66] D. W. Peaceman and H. H. Rachford. The numerical solution of parabolic and elliptic differential equations. *J. Soc. Indust. Appl. Math.*, 3:28–42, 1955.

[67] J. B. Perot. An analysis of the fractional step method. *J. Comput. Phys.*, 108:51–58, 1993.

[68] O. Pinaud. Transient simulations of a resonant tunneling diode. *J. Appl. Phys.*, 92(4): 1987–1994, 2002.

[69] A. Podolny, M. A. Zaks, B. Y. Rubinstein, A. A. Golovin, and A. A. Nepomnyashchy. Dynamics of domain walls governed by the convective Cahn–Hilliard equation. *Physica D*, 201(3):291–305, 2005.

[70] H. G. Roos, M. Stynes, and L. Tobiska. *Numerical Methods for Singularly Perturbed Differential Equations.: Convection-Diffusion and Flow Problems.*, volume 24. Springer, 1996.

[71] J. J. Shepherd. On the asymptotic solution of the Reynolds equation. *SIAM J. Appl. Math.*, 34(4):774–791, 1978.

[72] C-W Shu. Essentially non-oscillatory and weighted essentially non-oscillatory schemes for hyperbolic conservation laws. In *ICASE Report*, pages 325–432. Springer, 1997.

[73] C-W Shu and S. Osher. Efficient implementation of essentially non-oscillatory shock capturing schemes. *J. Comput. Phys.*, 77:439–471, 1988.

[74] G. I. Sivashinsky. Nonlinear analysis of hydrodynamic instability in laminar flames i. derivation of basic equations. *Acta Astronaut.*, 4:1177–1206, 1977.

[75] G. I. Sivashinsky. On flame propagation under conditions of stoichiometry. *SIAM J. Math. Anal.*, 39(1):190–193, 1980.

[76] G. I. Sivashinsky and D. Michelson. On irregular wavy flow of a liquid film down a vertical plane. *Prog. Theor. Phys.*, 63:2112–2114, 1980.

[77] G. L. Snider, I-H Tan, and E. L. Hu. Electron states in mesa-etched one-dimensional quantum well wires. *J. Appl. Phys.*, 68(6):2849–2853, 1990.

[78] M. Stanislavova and A. Stefanov. Asymptotic estimates and stability analysis of Kuramoto-Sivashinsky type models. *J. Evol. Equ.*, 11(3):605–635, 2011.

[79] F. Stern. Iteration methods for calculating self-consistent fields in semiconductor inversion layers. *J. Comput. Phys.*, 6(1):56–67, 1970.

[80] Yamada T. and Y. Kuramoto. A reduced model showing chemical turbulence. *Prog. Theor. Phys.*, 56(2):681–683, 1976.

[81] E. Tadmor and H. Nessyahu. Non-oscillatory central differencing for hyperbolic conservation laws. *J. Comput. Phys.*, 87:408–463, 1990.

[82] E. Tadmor and L. Xu-Dong. Third order nonoscillatory central scheme for hyperbolic conservation laws. *Numer. Math.*, 79:397–425, 1998.

[83] I-H Tan, G. L. Snider, L. D. Chang, and E. L. Hu. A self-consistent solution of schrödinger–poisson equations using a nonuniform mesh. *J. Appl. Phys.*, 68(8):4071–4076, 1990.

[84] E. F. Toro. Riemann solvers and numerical methods for fluid dynamics: A pratical introduction. *Springer Dordrecht Heidelberg London New York*, 2009.

[85] Y. Ugurlu and D. Kaya. Solutions of the cahn-hilliard equation. *Computers Math. Applic.*, 56(12):3038–3045, 2008.

[86] S. J. Watson. Crystal growth, coarsening and the convective Cahn-Hilliard equation. *International series of Numerical Mathematics*, 147:329–341, 2003.

[87] S. J. Watson, F. Otto, B. Y. Rubinstein, and S. H. Davis. Coarsening dynamics of the convective Cahn-Hilliard equation. *Physica D*, 178:127–148, 2003.

[88] D. J. Wollkind. Singular perturbation techniques: a comparison of the method of matched asymptotic expansions with that of multiple scales. *SIAM Review*, 19(3):502–516, 1977.

[89] X. Yan and S. Chi-Wang. Local discontinuous Galerkin methods for the Kuramoto-Sivashinsky equations and the Ito-type coupled KdV equations. *Comput. Methods Appl. Mech. Eng.*, 195:3430–3447, 2006.

[90] N. N. Yanenko. The method of fractional step for solving multi-dimensional problems of mathematical physics. *Novosibirsk, Nauka*, 1967.

[91] K. Yong-Jung, H. Youngsoo, and T. G. Myers. On the numerical solution of a driven thin film equation. *J. Comput. Phys.*, 227:7246–7263, 2008.

[92] N. J. Zabusky and M. D. Kruskal. Interaction of "Solitons" in a collisionless plasma and the recurrence of initial state. *Phys. Rev. Lett.*, 155(240), 1965.